Doctoral Thesis

# A microspectroscopic investigation of photoluminescence and electroluminescence in lead halide perovskites

(ハロゲン化鉛ペロブスカイトにおける光および電気励起発光の顕微分光学的研究)

Graduate School of Environmental Science
Hokkaido University

**Sankaramangalam Balachandran Bhagya Lakshmi**

September 2021

# Acknowledgment

I would like to express my sincere thanks to my Ph.D. supervisor Prof. Vasudevan Pillai Biju for providing all the guidance and assistance throughout my doctoral research. I am also thankful for Associate professor Yuta Takano and Assistant professors Ken-Ichi Yuyama and Palyam Subramanyam for their supports and active discussions. I thank Mrs. Atsuko Fujii for her time and administrative assistance. I also thank all my lab members Dr. Jahidul Islam, Dr. Devika Sasikumar, Dr. Sushant Ghimire, Dr. Lata Chouhan, Ajith Nair, Md. Shahjahan, Jeladhara Sobhanan, Sachith B. M., Danyang Chen, Hanjun Zhao, Feijun Xu, Zhijing Zhang, Dong Zhang, Dr. Takuya Okamoto for their active discussion and friendship. I thank the Japanese embassy, India for providing me with a MEXT scholarship. I thank all my Indian and international friends, who made my life in Japan much easier and colorful.

A warm thank you to all my teachers, classmates, friends, cousins, and family members from Kerala for their motivation and cheers.

Last but not the least, I am thankful to my family for the constant motivation they provided to pursue my research. I thank my mother, Dr. T. S. Geetha for the unbiased opinions and strength she gave me whenever I faced troubles during my life. My father, Adv. S. K. Balachandran had always been there for me in making rightful decisions. My brother, Harikrishnan S. B. has always motivated me to become a better person.

Finally, I thank god almighty for giving me enough strength to successfully finish what I have started.

# Abstract

Lead halide perovskites are gaining rapid attention in solar cells, LEDs, lasers, etc. on account of their attractive properties like easy synthesis, tunable bandgap, and excellent charge carrier dynamics. However, their commercialization is still hindered by certain factors, mainly being the stability concern. In this thesis, I carry out a microspectroscopic investigation of photoluminescence (PL) and electroluminescence (EL) in lead halide perovskites microcrystals for understanding the factors that decrease photoluminescence and electroluminescence efficiencies. This thesis has five chapters. In chapter 1, an introduction of lead halide perovskite by giving focus to its chemical structure, optoelectronic properties, various synthesis methods, and their applications is provided. Perovskite blinking is one of the main issues leading to the loss of photoluminescence and electroluminescence efficiency in devices, which is discussed in detail. In chapter 2, various methods like the pressure-induced solid-state method, antisolvent vapor-assisted crystallization, and inverse temperature crystallization to synthesize perovskites crystals are summarized. Various characterization methods like absorption spectroscopy, steady-state and time-resolved fluorescence spectroscopy, single-particle microspectroscopy, X-ray diffraction technique, scanning electron microscopy (SEM), and energy-dispersive X-ray spectroscopy (EDS) for understanding the properties are also discussed in detail. In chapter 3, photoluminescence studies on perovskite pellets synthesized by a solid-state, pressure-induced method are carried out. The synthesized perovskite pellet shows very good optical properties, which match those synthesized by wet chemical routes involving solvents like *N*, *N*-dimethylformamide, and dichloromethane. Due to the large thickness of the pellet samples, electroluminescence studies are not feasible. Photon recycling is a phenomenon seen in thick samples, in which emissions from the sample get reabsorbed and emitted multiple times. This phenomenon is known to improve solar cell efficiencies. The perovskite pellets synthesized by the pressure-induced method showed a distribution of energy states, confirmed by photoluminescence spectral and lifetime studies. From the photoluminescence lifetime studies, the rates of various charge carrier recombination processes are extracted. These rates reveal that energy transfer outweighs other radiative and nonradiative processes occurring in the pellet. This fact is clarified by preparing mixed halide perovskites which confirm nonradiative energy transfer in the photon recycling mechanism. In chapter 4, electroluminescence and photoluminescence studies are conducted on perovskite microcrystals using single-particle microspectroscopy and

fluorescence spectroscopy. An interesting phenomenon of EL blinking is observed from these microcrystals which are characterized by high-intensity and low-intensity EL bursts in the EL trajectories. The nature of EL blinking in perovskites is clarified with the help of statistical analysis. In a microcrystal showing multiple-emitting sites, truncated power-law behaviors for ON- and OFF-time probability densities are observed. Such a truncated behavior is commonly characterized as type-A blinking arising due to the charging-discharging processes. However, in an ensemble of crystals, a linear power-law behavior is seen for the ON- and OFF-time probability distributions. This is the signature of type-B blinking due to the charge carrier trapping-de-trapping processes. From these studies, $MAPbBr_3$ microcrystals show both the type of blinking. The main factor responsible for EL blinking is the migrating halide vacancies in the microcrystals, which act as EL quenchers. These vacancies randomly shift their locations. Such a mechanism dominates the whole microcrystal. The above studies made it possible to understand the origin and mechanism of EL blinking in perovskites. In chapter 5, the role of halide vacancies in EL blinking is studied. For this purpose, perovskite microcrystals of varying bromide compositions are prepared by varying the molar ratio of precursors. An under-stoichiometric sample, which is expected to carry many halide vacancies, shows a linear power-law behavior in the ON- and OFF-time probability densities. This behavior, as stated above, is typical of type-B blinking, which is due to the trapping and de-trapping of charge carriers. The trapping of charge carriers occurs due to the excess halide vacancies. However, a stoichiometric and an over-stoichiometric perovskite sample show type-A blinking as suggested by the truncated power-law behavior of the ON- and OFF-time probabilities. This is due to the charging-discharging mechanism resulting from the formation of trions and associated Auger-type nonradiative recombination. The role of halide vacancies in EL blinking is verified by analyzing $MAPbBr_3$ microcrystals post-treated with MABr solutions to fill the vacancies. An enhancement in the photo- or electroluminescence intensities of the MABr treated $MAPbBr_3$ microcrystals is verified by correlating single-particle microspectroscopic studies with SEM-EDS studies. The PL and EL experiments on lead halide perovskites help understand the low efficiencies of perovskite-based electroluminescent devices. The studies in this thesis help improve the efficiencies of perovskite-based optoelectronic, photovoltaic, and electroluminescent devices.

# Abbreviations and symbols

| | |
|---|---|
| Å | Angstrom |
| A | Lattice constant |
| ASE | Amplified spontaneous emission |
| AVC | Antisolvent vapor assisted crystallization |
| °C | Degree Celsius |
| CBM | Conduction band minimum |
| CHP | *N*-cyclohexyl pyrrolidone |
| $CsCO_3$ | Cesium carbonate |
| CsBr | Cesium bromide |
| $d_{hkl}$ | Interplanar spacing |
| DCM | Dichloromethane |
| DMF | *N, N*-dimethylformamide |
| DMSO | Dimethyl sulfoxide |
| EDS | Energy dispersive X-ray spectroscopy |
| $E_g$ | Bandgap energy |
| EL | Electroluminescence |
| EMCCD | Electron multiplying charge-coupled device |
| ETL | Electron transport layer |
| FABr | Formamidinium bromide |
| fs | Femtosecond |
| FWHM | Full width at half maximum |
| GPa | Gigapascal |
| *h*, *k*, or *l* | Miller indices |

| | |
|---|---|
| HTL | Hole transport layer |
| ITC | Inverse temperature crystallization |
| ITO | Indium tin oxide |
| k eV | Kilo electron volt |
| $k_1$ | Monomolecular recombination rate constant |
| $k_2$ | Bimolecular recombination rate constant |
| $k_3$ | Auger recombination rate constant |
| $k_{et}$ | The rate constant of energy transfer |
| $k_{ET}$ | The rate constant of electron transfer |
| $k_{nr}$ | The rate constant of nonradiative relaxation |
| $k_r$ | The rate constant of radiative relaxation |
| LARP | Ligand-assisted reprecipitation |
| LED | Light emitting diode |
| LHP | Lead halide perovskite |
| LUMO | Lowest unoccupied molecular orbital |
| M | Molar |
| MABr | Methylammonium bromide |
| MHz | Megahertz |
| mL | Milliliter |
| mmol | Millimole |
| ms | Millisecond |
| mW | Milliwatt |
| NA | Numerical aperture |
| NIR | Near-infrared |

| | |
|---|---|
| nm | Nanometer |
| ns | Nanosecond |
| OPA | Optical parametric amplifier |
| P(τ) | Probability distribution |
| PCE | Power-conversion efficiency |
| PEDOT:PSS | Poly(3,4-ethylenedioxythiophene)-polystyrene sulfonate |
| PeLED | Perovskite-based light emitting diode |
| PL | Photoluminescence |
| PLQY | Photoluminescence quantum yield |
| PMMA | Poly(methyl methacrylate) |
| PNC | Perovskite nanocrystal |
| PSC | Perovskite solar cell |
| QY | Quantum yield |
| RegA | Regenerative amplifier |
| RT | Room temperature |
| s | Second |
| SEM | Scanning electron microscope |
| SHG | Second harmonic generation |
| SOC | Spin orbit coupling |
| T | Temperature |
| $TiO_2$ | Titanium dioxide |
| UV | Ultraviolet |
| V | Voltage |
| v/v | Volume-by-volume |

| | |
|---|---|
| Vis | Visible |
| W | Watt |
| µm | Micrometer |
| µM | Micromolar |
| X | Cl or Br or I |
| XRD | X-ray diffraction |
| $\tau$ or $\tau_{av}$ | Photoluminescence lifetime or average photoluminescence lifetime |
| $\tau_c$ | Truncation time |
| $\lambda$ | Wavelength |

# Table of contents

# Chapter 1

# Introduction

**Abstract**

Metal halide perovskites are gaining a lot of popularity in the field of optoelectronic applications. These semiconductors offer attractive optical and electronic properties suitable for light-harvesting, light-emitting, and light-amplifying applications in the form of solar cells, LEDs, lasers, etc. In this chapter, I first briefly introduce the lead halide perovskite by describing its structure. Then, I discuss various methods to synthesize perovskite nanocrystals, microcrystals, and single crystals by methods like antisolvent vapor assisted crystallization, inverse temperature crystallization, ligand assisted reprecipitation method, etc. In the following section, its fundamental optical and electronic properties like bandgap, absorption, photoluminescence, charge carrier dynamics, and various types of defects are discussed. The next section is dedicated to the discussion of various applications using perovskite materials, especially in photovoltaic and light-emitting applications. Although perovskites have attractive optoelectronic properties as semiconducting material, their stability is still a bottleneck in their commercialization. Blinking in perovskites is a phenomenon in which the photoluminescence from perovskites shows stochastic fluctuation. By taking various examples from literature, I explain PL and EL blinking observed in various perovskite crystals. The origin of blinking, its mechanism, and ways to suppress blinking are discussed in this section. I also discuss the motivation for my research and various studies performed in each chapter of the thesis.

## 1.1 General Introduction

Perovskites refer to a class of compounds represented by a general formula $ABX_3$. A 3D framework of perovskite consists of corner-sharing $BX_6$ octahedra with the A-site cation filling the cuboctahedral cavities. Perovskite was first identified as $CaTiO_3$ by Gustav Rose in 1839 and named it after the Russian mineralogist Lev Perovski.[1] Following this discovery of oxide perovskite, metal halide perovskites like $CsPbX_3$ were synthesized in the laboratory having notable electronic and magnetic properties.[2] Metal halide perovskite can be purely inorganic when the A site is occupied by an inorganic ion like ($Cs^+$) or can be an organic-inorganic hybrid if the A site ion is an organic cation like methylammonium ($CH_3NH_3^+$/$MA^+$) or formamidinium ($CH_3(NH_2)_2^+$/$FA^+$). The B site ion is a divalent cation like $Pb^{2+}$ or $Sn^{2+}$, and X is a halide ion ($Cl^-$, $Br^-$, $I^-$).

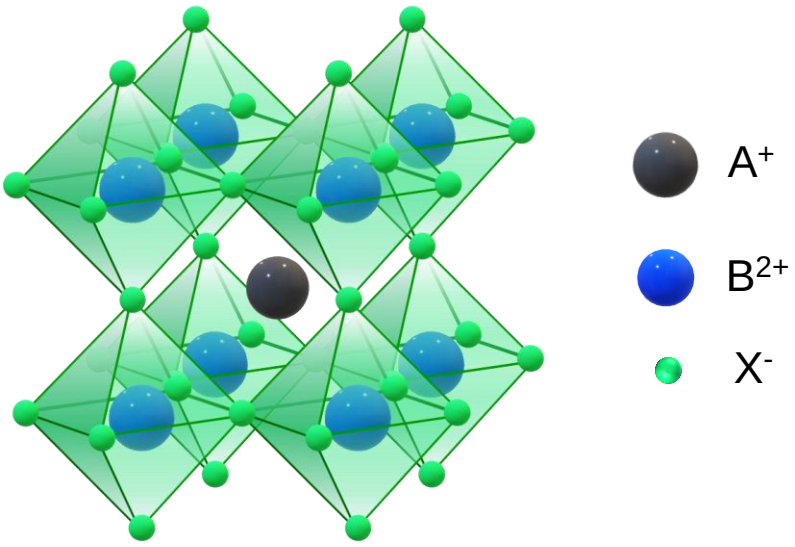


**Figure 1.** The perovskite crystal structure

Surprisingly, only a few ions fit the $ABX_3$ structure based on certain constraints like the tolerance factor and octahedral factor.[3] Both these factors decide the stability of the 3D structure above or below a certain limit can lead to distortions. The tolerance factor (t) introduced by Goldschmidt is given by the equation:

$$t = \frac{r_A + r_x}{\sqrt{2}(r_B + r_x)}$$

where, $r_A$, $r_B$, $r_X$ correspond to the ionic radii of the A site, B site, and X site ions. The ideal value lies between 0.81-1.00. A new equation for tolerance factor has been recently put forward by Bartel *et al.* to incorporate different kinds of perovskite structures other than $ABX_3$ crystal structure, like that of double perovskites with a formula $A_2BB'X_6$ and other nonperovskite structures.[4]

The next constraint to the crystal structure is given by the octahedral factor (μ), the ideal value of which lies between 0.44 and 0.90. It is given by the formula,

$$\mu = \frac{r_B}{r_x}$$

However, obeying the above constraints does not qualify their stability in the given phase. For example, the δ phase of $CsPbI_3$ or $FAPbI_3$ is not stable.

Although only a few ions fit the structural and stability criteria, metal halide perovskite possesses interesting optical and electronic properties. Absorption over a wide spectral range, large absorption cross-section, high photoluminescence quantum yield, bandgap tunability, impressive charge carrier dynamics, and a low lasing threshold is a few of them which have led to their rapid rise as photonic materials for the 21$^{st}$ century.[3] It was in 2009, the perovskite material started gaining rapid attention. In 2009, the first perovskite solar cells were designed by Miyasaka and co-workers.[5] The power conversion efficiency (PCE) from the $MAPbI_3$ based solar cells designed by them was 3.8 %. Since then, PCE has improved and reached 25 % to date.[5] The first room-temperature electroluminescence was achieved by Friend *et al.* in 2014 with an external quantum efficiency of 0.76 %.[7] Within a short period, the EQE increased to 20 % or more.[8,9,10,11] The first room-temperature lasing was observed in 2014 from $MAPbI_{3-x}Cl_x$ perovskite.[12] With progressing research, the threshold for perovskite lasing has reduced to 220 nJ/cm$^2$.[13]

### 1.2 Synthesis of perovskites

Perovskites are materials known to have very low formation energy. The standard Gibbs free energy of formation at 298 K was found to be negative for different kinds of $MAPbX_3$ (X= Cl, Br, I) perovskites.[14] Simple mixing of precursor solution at room temperature can result in a highly crystalline perovskite structure. By using controlled techniques, high-quality perovskite crystals can be synthesized. The synthesis of perovskite is highly cost-effective as compared to other semiconductor counterparts. Some of the most common

methods for perovskite synthesis are explained here. Based on the requirement, perovskite crystals can be synthesized at the nanoscale, microscale, or bulk level.[15]

An antisolvent vapor-assisted crystallization (AVC) method is used to synthesize perovskite microcrystals. Figure 2a shows the synthesis scheme of perovskite by the AVC method. This method involves the use of an antisolvent in which the perovskite has low solubility. Common examples of antisolvents for perovskite synthesis are dichloromethane, isopropanol, and chlorobenzene. In the presence of antisolvent vapors, the perovskite crystallizes from its solution in a good solvent like *N, N* dimethylformamide (DMF). By optimizing the concentration of precursor salt solutions and time for crystallization, high-quality perovskite micro or single crystals with low trap density and free of the crack can be synthesized. Bakr and co-workers synthesized $MAPbBr_3$ and $MAPbI_3$ single crystals in this way for the first time.[16,17]

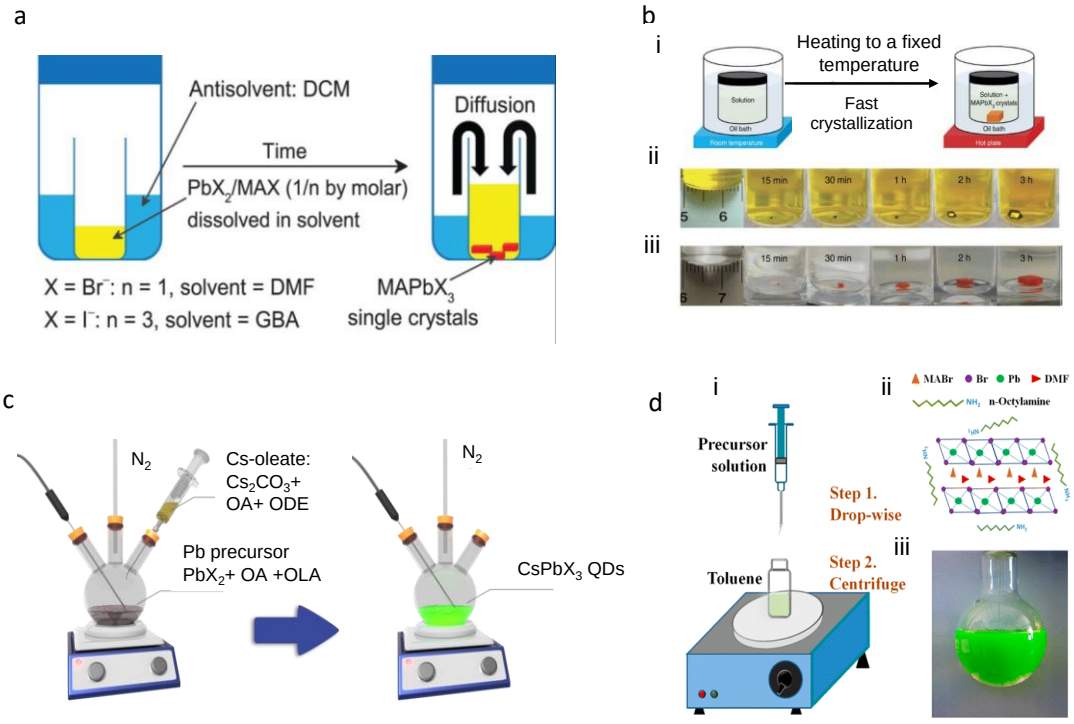


**Figure 2.** Various synthesis methods used for preparing perovskites. a) Antisolvent vapor-assisted crystallization method,[16] b) inverse temperature crystallization method i) scheme showing the synthesis method, ii) $MAPbI_3$ single crystal synthesis at 110 °C, and iii) $MAPbBr_3$ single crystal synthesis at 80 °C showing growing crystals at various intervals of time,[19] c) hot injection method (picture from www.ossila.com), and d) ligand assisted reprecipitation method i) scheme for synthesis, ii) illustration of starting materials, and iii) optical image of the $MAPbBr_3$ perovskite solution.[24]

The inverse temperature crystallization method (ITC) uses the retrograde solubility feature of perovskite crystals.[18,19] This is shown in Figure 2b. Perovskite is known to crystallize from a precursor solution by increasing the temperature. Perovskite single crystals of 5 mm or more can be grown in this way within 3 hours. This is one of the fastest methods to grow high-quality perovskite single crystals. $MAPbX_3$, $FAPbX_3$ (X= Cl, Br, I) single and microcrystals are synthesized mainly in this way. Seeding crystals into a fresh precursor solution can also decrease the time of crystallization. $CsPbBr_3$ single crystals synthesized by a high temperature (>600°C) Bridgeman method, can now be grown easily using this ITC method.[20]

Colloidal QDs of perovskites can be synthesized easily by the hot injection method (HI) (Figure 2c) and ligand-assisted reprecipitation methods (LARP) (Figure 2d). These methods employ organic ligands to control the growth and maintain the stability of the formed colloidal nanocrystals and quantum dots. Kovalenko and co-workers synthesized $CsPbX_3$ QDs of various sizes using the hot injection method.[13] It involves two steps. First, a $PbX_2$ precursor containing various ligands is prepared at a high temperature under inert conditions. Simultaneously the Cs precursor is also prepared at high temperature. Injection of the Cs precursor to the Pb precursor at high temperature followed by immediate arresting of the reaction using ice water bath results in the precipitation of colloidal $CsPbX_3$ QDs. The QDs are then extracted using nonpolar solvents by repeated centrifugation. By varying the temperature at the injection time, QDs or nanocrystals of various sizes can be synthesized. Several modifications of this method are seen nowadays to improve the quality of the QDs. It involves the choice of various organic ligands and precursor chemicals. $FAPbBr_3$, $MAPbI_3$ QDs can also be prepared using this strategy. By optimizing the synthesis conditions, quantum confinement can be achieved in the nanocrystals.

To prepare PNCs, a ligand-assisted reprecipitation method is used (Figure 2d).[21,22] $MAPbBr_3$ nanocrystals are prepared using this method. Precursor solution consisting of $PbBr_2$, MABr, and organic ligands like oleic acid, octadecene, alkyl ammonium bromide in a polar solvent like DMF is introduced dropwise into a nonpolar solution like toluene under stirring. Highly luminescent nanocrystals immediately precipitate out of the solution that is separated and stored after centrifugation. The size of perovskite QDs was ca 6 nm. Not only $MAPbBr_3$ but other perovskites could also be synthesized in this way.

Thin films of perovskites are often required for device-based applications and studies. By a one-step or two-step spin coating methods or simply by drop-casting the precursor solution and room temperature drying can result in pinhole-free smooth thin films.[23] Apart from the above-mentioned standard synthesis methods, several unconventional methods are also employed. Microwave-assisted methods,[24] ultrasonication methods,[25] ball milling,[26,27,28] and pressure-induced solid-state synthesis methods will all result in good quality perovskite crystals. [29,30,31]

### 1.3. Fundamental properties of perovskites

#### 1.3.1 Electronic structure

Lead halide perovskites are direct bandgap semiconductors. Their bandgap can be modulated by simply varying the ions in them. Lattice distortions affect the bandgap, with major contributions coming from varying halide ions. Lead and halide ions contribute to the frontier molecular orbitals. Varying the halide ions leads to changes in B-X bond length and bond angles based on their electronegativities.[32] This leads to changes in the contribution of respective atomic orbitals and thus bandgap. 'A' site cation has no direct contribution to the electronic structure of the bandgap. However, the size of the A-site cation will lead to lattice expansion or contraction based on which bandgap will be slightly affected.[33] The bandgap can be tuned across the visible spectrum from deep blue to near infra-red. The bandgap tuning has led to their utilization in the field of light-harvesting and light-emitting applications. Figure 3 shows the formation of molecular orbitals using lead and iodine atoms.

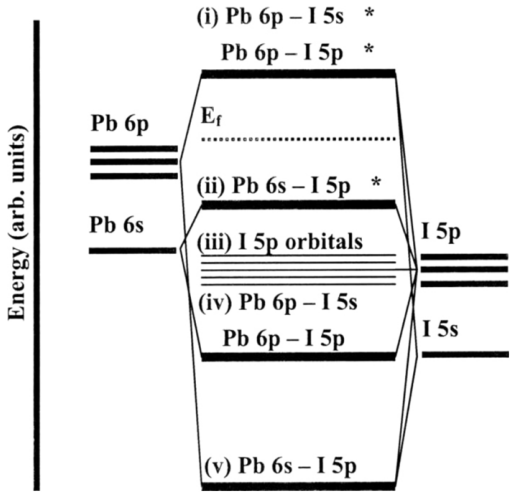


**Figure 3.** Electronic band energy diagram of $MAPbI_3$ perovskite without considering spin-orbit coupling.[3]

The 6s and 6p orbitals of lead and 5s and 5p orbitals of iodine contribute to the formation of molecular orbitals in the energy level diagram. This molecular orbital formation ignores any form of spin-orbit coupling. The valence band minimum (VBM) is contributed by the iodine 5p and Pb 6s in a 3:1 ratio, while the conduction band maximum (CBM) has a majority contribution from lead 6p orbitals along with contributions from p orbitals of iodine. In the absence of spin-orbit coupling, the CBM has a three-fold degeneracy, while the VBM remains nondegenerate. However, when the spin-orbit coupling is taken into account, the degenerate states of CBM undergo splitting. Such a splitting causes dispersion of CBM energy states and hence lowers the bandgap. Unlike the case of conventional semiconductors that shows splitting in VBM, the perovskite band structure is called inverted because the splitting occurs in the CBM.

### 1.3.2 Absorption and photoluminescence

Metal halide perovskite posses a large absorption coefficient. This is one of the reasons for their success in photovoltaic applications. The absorption edge is very sharp, arising out of their direct bandgap nature. Absorption processes below the bandgap are also seen as a result of the tailing of the band edges. This phenomenon is called Urbach tailing and is caused by the presence of intrinsic defects or due to impurity doping. Distribution of closely spaced energy states close to the valence band maximum and conduction band minimum will lead to the tailing. The absorption of lead halide perovskite can be tuned over a wide spectral range in the visible region by changing the halide ions. Figure 4 shows the absorption features of $CsPbBr_3$ perovskite by varying the halide ions. A change in the A-site cation has however less role in the tuning of the bandgap and hence the absorption. However, the influence of A-site cation in the bandgap can be seen with the distortion of the ideal crystal structure. A deviation from the ideal B-X-B angle in the $ABX_3$ crystal structure is observed by changing the A-site cation in an $APbI_3$ perovskite. An increase in bandgap from 1.48 for α-$FAPbI_3$ to 1.67 for γ-$CsPbI_3$ is seen corresponding to a decrease in B-X-B bong angle.[34,35]

Halide-dependent tuning of emission color is useful in various device-based applications. Apart from the halide-dependent tuning of bandgap, dimensionality reduction also causes appreciable shifts in absorption and emission features in lead halide perovskites.[3] A 2D perovskite exhibit strong excitonic features in the absorption spectra as compared to 3D perovskites.[3] The changes in the absorption and emission features can

also be observed with changes in perovskite crystal size. When the size of the perovskite crystals lies below the Bohr exciton diameter, it starts showing quantum confinement properties. Fine color tunability across the whole visible spectral range can be achieved. Kovalenko and co-workers synthesized $CsPbBr_3$ perovskite NCs with 'wide color gamut' adding more pure color options in the Commission Inter-nationale de I'Eclairage (CIE) color chart.[21] This is shown in Figures 4a, b, c and d. By simply varying the halide ion, the emission color could be tuned from deep blue to near-infrared colors.

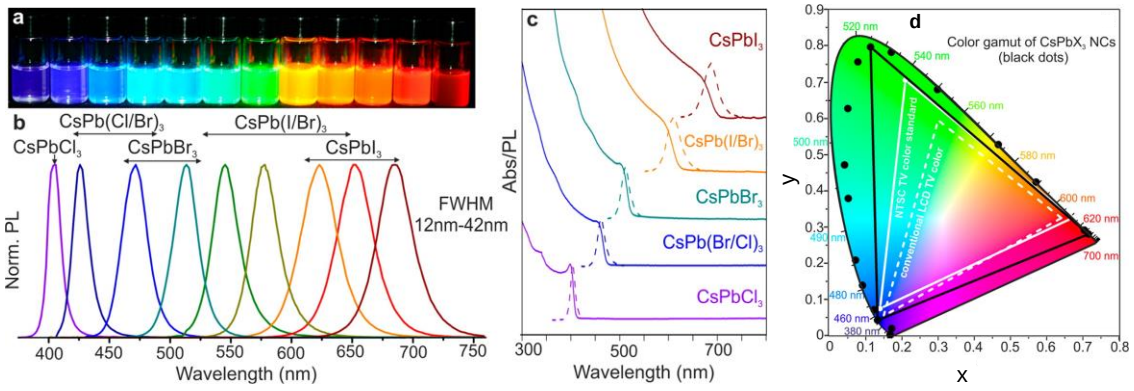


**Figure 4.** Absorption and emission properties of metal halide perovskites: (a,b) tunable emission from $CsPbX_3$ QDs across the entire visible spectrum, b) absorption spectra of $CsPbX_3$ perovskite of varying halide composition and, c) wide color gamut from $CsPbBr_3$ QDs for display applications.[21]

### 1.3.3 Charge carrier dynamics

Absorption of light by perovskite materials excites the charge carriers to higher energy states, leaving a hole behind at the ground state. The fate of these charge carriers is responsible for the optoelectronic properties of the perovskite. Whether the photogenerated charge carriers behave as free carriers or excitons depends on the nature of the material. For solar cells applications, the formation of free carriers with very low binding energy is favored. In contrast, for a light-emitting device, excited-state species with high exciton binding energy will lead to a high probability of radiative relaxation.

Perovskite shows a lifetime ranging from nanoseconds in quantum dots to several microseconds in single crystals or thin films. In the case of lead halide perovskite, various ways in which a charge carrier relax are given in the Figure 5.

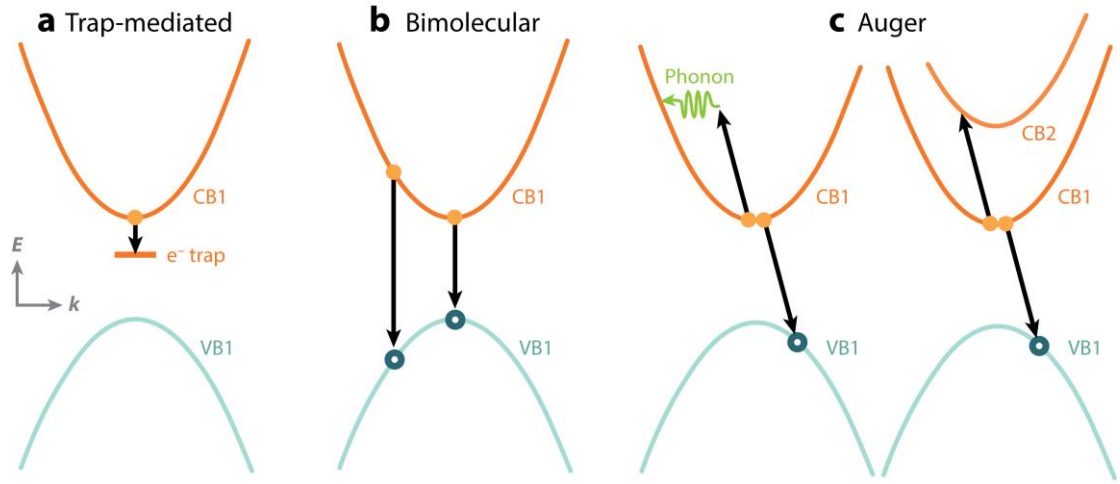


**Figure 5.** Various modes of charge carrier recombination in lead halide perovskites. a) Monomolecular trap-assisted recombination, b) bimolecular recombination of an electron, and a hole, and c) Auger-recombination involving trion states.[36]

The rate equation for recombination involving a charge carrier density n (t) can be represented as follows. Here it is assumed that free carriers are formed upon photo or electro-excitation.

$$\frac{dn}{dt} = -k_3 n^3 - k_2 n^2 - k_1 n$$

where $k_1$ is the rate constant for monomolecular recombination which involves excitonic recombination or trap-assisted recombination. Here the recombination depends only on the concentration of either of the two species. $k_2$ is the bimolecular recombination rate constant involving an electron-hole pair. $k_3$ is the Auger recombination rate constant. The Auger process involves many species and many steps. It is the relative contribution of each of these processes that will determine their capability in device-based applications like LED, laser, or solar cells.

The total rate constant r (n) is a sum of all three recombination processes and which is known to affect the diffusion length, $L_D$ as follows:

$$L_D(n) = \sqrt{\frac{\mu k_B T}{r(n) e}}$$

where μ is the mobility of charge carriers, $k_B$ is the Boltzmann constant, T is the temperature, and e is the electronic charge.

### 1.3.4 Defects

Not all recombination processes lead to radiative events. Defects in the crystal structure act as centers of nonradiative recombination. Energetically, they are called trap states. Nonradiative recombination processes in a semiconductor material lower its luminescence efficiency. In the case of perovskites, several types of defects are known to exist. Below is a figure showing various traps present in lead halide perovskites.[37]

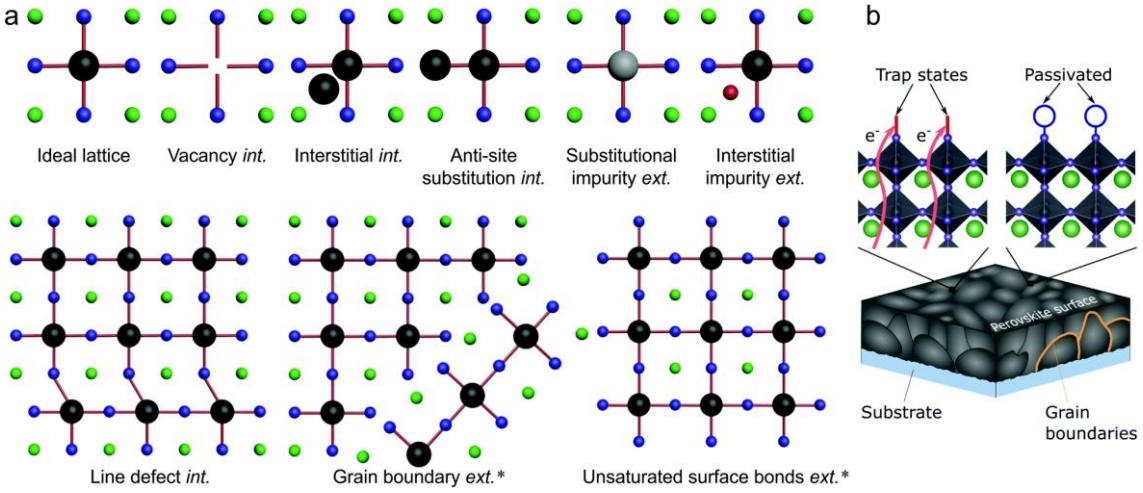


**Figure 6.** a) Various kinds of defects observed in lead halide perovskite and b) defect passivation methods.[37]

$MAPbI_3$ is known to have 12 types of defects, namely the vacancy defects, $V_{MA}$, $V_{Pb}$, $V_I$; the interstitial defects $MA_i$, $Pb_i$, $I_i$; antisite occupancy defects, $MA_{Pb}$, $MA_I$, $Pb_{MA}$, $Pb_I$, and $I_{Pb}$. In general, the defects with high formation energy would be present as deep levels within the bandgap, and the defects with low formation energy would result in shallow energy states within the bandgap. However, some exceptions are known. The $I_{Pb}$, $I_{MA}$, $Pb_i$, $Pb_I$, $V_I$ are known to form deep states. The defects which are known to form shallow states are $V_{Pb}$, $V_{MA}$, $MA_{Pb}$, and $I_i$ and have acceptor characteristics and the defects, $MA_i$, $V_I$, and $MA_I$ also form shallow states with a donor characteristic. [38]

In the case of $MAPbBr_3$ single crystals, first-principle calculations suggest the following defects, $MA_i$, $Pb_{MA}$, $V_{Br}$, $Pb_i$, $MA_{Pb}$, and $Pb_{Br}$.[38] Apart from the point defects, other defects, like surface defects due to the presence of dangling bonds, structural defects like screw-dislocation, line defects and, grain boundaries are also present in lead halide perovskite as can be seen in Figure 6.

The nature of the traps, whether is it shallow or deep, is still conflicting in various reports. However, it is understood that perovskites are highly defect-tolerant and hence the nature of the traps in perovskites are often associated with shallow traps. This can be seen from Figure 7 where defect intolerant semiconductors like GaAs or CdTe form deep trap levels while perovskite shows shallow trap levels or intraband levels.[39] The de-trapping process occurs even at room temperature utilizing thermal energy. Hence the defects in optimum concentration do not affect their optoelectronic properties.

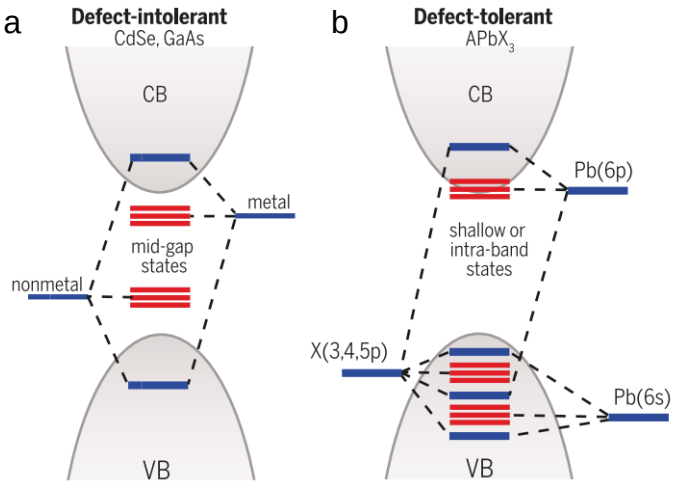


**Figure 7.** a) Defect levels in CdSe, GaAs semiconductors, and b) defect levels in perovskites.[39]

Several techniques are used to passivate the defect states. Light soaking in a nitrogen atmosphere is known to remove shallow defect states in (FA, MA, Cs)$Pb(I_{1-x}Br_x)_3$ perovskite films.[40] KI-based defect passivation methods are also known.[41] Various kinds of Lewis acids and Lewis bases can also passivate surface defects. Benzylamine and Cu(thiourea) can attach to Pb and I simultaneously and satisfy their dangling bonds.[42,43]

### 1.4 Applications of perovskites

#### 1.4.1 Principle of solar cell and LED

In both the cases of solar cells and LED, a photoirradiation or electrical excitation introduces charges into conduction bands. Several pathways open up for their relaxation. In the case of solar cells, charge separation towards oppositely charged electrodes is highly favored to generate the photocurrent. However, in the case of LEDs, a high rate of charge recombination is preferred. Apart from the active perovskite layer which acts as the center of charge generation and recombination, several charge transport layers are

utilized to either separate the charges from the perovskite layer (in solar cells) or to confine charges within the perovskite layer (in LED). The success of a good solar cell or LED lies in the above-said processes. Transport layers should have appropriately placed conduction and valence band levels for charge injection or separation. Below shown is a solar cell and an LED device configuration using perovskite as active layers.

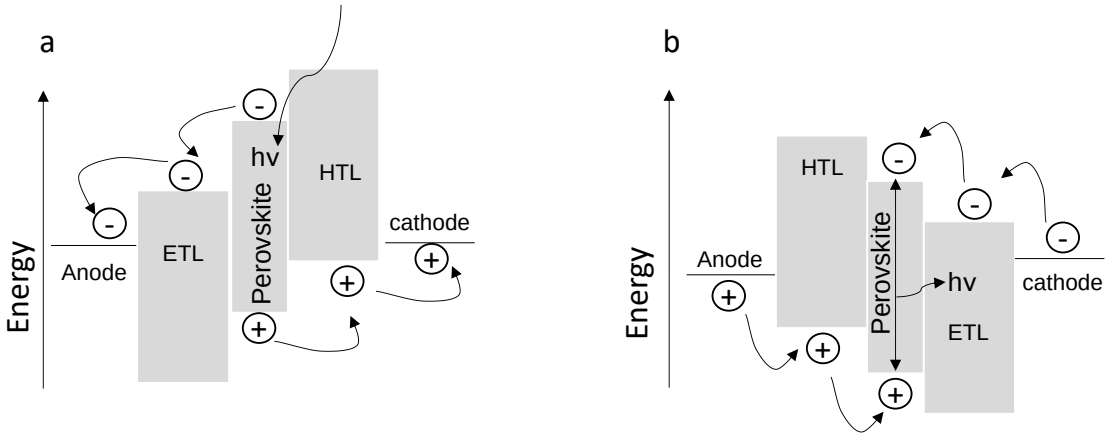


**Figure 8.** a) A device configuration of perovskite solar cell, and b) a device configuration of perovskite LED. ETL- electron transport layer, HTL- hole transport layer.

### 1.4.2 Perovskite solar cells

Perovskite was initially used as a sensitizer in solar cells.[4] However, with their attractive properties like large absorption cross-section, absorption over a wide spectral range, ambipolar charge transport, high PLQY, large diffusion coefficient, long carrier lifetime, etc. to name a few, perovskites became the active layer in solar cells. In 2009, when Miyasaka *et al.* designed the hybrid organic-inorganic perovskite solar cells, the power conversion efficiency (PCE) was very low, at about 3.8%.[5] The PCE as of today has gone up to 25%. Theoretical calculations have exceeded the Shockley-Queisser limit of 30% considering that only radiative recombination can take place within the material.[44] Several modifications in the solar cell device architecture from a simple planar heterojunction to mesosuperstructured[45] and tandem cells[46,47] have improved the long-range carrier migration across various charge transport layers. However, the presence of sub-bandgap defects in perovskite is known to interfere with the recombination of charge carriers and hence decrease the PLQY and open-circuit voltage associated with perovskite solar cells (PSCs).[48] Thus, research progressed to fill these traps by defect passivation and doping.[48,49,50] Hysteresis in the current vs voltage curve in PSCs is another issue affecting its growth.[50] Ion migration under an external electric field is the main cause of this

hysteresis.[51] Using fullerenes and $TiO_2$ over the perovskite active layer improves the electronic contact with various charge transport layers. This has allowed reducing hysteresis in the current vs voltage curve.[51,52] Stability concern about perovskite materials is a bottleneck towards its commercialization. The degradation of perovskite is caused by the presence of moisture, oxygen, and heat[53,54,55] Various encapsulation techniques are tried to sustain the material stability and elongate the operational lifetime of perovskite-based devices.[54] Howsoever, the operation lifetime is tens of magnitude lower than that of silicon and other inorganic semiconductor-based solar cells.

### 1.4.3 Perovskites light-emitting diodes

Although perovskites were studied mainly for solar cell applications, it turns out that a good solar cell should also work as a good LED. The properties that attracted metal halide perovskites towards light-emitting applications are the high PLQY, tunable bandgap across the whole visible spectrum (1.7-2.3eV), size-dependent wide color gamut (400-700 nm), narrow emission line width (<100meV) with a full width half maximum as low as 12 nm.[3] Figure 9a shows a PeLED device architecture involving various transport layers like hole transport layer (HTL), electron transport layer (ETL) as well as conducting electrodes. Figure 9b shows the absorption and emission features (PL and EL) of the perovskite-based LED device as prepared using a $MAPbX_3$ perovskite.

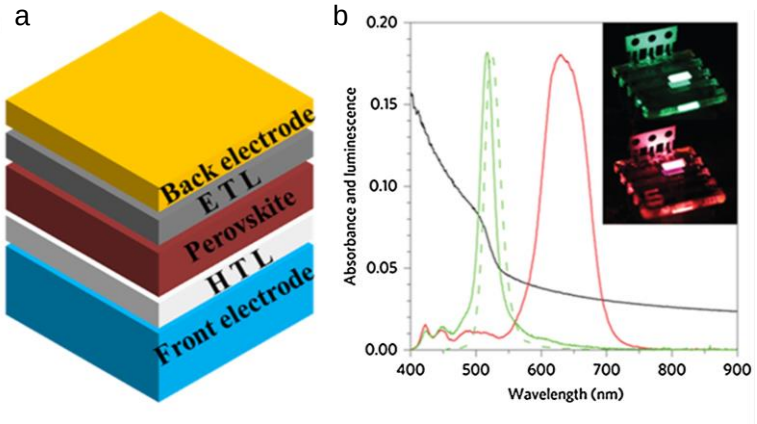


**Figure 9.** a) A typical perovskite LED structure, and b) absorption (black), normalized EL spectra (green solid), and normalized PL spectra of $MAPbBr_3$ perovskite (green, dashed), normalized EL spectrum (red) from $MAPbBr_2I$. Inset shows the respective EL devices.[7]

Although perovskite electroluminescence studies began in the 1990s,[56,57,58,59] the first room-temperature electroluminescence was observed in 2014 by Friend *et al.* with a

reported EQE of 0.76% and 0.1% from a mixed halide $MAPbI_{3-x}Cl_x$ and $MAPbBr_3$ perovskite respectively.[7] Here, the EQE was found to increase with the current density just like how PLQY increased with excitation density increase. A double heterojunction structure (ITO/PEDOT: PSS/Perovskite/F8/Ca/Ag) was utilized to confine the charge carriers injected into the emissive perovskite layer of nanometer thickness. Such an architecture leads to improved radiative bimolecular recombination assisted by the quantum well structure. A low EQE as compared to PLQE suggested that nonradiative losses occur as a result of leakage current in such LEDs. Also, losses are due to low surface coverage of perovskite films leading to electrical shunts. Their studies have shown the need for improving surface coverage of the perovskite layer. Optimizing film thickness, use of charge transport layers of appropriate energy levels for charge injection and transport, can further improve EQE.

By solvent engineering and defect passivation techniques, the efficiencies of perovskite LEDs were improved over the years.[53,56,60] Sequential deposition of perovskites precursors under vapor phase or in solution-phase had led to the formation of smooth films with fewer defects. Apart from EQE, other factors affecting the commercialization of PeLED include low operational stability, material degradation under moisture or oxygen, or Joule heating.[53,55] Controversially, humidity at controlled levels is known to heal surface defects and improve their performance.[61] Figure 10 shows a comparison of efficiencies of LEDs based on organic semiconductors, other inorganic QD semiconductors, and perovskites. It can be seen that within a short period, perovskite has achieved rapid progress in efficiency as compared to other contenders.

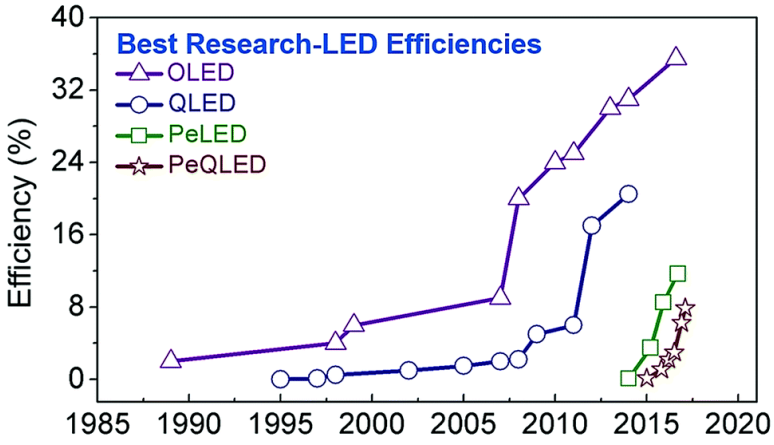


**Figure 10.** A chart showing efficiencies of organic LED, inorganic quantum dot LEDs perovskite LEDs, and perovskite quantum dot LEDs.[62]

### 1.4.4. Lasing and amplified spontaneous emission

Apart from solar cells and LED applications, perovskites are well known to show low threshold lasing. Similar to LED, lasing in perovskite was also a low-temperature phenomenon. Over the years, the threshold for lasing has come down from 2μJ/cm$^2$ to 220 nJ/cm$^2$.[13,63,64,65,66,67] Various modes of optically pumped lasing like whispering gallery mode, random lasing and Fabry-Peröt lasing could be achieved from nanocavities, microcrystal networks, spherical resonators, etc.[13,63-67] Figure 11 shows lasing from $APbX_3$ (A= Cs, MA, FA, and X= Cl, Br, I) perovskite rods and nanoplates.

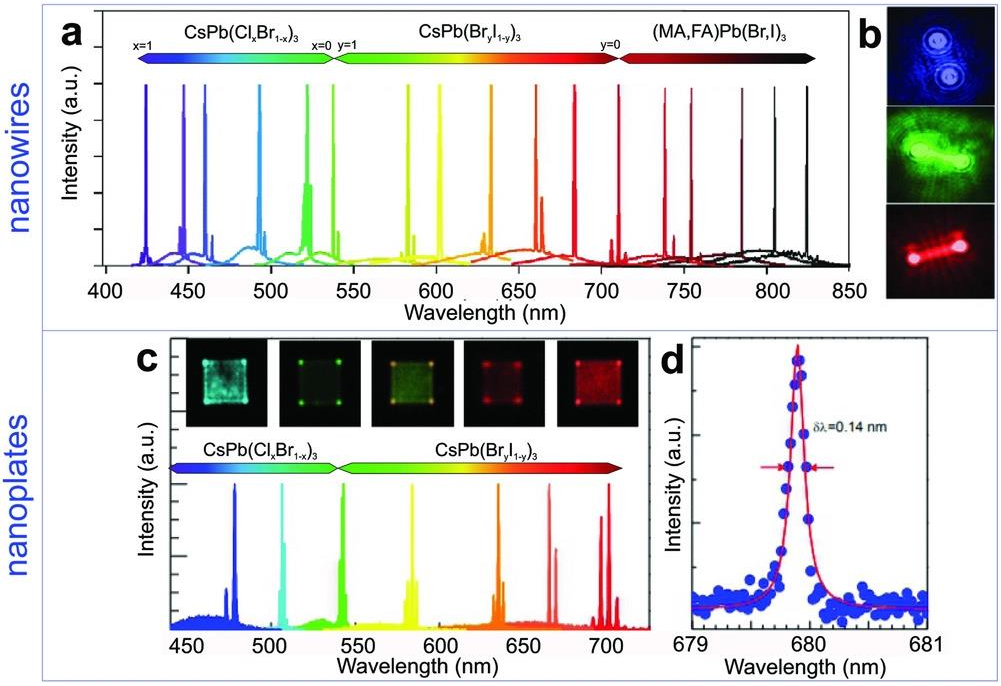


**Figure 11.** (a) Lasing showed by $APbX_3$ perovskite nanowires of varying A and X site composition, (b) an image showing the nanowires under lasing, (c) lasing from nanoplates of $CsPbX_3$. Inset: the image showing the lasing in nanoplates, and (d) example of a lasing spectrum with a Q factor of 4850.[67]

Their role as photodetectors and sensors is also gaining a lot of popularity these days,[58,59,60] Over a short span of time, perovskites have turned out to be the material for the millennium. However, research is still impeded by certain limitations degradation by moisture, oxygen, and short operational lifetime. Apart from these, they are at par with conventional organic and inorganic semiconductors like GaAs, and Si and their tremendous improvement in efficiency can replace the flatlining silicon semiconductor industry in the near future.

### 1.5 Blinking phenomenon.

#### 1.5.1 Photoluminescence blinking in perovskites

It is known from earlier reports that chalcogenide QDs show a peculiar property called intermittency or blinking.[71,72,73,74,75] It is a process in which quantum dots show discontinuity in emission upon its photoexcitation. With the introduction of single-particle imaging and microspectroscopic techniques, blinking could be characterized as random fluctuations in the PL intensity. The fluctuations were defined as ON and OFF based on a threshold value. The ON states were a result of radiative recombination events in a quantum dot when it emits, and OFF states are a result of nonradiative recombination leading to no emission. The ON and OFF processes are independent of each other and OFF state recovery is assisted by one or more pathways. There is no fixed time in which the QD exists in a particular state. Such a stochastic process is difficult to be followed, however, a statistical analysis of ON- and OFF-time probabilities can give an understanding of the charge carrier dynamics within the QDs. Such single particle studies could give insights into the behavior of individual particles which otherwise were averaged out in steady-state fluorescence studies. Similar to chalcogenide QDs, perovskite materials are also known to show blinking.[76-89]

Blinking is a highly unfavorable process for light-emitting applications such as LEDs and lasers. Nonradiative losses in emission are evident in the blinking trajectory characterized by the OFF events. The first observations of PL blinking in perovskite came from large nanocrystals beyond the quantum confinement regime. Scheblykin and co-workers observed 'giant photoluminescence blinking' of large $MAPbI_3$ nanocrystals as well as from localized regions in micro-sized crystals (Figure 12).[76]

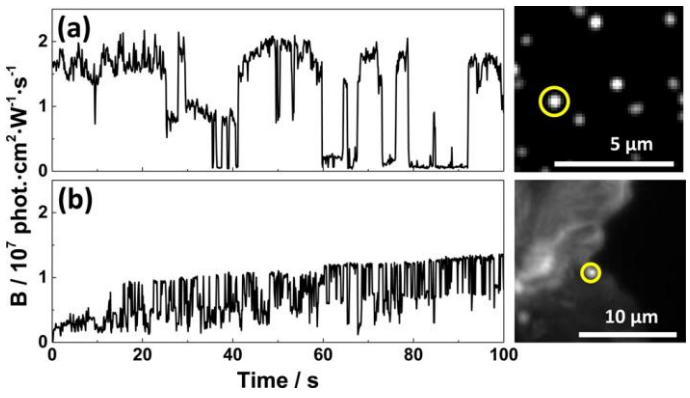


**Figure 12.** Giant PL blinking observed from a) a $MAPbI_3$ NC and, b) an area on a large $MAPbI_3$ crystal.[76]

The amplitude of such blinking was 5 orders of magnitude greater than individual dye molecules under similar excitation conditions. Such blinking was seen pronounced at lower excitation densities as opposed to the blinking fluctuations observed for dye molecules at higher excitation power.

Following this, PL blinking was observed from $MAPbX_3$ (X= Br, I) nanocrystals of different morphologies like dots, rods, plates, and sheets.[77] Such shape correlated blinking was also associated with the density of traps present in different shapes which was also supported by lifetime studies. In the case of $MAPbBr_3$ film of nanoparticles, blinking was observed as a result of charge migration across nanocrystals in a film which on accumulation at grain boundaries, lead to nonradiative Auger recombination.[78] Here, the charging and discharging of nanoparticles leads to the blinking phenomenon where the OFF state is a result of nonradiative Auger recombination. A statistical analysis of ON- and OFF-time probability distribution was characterized by a truncated power-law behavior described as $P(\tau) \propto \tau^a e^{-\tau/\tau_c}$, where 'a' is the power-law exponent. However, blinking was not observed from isolated $MAPbBr_3$ particles because of the balanced charge movement within them. PL blinking from $MAPbBr_3$ nanocrystals of 10-50 nm size synthesized without any capping ligands proves the role of surface charge traps as a cause of longer OFF-times.[79] These traps were attributed to undercoordinated $Pb^{2+}$ atoms, or, in essence, halide vacancies, at the surface of these nanocrystals. $CsPbBr_3$ NC and $CsPbI_3$ with weak quantum confinement showed PL blinking which was also attributed to nonradiative Auger recombination from charged excitons.[80] The blinking was characterized as type-A based on its correlation with lifetime studies. A truncated power-law behavior with an exponential cut-off, in this case, is a signature of the charging and discharging of quantum dots. Super-resolution microscopy studies on large $MAPbI_3$ rods of hundreds of nanometer sizes proved that these particles could blink as a whole.[81] Here, a linear power-law behavior ($P(\tau_{ON/OFF}) \propto \tau^a$) where 'a' is the power-law exponent for the ON and OFF-time for blinking in $MAPbI_3$ nanorods was noticed for the first time. This behavior suggests a trapping-de-trapping mechanism for blinking. An increase in the excitation density decreased the OFF times as well as suppressed PL blinking which is associated with trap-filling. PL blinking dependence under different atmospheres such as vacuum, nitrogen, and air showed increased blinking in a nitrogen atmosphere as compared to vacuum or air. However, the OFF-time duration in nitrogen was several orders times less than that in vacuum and air. Here the role of the atmosphere in the

formation and suppression of surface trap-states, as well as the role of oxygen or water molecules in PL fluctuations, could be understood.

The co-existence of type-A and type-B blinking was observed in $FAPbBr_3$ QDs.[82] In addition to charging-discharging of trions trapping-de-trapping mechanisms, diffusion-controlled electron transfer processes also contributed to the type-A mechanism in $FAPbBr_3$ QDs. PL flickering seen in perovskite nanocrystals, unlike PL blinking, shows multistate intensity fluctuations, which occurs as a result of excess charges trapped within a nanocrystal.[83]

The mechanism for such PL blinking was discussed as 'Quenching site model' or 'Emitting site model'. Several charge carrier traps are located in the crystal which is associated with chemical defects or crystal defects like ion vacancies. The activation and deactivation of such defects or trap states cause blinking in this example (Figure 13a). Super trap models are used to explain blinking in larger perovskite crystals.[84] According to this model, a single super trap provides a more efficient recombination channel than a large number of other forms of quenching sites existing in the material. The super traps are a quasi-stable complex of a hole trap and an electron trap located close to each other like that of a donor-acceptor (DA) pair. Activation and deactivation of these super traps result in blinking. This is shown in Figure 13b. In the case of thin films, accumulation of mobile charges at grain boundaries and resulting nonradiative Auger recombination is said to be the cause of PL blinking (Figure 13c).

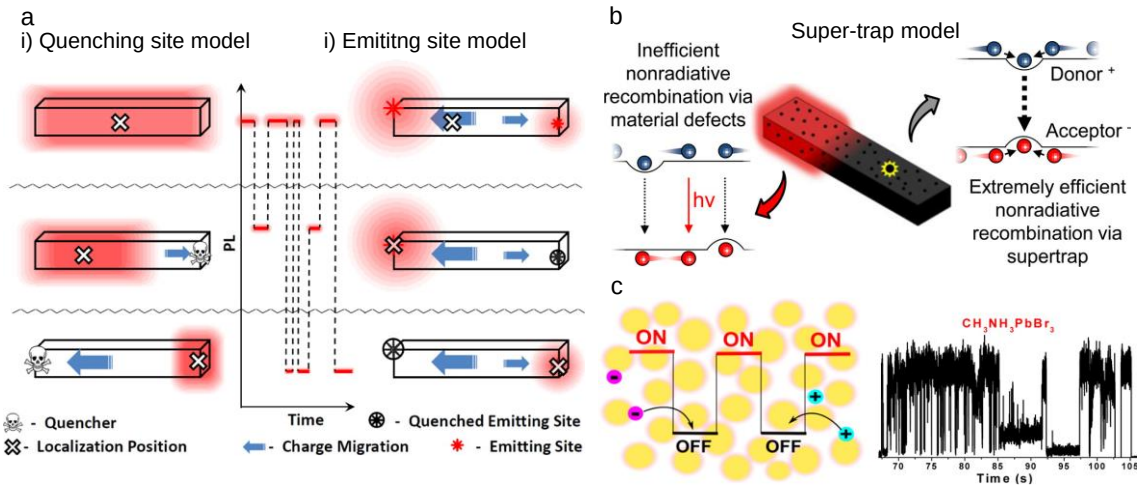


**Figure 13.** PL blinking mechanisms in perovskite a) the quenching and emitting site model[66] b) the super trap model,[84] c) Auger recombination model based on charge migration and accumulation.[88]

The blinking in perovskite shows excitation power dependence,[75] temperature dependence[86] as well as environment dependence in various gases as well as polymers.[87]

Several types of research have been undertaken to suppress PL blinking. One example is the post-synthetic surface modification strategy for blinking suppression. Surface treatment of $FAPbBr_3$ NCs with sodium thiocyanate (NaSCN) was found to suppress PL flickering.[88] Perovskite/semiconductor/core/shell/ QDs configuration as in the case of $CsPbBr_3$/CdS core/shell QDs shows nonblinking features along with high stability.[89] This is similar to conventional core/shell QDs which provide reduced electronic traps and improved stability. Blinking free PL-time traces were achieved in Cs-based single halide nanocrystals at a low temperature of 6K.[90] Some recent studies also indicated that tuning of perovskite by varying the halide composition has a great impact on blinking behavior.[91] It turned out that simple mixing of two perovskite solutions of different halides resulted in perovskites with 71% non-blinking behavior with > 99% ON time fraction. The mixing of halogens causes the reduction of interior traps in perovskite nanocrystals. Such alloyed type mixed halide perovskite thus exhibits reduced Auger recombination thereby suppressing the blinking.

### 1.5.2 Electroluminescence blinking in perovskites

Although hundreds of reports discuss the origin of PL blinking and ways to suppress it, there are seldom reports on electroluminescence blinking. Analogous to PL blinking, EL blinking is also reported from perovskite. Here the perovskite is excited electrically rather than optically. Nguyen *et al.* reported EL blinking from $MAPbBr_3$ single crystals.[92] The EL blinking trajectory obtained from $MAPbBr_3$ single crystal is shown in Figure 14a. A suggested explanation for EL blinking is the trapping of charge carriers in sub-bandgap trap states located at crystal edges and corners. Here the competing radiative and nonradiative process results in EL blinking. Another report on EL blinking was made by Vacha and co-workers from $CsPbBr_3$ nanocrystal aggregates.[93] Here, the funneling of charge carriers to large nanocrystal and their subsequent recombination result in EL blinking behavior. Here the particle-selective nature of carrier recombination leads to EL blinking mechanism. The EL trajectories collected from the nanocrystal aggregates are shown in Figure 14b.

So far, there are no reports on the EL blinking mechanism. However, several studies have been performed to understand electric field-related effects on perovskites.

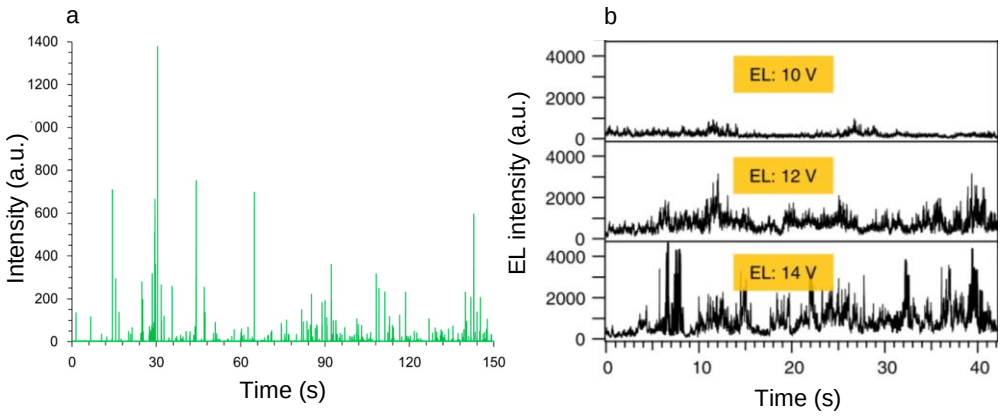


**Figure 14.** EL blinking observed in a) $MAPbBr_3$ single-crystal perovskite,[82] and b) $CsPbBr_3$ nanocrystal aggregates at various voltages.[93]

### 1.6. Motivation

Metal halide perovskite research has given greater insights into their attractive optoelectronic properties and charge carrier dynamics within these semiconducting materials. Most of the researches are dedicated to improving these properties by overcoming the challenges associated with material stability and reducing nonradiative losses in device-based applications. In my thesis, I focus mainly on understanding the charge carrier dynamics within perovskite microstructures in the context of electroluminescence blinking.

In chapter 2, I explain the synthesis of perovskite microcrystals and pellets used for my studies and various characterization techniques used for evaluating the optical and electronic properties of perovskites. I used Kubelka-Munk diffuse reflectance spectroscopy to calculate the bandgap of the synthesized perovskite and time-resolved fluorescence studies for understanding the charge carrier recombination processes. I also used steady-state PL spectroscopy, X-ray diffraction, scanning electron microscopy, and energy-dispersive x-ray diffraction to characterize the perovskites. A single-particle imaging instrument was used to study electroluminescence blinking.

In chapter 3, I discuss the synthesis of $CsPbBr_3$, $FAPbBr_3$, and $FAPb(Br, I)_3$ perovskite pellets using a pressure-induced solid-state method. These polycrystalline perovskite pellets showed photoluminescence and bandgap features similar to that of solution-processed perovskites. The time-resolved photoluminescence studies also reveal PL lifetime comparable to that of solution-processed ones. An attempt was made to use the perovskite pellets prepared by this method as an emitting layer in an electroluminescent

device. However, the thickness of the synthesized perovskite couldn't be optimized for LED applications. The existence of distributed band gaps within these perovskites encouraged me to study the role of nonradiative energy transfer in photon recycling in these thick perovskite pellets. I found that nonradiative energy transfer plays a dominant role in photon recycling.

In chapter 4, I discuss the synthesis of $MAPbBr_3$ perovskite microcrystals using AVC and ITC methods. I observed electroluminescence blinking from single perovskite microcrystals. The electrically excited $MAPbBr_3$ showed EL spectral and intensity fluctuations. The presence of multiple emitting centers in a large $MAPbBr_3$ microcrystal also resulted in EL blinking phenomenon. Statistical analyses were performed using the information obtained from the EL trajectories collected from an ensemble of microcrystals as well as the individual emitting centers within a microcrystal. Based on the observation of a truncated power-law behavior for ON- and OFF-time probability for individual emitting centers within a perovskite crystal, I assign the type-A EL blinking mechanism involving the charging and discharging process. On the other hand, the ensemble of microcrystals showed a linear power-law behavior which I assign as type-B EL blinking behavior as a result of the charge trapping-de-trapping processes. Here, the switching of quenching and emitting sites is assisted by the migrating traps, which are usually the halide vacancies.

In chapter 5, I discuss the role of halide vacancies in EL blinking. For this, I synthesize $MAPbBr_3$ microcrystals of varying bromide composition, namely using under-stoichiometric, stoichiometric, and over-stoichiometric precursor solution by simply changing the precursor concentration ratio (MABr: $PbBr_2$) and study the EL blinking from them. An under-stoichiometric $MAPbBr_3$ sample showed a linear-power-law behavior for ON- and OFF-time probabilities which is a signature of the trapping-de-trapping mechanism for EL blinking. The presence of halide vacancies in an under-stoichiometric perovskite sample is the reason for type-B EL blinking. But upon changing the sample to stoichiometric and over stoichiometric ratio, the blinking behavior changes to type-A. Such a change is associated with the filling of halide vacancies with the EL blinking taking the charging-discharging route. PL lifetime studies and EDS studies support the proposed EL blinking mechanism.

Finally, I summarized my studies and provided future perspectives of the current work.

## References


1. Paufler, P. Structure of Materials. An Introduction to Crystallography, Diffraction and Symmetry. By Marc De Graef and Michael E. McHenry. Pp. Xxxi+844. Cambridge: Cambridge University Press. 3rd Printing, 2010. Price (Hardback) USD 118.00. ISBN: 978-0521651516. *Acta Crystallogr. Sect. A Found. Crystallogr.* **2012**, *68*, 523–523.

2. MØLLER, C. K. Crystal Structure and Photoconductivity of Cæsium Plumbohalides. *Nature* **1958**, *182*, 1436–1436.

3. Manser, J. S.; Christians, J. A.; Kamat, P. V. Intriguing Optoelectronic Properties of Metal Halide Perovskites. *Chem. Rev.* **2016**, *116*, 12956–13008.

4. Bartel, C. J.; Sutton, C.; Goldsmith, B. R.; Ouyang, R.; Musgrave, C. B.; Ghiringhelli, L. M.; Scheffler, M. New Tolerance Factor to Predict the Stability of Perovskite Oxides and Halides. *Sci. Adv.* **2019**, *5* (2), eaav0693.

5. Kojima, A.; Teshima, K.; Shirai, Y.; Miyasaka, T. Organometal Halide Perovskites as Visible-Light Sensitizers for Photovoltaic Cells. *J. Am. Chem. Soc.* **2009**, *131*, 6050–6051.

6. NREL 2021 PCE Efficiency Chart

7. Tan, Z.-K.; Moghaddam, R. S.; Lai, M. L.; Docampo, P.; Higler, R.; Deschler, F.; Price, M.; Sadhanala, A.; Pazos, L. M.; Credgington, D.; Hanusch, F.; Bein, T.; Snaith, H. J.; Friend, R. H. Bright Light-Emitting Diodes Based on Organometal Halide Perovskite. *Nat. Nanotechnol.* **2014**, *9*, 687–692.

8. Xiao, Z.; Kerner, R. A.; Zhao, L.; Tran, N. L.; Lee, K. M.; Koh, T.-W.; Scholes, G. D.; Rand, B. P. Efficient Perovskite Light-Emitting Diodes Featuring Nanometre-Sized Crystallites. *Nat. Photonics* **2017**, *11*, 108–115.

9. Cao, Y.; Wang, N.; Tian, H.; Guo, J.; Wei, Y.; Chen, H.; Miao, Y.; Zou, W.; Pan, K.; He, Y.; Cao, H.; Ke, Y.; Xu, M.; Wang, Y.; Yang, M.; Du, K.; Fu, Z.; Kong, D.; Dai, D.; Jin, Y.; Li, G.; Li, H.; Peng, Q.; Wang, J.; Huang, W. Perovskite Light-Emitting Diodes Based on Spontaneously Formed Submicrometre-Scale Structures. *Nature* **2018**, *562*, 249–253.

10. Chiba, T.; Hayashi, Y.; Ebe, H.; Hoshi, K.; Sato, J.; Sato, S.; Pu, Y.-J.; Ohisa, S.; Kido, J. Anion-Exchange Red Perovskite Quantum Dots with Ammonium Iodine Salts for Highly Efficient Light-Emitting Devices. *Nat. Photonics* **2018**, *12*, 681–687.

11. Zhao, B.; Bai, S.; Kim, V.; Lamboll, R.; Shivanna, R.; Auras, F.; Richter, J. M.; Yang, L.; Dai, L.; Alsari, M.; She, X.-J.; Liang, L.; Zhang, J.; Lilliu, S.; Gao, P.; Snaith, H. J.; Wang, J.; Greenham, N. C.; Friend, R. H.; Di, D. High-Efficiency Perovskite–Polymer Bulk Heterostructure Light-Emitting Diodes. *Nat. Photonics* **2018**, *12*, 783–789.

12. Sutherland, B. R.; Sargent, E. H. Perovskite Photonic Sources. *Nat. Photonics* **2016**, *10*, 295–302.

13. Zhu, H.; Fu, Y.; Meng, F.; Wu, X.; Gong, Z.; Ding, Q.; Gustafsson, M. V.; Trinh, M. T.; Jin, S.; Zhu, X.-Y. Lead Halide Perovskite Nanowire Lasers with Low Lasing Thresholds and High Quality Factors. *Nat. Mater.* **2015**, *14*, 636–642.

14. Senocrate, A.; Kim, G. Y.; Grätzel, M.; Maier, J. Thermochemical Stability of Hybrid Halide Perovskites. *ACS Energy Lett.* **2019**, *4* (12), 2859–2870.

15. Kim, Y.-H.; Kim, S.; Jo, S. H.; Lee, T.-W. Metal Halide Perovskites: From Crystal Formations to Light-Emitting-Diode Applications. *Small Methods* **2018**, *2*, 1800093.

16. Shi, D.; Adinolfi, V.; Comin, R.; Yuan, M.; Alarousu, E.; Buin, A.; Chen, Y.; Hoogland, S.; Rothenberger, A.; Katsiev, K.; Losovyj, Y.; Zhang, X.; Dowben, P. A.; Mohammed, O. F.; Sargent, E. H.; Bakr, O. M. Low Trap-State Density and Long Carrier Diffusion in Organolead Trihalide Perovskite Single Crystals. *Science* **2015**, *347*, 519–522.

17. Liao, Q.; Hu, K.; Zhang, H.; Wang, X.; Yao, J.; Fu, H. Perovskite Microdisk Microlasers Self-Assembled from Solution. *Adv. Mater.* **2015**, *27*, 3405–3410.

18. Saidaminov, M. I.; Abdelhady, A. L.; Maculan, G.; Bakr, O. M. Retrograde Solubility of Formamidinium and Methylammonium Lead Halide Perovskites Enabling Rapid Single Crystal Growth. *Chem. Commun.* **2015**, *51*, 17658–17661.

19. Saidaminov, M. I.; Abdelhady, A. L.; Murali, B.; Alarousu, E.; Burlakov, V. M.; Peng, W.; Dursun, I.; Wang, L.; He, Y.; Maculan, G.; Goriely, A.; Wu, T.; Mohammed, O. F.; Bakr, O. M. High-Quality Bulk Hybrid Perovskite Single Crystals within Minutes by Inverse Temperature Crystallization. *Nat. Commun.* **2015**, *6*, 7586.

20. Dirin, D. N.; Cherniukh, I.; Yakunin, S.; Shynkarenko, Y.; Kovalenko, M. V. Solution-Grown $CsPbBr_3$ Perovskite Single Crystals for Photon Detection. *Chem. Mater.* **2016**, *28*, 8470–8474.

21. Protesescu, L.; Yakunin, S.; Bodnarchuk, M. I.; Krieg, F.; Caputo, R.; Hendon, C. H.; Yang, R. X.; Walsh, A.; Kovalenko, M. V. Nanocrystals of Cesium Lead Halide Perovskites ($CsPbX_3$, X = Cl, Br, and I): Novel Optoelectronic Materials Showing Bright Emission with Wide Color Gamut. *Nano Lett.* **2015**, *15*, 3692–3696.

22. Schmidt, L. C.; Pertegás, A.; González-Carrero, S.; Malinkiewicz, O.; Agouram, S.; Mínguez Espallargas, G.; Bolink, H. J.; Galian, R. E.; Pérez-Prieto, J. Nontemplate Synthesis of $CH_3NH_3PbBr_3$ Perovskite Nanoparticles. *J. Am. Chem. Soc.* **2014**, *136*, 850–853.

23. Zhang, F.; Zhong, H.; Chen, C.; Wu, X.; Hu, X.; Huang, H.; Han, J.; Zou, B.; Dong, Y. Brightly Luminescent and Color-Tunable Colloidal $CH_3NH_3PbX_3$ (X = Br, I, Cl) Quantum Dots: Potential Alternatives for Display Technology. *ACS Nano* **2015**, *9*, 4533–4542.

24. Dunlap-Shohl, W. A.; Zhou, Y.; Padture, N. P.; Mitzi, D. B. Synthetic Approaches for Halide Perovskite Thin Films. *Chem. Rev.* **2019**, *119*, 3193–3295.

25. Pan, Q.; Hu, H.; Zou, Y.; Chen, M.; Wu, L.; Yang, D.; Yuan, X.; Fan, J.; Sun, B.; Zhang, Q. Microwave-Assisted Synthesis of High-Quality "All-Inorganic" CsPbX3 (X = Cl, Br, I) Perovskite Nanocrystals and Their Application in Light Emitting Diodes. *J. Mater. Chem. C* **2017**, *5*, 10947–10954.

26. Jang, D. M.; Kim, D. H.; Park, K.; Park, J.; Lee, J. W.; Song, J. K. Ultrasound Synthesis of Lead Halide Perovskite Nanocrystals. *J. Mater. Chem. C* **2016**, *4*, 10625–10629.

27. Zhu, Z. Y.; Yang, Q. Q.; Gao, L. F.; Zhang, L.; Shi, A. Y.; Sun, C. L.; Wang, Q.; Zhang, H. L. Solvent-Free Mechanosynthesis of Composition-Tunable Cesium Lead Halide Perovskite Quantum Dots. *J. Phys. Chem. Lett.* **2017**, *8*, 1610–1614.

28. Protesescu, L.; Yakunin, S.; Nazarenko, O.; Dirin, D. N.; Kovalenko, M. V. Low-Cost Synthesis of Highly Luminescent Colloidal Lead Halide Perovskite Nanocrystals by Wet Ball Milling. *ACS Appl. Nano Mater.* **2018**, *1*, 1300–1308.

29. Karmakar, A.; Askar, A. M.; Bernard, G. M.; Terskikh, V. V.; Ha, M.; Patel, S.; Shankar, K.; Michaelis, V. K. Mechanochemical Synthesis of Methylammonium Lead Mixed-Halide Perovskites: Unraveling the Solid-Solution Behavior Using Solid-State NMR. *Chem. Mater.* **2018**, *30*, 2309–2321.

30. Pal, P.; Saha, S.; Banik, A.; Sarkar, A.; Biswas, K. All-Solid-State Mechanochemical Synthesis and Post-Synthetic Transformation of Inorganic Perovskite-Type Halides. *Chem. - A Eur. J.* **2018**, *24*, 1811–1815.

31. Ghimire, S.; Takahashi, K.; Takano, Y.; Nakamura, T.; Biju, V. Photon Recycling by Energy Transfer in Piezochemically Synthesized and Close-Packed Methylammonium Lead Halide Perovskites. *J. Phys. Chem. C* **2019**, *123*, 27752–27758.

32. Bhagyalakshmi, S. B.; Ghimire, S.; Takahashi, K.; Yuyama, K. ichi; Takano, Y.; Nakamura, T.; Biju, V. Nonradiative Energy Transfer through Distributed Bands in Piezochemically Synthesized Cesium and Formamidinium Lead Halide Perovskites. *Chem. - A Eur. J.* **2020**, *26*, 2133–2137.

33. Koutselas, I. B.; Ducasse, L.; Papavassiliou, G. C. Electronic Properties of Three- and Low-Dimensional Semiconducting Materials with Pb Halide and Sn Halide Units. *J. Phys. Condens. Matter* **1996**, *8*, 1217–1227.

34. Amat, A.; Mosconi, E.; Ronca, E.; Quarti, C.; Umari, P.; Nazeeruddin, M. K.; Grätzel, M.; De Angelis, F. Cation-Induced Band-Gap Tuning in Organohalide Perovskites: Interplay of Spin–Orbit Coupling and Octahedra Tilting. *Nano Lett.* **2014**, *14*, 3608–3616.

35. Stoumpos, C. C.; Kanatzidis, M. G. The Renaissance of Halide Perovskites and Their Evolution as Emerging Semiconductors. *Acc. Chem. Res.* **2015**, *48*, 2791–2802.

36. Herz, L. M. Charge-Carrier Dynamics in Organic-Inorganic Metal Halide Perovskites. *Annu. Rev. Phys. Chem.* **2016**, *67*, 65–89.

37. Jin, H.; Debroye, E.; Keshavarz, M.; Scheblykin, I. G.; Roeffaers, M. B. J.; Hofkens, J.; Steele, J. A. It's a Trap! On the Nature of Localised States and Charge Trapping in Lead Halide Perovskites. *Mater. Horizons* **2020**, *7*, 397–410.

38. Ball, J. M.; Petrozza, A. Defects in Perovskite-Halides and Their Effects in Solar Cells. *Nat. Energy* **2016**, *1*, 16149.

39. Kovalenko, M. V.; Protesescu, L.; Bodnarchuk, M. I. Properties and Potential Optoelectronic Applications of Lead Halide Perovskite Nanocrystals. *Science* **2017**, *358*, 745–750.

40. Guo, D.; Andaji Garmaroudi, Z.; Abdi-Jalebi, M.; Stranks, S. D.; Savenije, T. J. Reversible Removal of Intermixed Shallow States by Light Soaking in Multication Mixed Halide Perovskite Films. *ACS Energy Lett.* **2019**, *4*, 2360–2367.

41. Wang, F.; Bai, S.; Tress, W.; Hagfeldt, A.; Gao, F. Defects Engineering for High-Performance Perovskite Solar Cells. *npj Flex. Electron.* **2018**, *2*, 22.

42. Ye, S.; Rao, H.; Zhao, Z.; Zhang, L.; Bao, H.; Sun, W.; Li, Y.; Gu, F.; Wang, J.; Liu, Z.; Bian, Z.; Huang, C. A Breakthrough Efficiency of 19.9% Obtained in Inverted Perovskite Solar Cells by Using an Efficient Trap State Passivator Cu(Thiourea)I. *J. Am. Chem. Soc.* **2017**, *139*, 7504–7512.

43. Zhou, Y.; Wang, F.; Cao, Y.; Wang, J.-P.; Fang, H.-H.; Loi, M. A.; Zhao, N.; Wong, C.-P. Benzylamine-Treated Wide-Bandgap Perovskite with High Thermal-Photostability and Photovoltaic Performance. *Adv. Energy Mater.* **2017**, *7*, 1701048.

44. Shockley, W.; Queisser, H. J. Detailed Balance Limit of Efficiency of P-n Junction Solar Cells. *J. Appl. Phys.* **1961**, *32*, 510–519.

45. Lee, M. M.; Teuscher, J.; Miyasaka, T.; Murakami, T. N.; Snaith, H. J. Efficient Hybrid Solar Cells Based on Meso-Superstructured Organometal Halide Perovskites. *Science* **2012**, *338*, 643–647.

46. Leijtens, T.; Bush, K. A.; Prasanna, R.; McGehee, M. D. Opportunities and Challenges for Tandem Solar Cells Using Metal Halide Perovskite Semiconductors. Nat. Energy **2018**, *3*, 828–838.

47. Werner, J.; Niesen, B.; Ballif, C. Perovskite/Silicon Tandem Solar Cells: Marriage of Convenience or True Love Story? – An Overview. *Adv. Mater. Interfaces* **2018**, *5*, 1700731.

48. Aydin, E.; Bastiani, M.; Wolf, S. Defect and Contact Passivation for Perovskite Solar Cells. *Adv. Mater.* **2019**, *31*, 1900428.

49. Jiang, Q.; Zhao, Y.; Zhang, X.; Yang, X.; Chen, Y.; Chu, Z.; Ye, Q.; Li, X.; Yin, Z.; You, J. Surface Passivation of Perovskite Film for Efficient Solar Cells. *Nat. Photonics* **2019**, *13*, 460–466.

50. Choi, H.; Jeong, J.; Kim, H.-B.; Kim, S.; Walker, B.; Kim, G.-H.; Kim, J. Y. Cesium-Doped Methylammonium Lead Iodide Perovskite Light Absorber for Hybrid Solar Cells. *Nano Energy* **2014**, *7*, 80–85.

51. Snaith, H. J.; Abate, A.; Ball, J. M.; Eperon, G. E.; Leijtens, T.; Noel, N. K.; Stranks, S. D.; Wang, J. T.-W.; Wojciechowski, K.; Zhang, W. Anomalous Hysteresis in Perovskite Solar Cells. *J. Phys. Chem. Lett.* **2014**, *5*, 1511–1515.

52. Shao, Y.; Xiao, Z.; Bi, C.; Yuan, Y.; Huang, J. Origin and Elimination of Photocurrent Hysteresis by Fullerene Passivation in $CH_3NH_3PbI_3$ Planar Heterojunction Solar Cells. *Nat. Commun.* **2014**, *5*, 5784.

53. Cho, H.; Kim, Y.-H.; Wolf, C.; Lee, H.-D.; Lee, T.-W. Improving the Stability of Metal Halide Perovskite Materials and Light-Emitting Diodes. *Adv. Mater.* **2018**, *30*, 1704587.

54. Lv, W.; Li, L.; Xu, M.; Hong, J.; Tang, X.; Xu, L.; Wu, Y.; Zhu, R.; Chen, R.; Huang, W. Improving the Stability of Metal Halide Perovskite Quantum Dots by Encapsulation. *Adv. Mater.* **2019**, *31*, 1900682.

55. Wozny, S.; Yang, M.; Nardes, A. M.; Mercado, C. C.; Ferrere, S.; Reese, M. O.; Zhou, W.; Zhu, K. Controlled Humidity Study on the Formation of Higher Efficiency Formamidinium Lead Triiodide-Based Solar Cells. *Chem. Mater.* **2015**, *27*, 4814–4820.

56. Wei, Z.; Xing, J. The Rise of Perovskite Light-Emitting Diodes. *J. Phys. Chem. Lett.* **2019**, *10*, 3035–3042.

57. Hong, X.; Ishihara, T.; Nurmikko, A. V. Photoconductivity and Electroluminescence in Lead Iodide Based Natural Quantum Well Structures. *Solid State Commun.* **1992**, *84*, 657–661.

58. Era, M.; Morimoto, S.; Tsutsui, T.; Saito, S. Organic-inorganic Heterostructure Electroluminescent Device Using a Layered Perovskite Semiconductor $(C_6H_5C_2H_4NH_3)_2PbI_4$. *Appl. Phys. Lett.* **1994**, *65*, 676–678.

59. Hattori, T.; Taira, T.; Era, M.; Tsutsui, T.; Saito, S. Highly Efficient Electroluminescence from a Heterostructure Device Combined with Emissive Layered-Perovskite and an Electron-Transporting Organic Compound. *Chem. Phys. Lett.* **1996**, *254*, 103–108.

60. Jeon, N. J.; Noh, J. H.; Kim, Y. C.; Yang, W. S.; Ryu, S.; Seok, S. Il. Solvent Engineering for High-Performance Inorganic–Organic Hybrid Perovskite Solar Cells. *Nat. Mater.* **2014**, *13*, 897–903.

61. You, J.; Yang, Y. (Michael); Hong, Z.; Song, T.-B.; Meng, L.; Liu, Y.; Jiang, C.; Zhou, H.; Chang, W.-H.; Li, G.; Yang, Y. Moisture Assisted Perovskite Film Growth for High Performance Solar Cells. *Appl. Phys. Lett.* **2014**, *105*, 183902.

62. Deng, W.; Fang, H.; Jin, X.; Zhang, X.; Zhang, X.; Jie, J. Organic–Inorganic Hybrid Perovskite Quantum Dots for Light-Emitting Diodes. *J. Mater. Chem. C* **2018**, *6*, 4831–4841.

63. Eaton, S. W.; Lai, M.; Gibson, N. A.; Wong, A. B.; Dou, L.; Ma, J.; Wang, L. W.; Leone, S. R.; Yang, P. Lasing in Robust Cesium Lead Halide Perovskite Nanowires. *Proc. Natl. Acad. Sci. U. S. A.* **2016**, *113*, 1993–1998.

64. Jia, Y.; Kerner, R. A.; Grede, A. J.; Rand, B. P.; Giebink, N. C. Continuous-Wave Lasing in an Organic-Inorganic Lead Halide Perovskite Semiconductor. *Nat. Photonics* **2017**, *11*, 784–788.

65. Du, W.; Zhang, S.; Shi, J.; Chen, J.; Wu, Z.; Mi, Y.; Liu, Z.; Li, Y.; Sui, X.; Wang, R.; Qiu, X.; Wu, T.; Xiao, Y.; Zhang, Q.; Liu, X. Strong Exciton-Photon Coupling and Lasing Behavior in All-Inorganic $CsPbBr_3$ Micro/Nanowire Fabry-Pérot Cavity. *ACS Photonics* **2018**, *5*, 2051–2059.

66. Jiang, L.; Liu, R.; Su, R.; Yu, Y.; Xu, H.; Wei, Y.; Zhou, Z. K.; Wang, X. Continuous Wave Pumped Single-Mode Nanolasers in Inorganic Perovskites with Robust Stability and High Quantum Yield. *Nanoscale* **2018**, *10*, 13565–13571.

67. Makarov, S.; Furasova, A.; Tiguntseva, E.; Hemmetter, A.; Berestennikov, A.; Pushkarev, A.; Zakhidov, A.; Kivshar, Y. Halide-Perovskite Resonant Nanophotonics. *Adv. Opt. Mater.* **2019**, *7*, 1–19.

68. Wang, H.; Kim, D. H. Perovskite-Based Photodetectors: Materials and Devices. *Chem. Soc. Rev.* **2017**, *46*, 5204–5236.

69. Zhang, F.; Yang, B.; Zheng, K.; Yang, S.; Li, Y.; Deng, W.; He, R. Formamidinium Lead Bromide ($FAPbBr_3$) Perovskite Microcrystals for Sensitive and Fast Photodetectors. *Nano-Micro Lett.* **2018**, *10*, 1–8.

70. Zhu, Z.; Sun, Q.; Zhang, Z.; Dai, J.; Xing, G.; Li, S.; Huang, X.; Huang, W. Metal Halide Perovskites: Stability and Sensing-Ability. *J. Mater. Chem. C* **2018**, *6*, 10121–10137.

71. Nirmal, M.; Dabbousi, B. O.; Bawendi, M. G.; Macklin, J. J.; Trautman, J. K.; Harris, T. D.; Brus, L. E. Fluorescence Intermittency in Single Cadmium Selenide Nanocrystals. *Nature* **1996**, *383*, 802–804.

72. Galland, C.; Ghosh, Y.; Steinbrück, A.; Sykora, M.; Hollingsworth, J. A.; Klimov, V. I.; Htoon, H. Two Types of Luminescence Blinking Revealed by Spectroelectrochemistry of Single Quantum Dots. *Nature* **2011**, *479*, 203–207.

73. Efros, A. L.; Nesbitt, D. J. Origin and Control of Blinking in Quantum Dots. *Nat. Nanotechnol.* **2016**, *11*, 661–671.

74. Peterson, J. J.; Nesbitt, D. J. Modified Power Law Behavior in Quantum Dot Blinking: A Novel Role for Biexcitons and Auger Ionization. *Nano Lett.* **2009**, *9*, 338–345.

75. Ye, M.; Searson, P. C. Blinking in Quantum Dots: The Origin of the Grey State and Power Law Statistics. *Phys. Rev. B* **2011**, *84*, 125317.

76. Tian, Y.; Merdasa, A.; Peter, M.; Abdellah, M.; Zheng, K.; Ponseca, C. S.; Pullerits, T.; Yartsev, A.; Sundström, V.; Scheblykin, I. G. Giant Photoluminescence Blinking of Perovskite Nanocrystals Reveals Single-Trap Control of Luminescence. *Nano Lett.* **2015**, *15*, 1603–1608.

77. Zhu, F.; Men, L.; Guo, Y.; Zhu, Q.; Bhattacharjee, U.; Goodwin, P. M.; Petrich, J. W.; Smith, E. A.; Vela, J. Shape Evolution and Single Particle Luminescence of Organometal Halide Perovskite Nanocrystals. *ACS Nano* **2015**, *9*, 2948–2959.

78. Wen, X.; Ho-Baillie, A.; Huang, S.; Sheng, R.; Chen, S.; Ko, H. C.; Green, M. A. Mobile Charge-Induced Fluorescence Intermittency in Methylammonium Lead Bromide Perovskite. *Nano Lett.* **2015**, *15*, 4644–4649.

79. Tachikawa, T.; Karimata, I.; Kobori, Y. Surface Charge Trapping in Organolead Halide Perovskites Explored by Single-Particle Photoluminescence Imaging. *J. Phys. Chem. Lett.* **2015**, *6*, 3195–3201.

80. Park, Y. S.; Guo, S.; Makarov, N. S.; Klimov, V. I. Room Temperature Single-Photon Emission from Individual Perovskite Quantum Dots. *ACS Nano* **2015**, *9*, 10386–10393.

81. Yuan, H.; Debroye, E.; Caliandro, G.; P. F. Janssen, K.; van Loon, J.; E. A. Kirschhock, C.; A. Martens, J.; Hofkens, J.; B. J. Roeffaers, M. Photoluminescence Blinking of Single-Crystal Methylammonium Lead Iodide Perovskite Nanorods Induced by Surface Traps. *ACS Omega* **2016**, *1*, 148–159.

82. Trinh, C. T.; Minh, D. N.; Ahn, K. J.; Kang, Y.; Lee, K. G. Organic-Inorganic FAPbBr 3 Perovskite Quantum Dots as a Quantum Light Source: Single-Photon Emission and Blinking Behaviors. *ACS Photonics* **2018**, *5*, 4937–4943.

83. Seth, S.; Ahmed, T.; Samanta, A. Photoluminescence Flickering and Blinking of Single $CsPbBr_3$ Perovskite Nanocrystals: Revealing Explicit Carrier Recombination Dynamics. *J. Phys. Chem. Lett.* **2018**, *9*, 7007–7014.

84. Merdasa, A.; Tian, Y.; Camacho, R.; Dobrovolsky, A.; Debroye, E.; Unger, E. L.; Hofkens, J.; Sundström, V.; Scheblykin, I. G. "supertrap" at Work: Extremely Efficient Nonradiative Recombination Channels in $MAPbI_3$ Perovskites Revealed by Luminescence Super-Resolution Imaging and Spectroscopy. *ACS Nano* **2017**, *11*, 5391–5404.

85. Gibson, N. A.; Koscher, B. A.; Alivisatos, A. P.; Leone, S. R. Excitation Intensity Dependence of Photoluminescence Blinking in $CsPbBr_3$ Perovskite Nanocrystals. *J. Phys. Chem. C* **2018**, *122*, 12106–12113.

86. Gerhard, M.; Louis, B.; Camacho, R.; Merdasa, A.; Li, J.; Kiligaridis, A.; Dobrovolsky, A.; Hofkens, J.; Scheblykin, I. G. Microscopic Insight into Non-Radiative Decay in Perovskite Semiconductors from Temperature-Dependent Luminescence Blinking. *Nat. Commun.* **2019**, *10*, 1–12.

87. Galisteo-López, J. F.; Calvo, M. E.; Rojas, T. C.; Míguez, H. Mechanism of Photoluminescence Intermittency in Organic–Inorganic Perovskite Nanocrystals. *ACS Appl. Mater. Interfaces* **2019**, *11*, 6344–6349.

88. Yarita, N.; Tahara, H.; Saruyama, M.; Kawawaki, T.; Sato, R.; Teranishi, T.; Kanemitsu, Y. Impact of Postsynthetic Surface Modification on Photoluminescence Intermittency in Formamidinium Lead Bromide Perovskite Nanocrystals. *J. Phys. Chem. Lett.* **2017**, *8*, 6041–6047.

89. Tang, X.; Yang, J.; Li, S.; Liu, Z.; Hu, Z.; Hao, J.; Du, J.; Leng, Y.; Qin, H.; Lin, X.; Lin, Y.; Tian, Y.; Zhou, M.; Xiong, Q. Single Halide Perovskite/Semiconductor Core/Shell Quantum Dots with Ultrastability and Nonblinking Properties. *Adv. Sci.* **2019**, *6*, 1900412.

90. Rainoì, G.; Nedelcu, G.; Protesescu, L.; Bodnarchuk, M. I.; Kovalenko, M. V.; Mahrt, R. F.; Stöferle, T. Single Cesium Lead Halide Perovskite Nanocrystals at Low Temperature: Fast Single-Photon Emission, Reduced Blinking, and Exciton Fine Structure. *ACS Nano* **2016**, *10*, 2485–2490.

91. Zhang, A.; Dong, C.; Ren, J. Tuning Blinking Behavior of Highly Luminescent Cesium Lead Halide Nanocrystals through Varying Halide Composition. *J. Phys. Chem. C* **2017**, *121*, 13314–13323.

92. Nguyen, V. C.; Katsuki, H.; Sasaki, F.; Yanagi, H. Single-Crystal Perovskite $CH_3NH_3PbBr_3$ Prepared by Cast Capping Method for Light-Emitting Diodes. *Jpn. J. Appl. Phys.* **2018**, *57*, 04FL10.

93. Sharma, D. K.; Hirata, S.; Vacha, M. Single-Particle Electroluminescence of $CsPbBr_3$ Perovskite Nanocrystals Reveals Particle-Selective Recombination and Blinking as Key Efficiency Factors. *Nat. Commun.* **2019**, *10*, 4499.

# Chapter 2

# Experiments

**Abstract**

This chapter consolidates different experimental methods used for synthesizing the perovskite materials, characterization using various spectroscopic techniques and instrumentation, and the basic principles relating to them. I utilized various crystallization techniques to synthesize lead halide perovskite as nanocrystals and microcrystals. A pressure-induced solid-state synthesis was used to prepare perovskite pellets. These perovskites were used as such or in the form of films or solutions for studying their properties. For electroluminescence blinking-related studies, an LED device was fabricated. The physical properties of perovskite like absorption, emission, and bandgap were estimated using UV-visible absorption spectroscopy, steady-state fluorescence spectroscopy, and diffuse reflectance spectroscopy, respectively. The morphology of perovskite was studied using scanning electron microscopy. The crystal phase of perovskite was studied using powder and single-crystal X-ray diffraction spectroscopy. Elemental mapping studies were performed using energy-dispersive X-ray spectroscopy. Fluorescence blinking studies were performed using single-molecule imaging and microspectroscopy. To understand the charge carrier dynamics under photoexcitation, time-resolved fluorescence spectroscopy equipped with an ultrafast pulsed laser and LED systems working in the range of femtosecond to nanosecond time resolution, was used.

## 2.1 Materials

I used the following chemicals and materials for my studies. Cesium bromide (CsBr, >90.0%, Tokyo chemical Industry (TCI)), lead bromide ($PbBr_2$, ≥ 98%, Aldrich), formamidinium lead bromide (FABr, > 98%, TCI), lead iodide ($PbI_2$, >99%, Aldrich), methylammonium bromide ($CH_3NH_3Br$, >98%, Tokyo Chemical Industry (TCI)), *N*-cyclohexyl-2-pyrrolidone (CHP) (98%, Aldrich), deoxidised *N*,*N*-dimethylformamide (DMF), (FUJIFILM Wako Pure chemical Corporation (WAKO)), dichloromethane (DCM,WAKO), hexadecyl amine ($C_{16}H_{35}N$, >95%, TCI), hexadecene ($C_{16}H_{32,}$ >90%, TCI), oleic acid ($C_{18}H_{34}O_2$, >85%, TCI), cesium acetate ( $CH_3COOCs$, 99.9%, Aldrich), hexane (WAKO), cesium carbonate ($CsCO_3$, 99%, Aldrich), octadecene ($C_{18}H_{36}$, > 90% TCI), oleylamine ($C_{18}H_{37}N$, >50%, TCI), isopropanol ($C_3H_8O$, 99.7%, WAKO), toluene (99.5%, WAKO), PEDOT: PSS ((3,4-ethylenedioxythiophene)- poly(styrene sulphonate), 1.3 wt% dispersion in water, Aldrich), PEDOT: PSS (3,4-ethylenedioxythiophene)-poly (styrene sulphonate) (HTL Solar 3, Ossila), 1-butanol (99%, WAKO), methanol (99.8 %, WAKO), ITO-coated glass (surface resistivity 15-25 Ω/sq. slide, Aldrich), and cover glass (Matsunami Neo Cover Glass, 25 x 50 $mm^2$, thickness 0.13- 0.17 mm). The ITO-coated glass substrates were used after cleaning with water, isopropanol, and acetone in batches, and finally with water and dried. All the other chemicals were used as such or after drying it under an inert atmosphere.

## 2.2 Samples

### 2.2.1 Pressure-induced solid-state synthesis of perovskite pellets

#### Synthesis of $CsPbBr_3$ and $FAPbBr_3$ perovskites

Perovskite precursor salts were weighed and mixed in a definite ratio. A 1:1.25 mol ratio of CsBr and $PbBr_2$ was used for synthesizing $CsPbBr_3$ perovskite, and a 1.25:1.35 mol ratio of FABr and $PbBr_2$ for $FAPbBr_3$ perovskite. Using a hand mortar, the precursor salts were ground and was transferred to a glass vial. By flipping the vial upside down for some minutes, the salts were mixed homogenously. A silicon rubber chamber with a diameter of 20 mm was prepared. The precursor salt mixture was transferred to this chamber. Using a hydraulic press machine, 2.4 GPa pressure was applied over this solid solution for 30 minutes. After releasing the pressure, the formed perovskite pellet was carefully removed from the chamber and was stored in air-tight containers.

**Synthesis of the $FAPb(BrI)_3$ perovskite pellet**

FABr, $PbBr_2$ and $PbI_2$ salts were weighed (0.75 mmol, 0.75 mmol, 0.25 mmol respectively). The salts were ground in a hand mortar separately before being mixed. After transferring to a silicon chamber, a pressure of 2.4 GPa was applied over this precursor salt mixture for 30 minutes. After the release of pressure, $FAPb(BrI)_3$ perovskite pellet was formed. The pellet was stored in air-tight containers to prevent degradation. A scheme of the above synthesis is shown below:

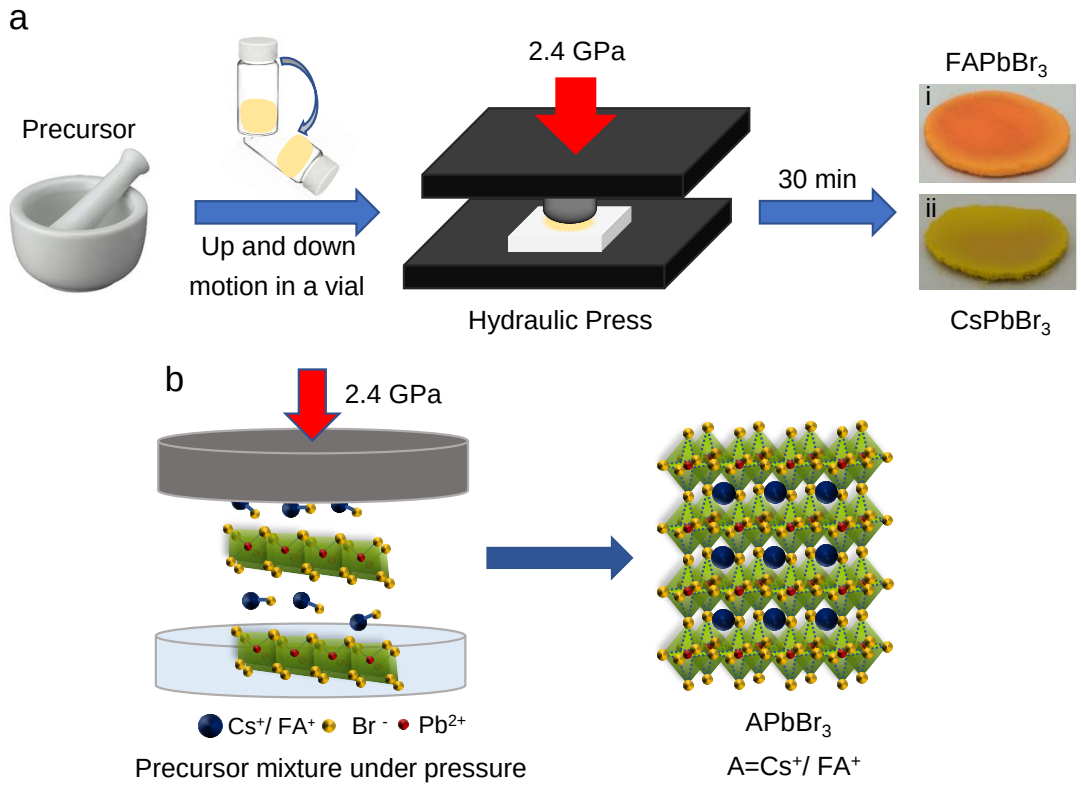


**Figure 1.** A scheme showing the synthesis of perovskite pellets by the pressure-induced solid-state method.[7]

**2.2.2 Antisolvent vapor-assisted crystallization method (AVC)**

The microcrystals were prepared following the method developed by Schmidt *et al.*[1] $PbBr_2$ (690 mg), and MABr (210 mg) was weighed and dissolved in 5 mL DMF separately. 1 mL was taken from each of these solutions and mixed to get the precursor solution. 100 µL of this precursor solution was dropped on an ITO glass placed on a silicon stage inside a glass chamber. The glass chamber was prefilled with an antisolvent for perovskite, DCM to a level just below the stage. The crystals nucleated immediately and grew overnight. Perovskite microcrystals of size 40- 150 µm were formed by this

method. By controlling the time of growth or concentration of precursor solution, we can control the size of the crystals formed. The scheme for synthesis is shown in Figure 2.

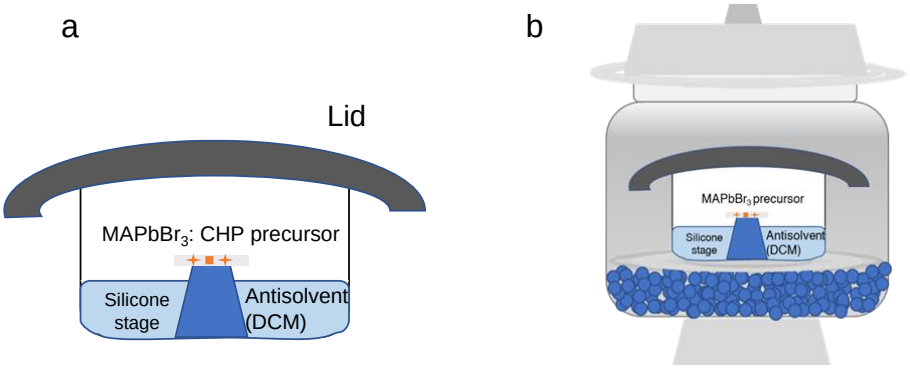


**Figure 2.** Schemes showing the synthesis of $MAPbBr_3$ microcrystals by antisolvent vapor-assisted crystallization, a) in an open environment, and b) inside a desiccator under a moisture-free environment.

### 2.2.3 Inverse temperature crystallization method (ITC)

$PbBr_2$ and MABr were weighed and dissolved in DMF to get a 0.01 M solution. It was supplemented with 5% (volume) of N-cyclohexyl-2-pyrrolidone (CHP), which was for controlling the crystal growth and size.[8] 2 µL of this solution was dropped on an ITO glass kept on a hot plate preheated to 200 °C. Within seconds, $MAPbBr_3$ microcrystals nucleated and grew to 10 µm sized crystals. Using a 1M precursor solution, larger microcrystals of 40 µm size could be obtained this way. Certain properties of the additive, like low vapor pressure, apolar ring, and a high boiling point was useful in controlling the kinetics of crystal growth and size of crystals. Figure 3 shows the scheme of perovskite microcrystal synthesis by the ITC method.

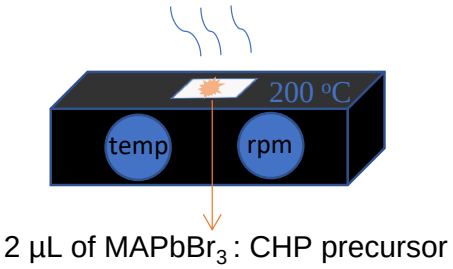


**Figure 3.** Scheme showing the synthesis of $MAPbBr_3$ microcrystals by inverse temperature crystallization (ITC) for smaller crystals.

The structure of CHP used as the additive during AVC and ITC methods for controlling the crystal sizes is shown below:

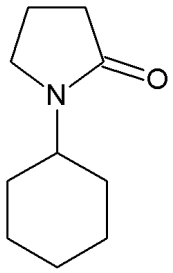


**Figure 4.** The structure of *N*-cyclohexyl-2-pyrrolidone (CHP) used as an additive to control the crystal size.

### 2.3 LED device fabrication

Chapters 4 and 5 of this thesis involves electroluminescence studies using perovskite. Perovskite microcrystals were used for electroluminescence studies. The microcrystals grown on one ITO glass were sandwiched with another ITO-coated glass substrate as shown in the figure. The LED was fabricated without using any charge transport layer. However, a polymer spacer is used to prevent short-circuiting. Figure 5 shows the scheme of the LED device fabrication for electroluminescence measurements.

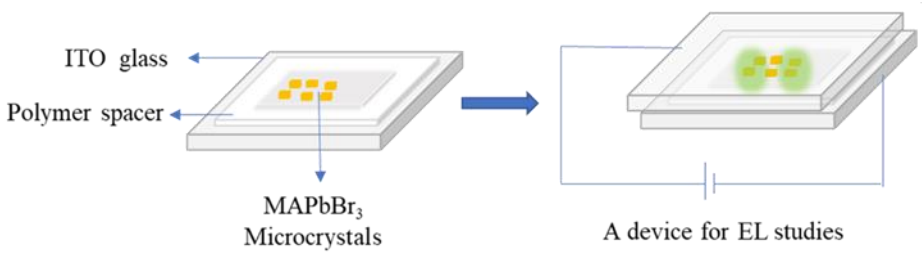


**Figure 5.** LED set up for microcrystal electroluminescence studies.

### 2.4 Methods

#### 2.4.1. UV-vis absorption and diffuse reflectance spectroscopy

Absorption and diffused reflectance studies were performed using Evolution 220 UV-visible spectrophotometer by ThermoScientific. The optical setup for absorption studies is shown in Figure 6 below:

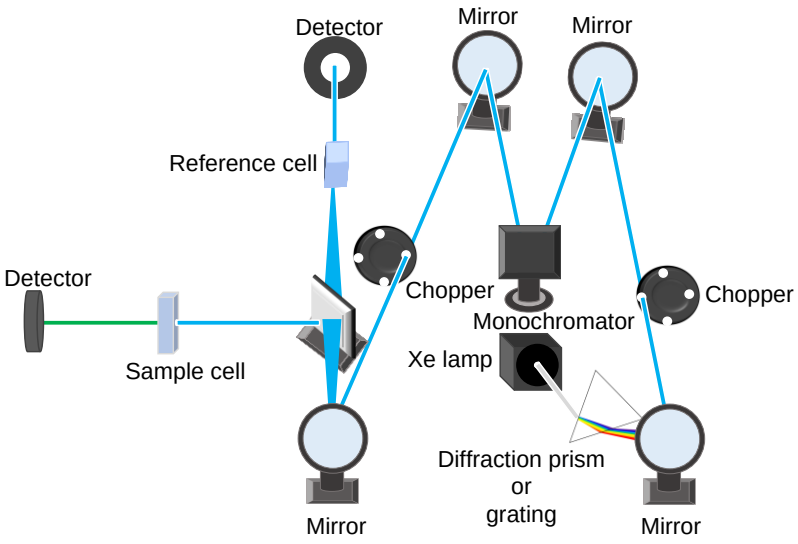


**Figure 6.** Schematic representation of optics inside the spectrophotometer.

The absorbance of material can be calculated by Beer-Lamberts law. Since the above method can be used only for dilute solutions with no scattering effects, solid samples are difficult to be characterized by this method. Hence, I used diffused reflectance spectroscopy (DRS) to study the bandgap features of my sample. The principle of DRS is discussed here.

Heterogeneous samples show a scattering of light in random directions shown below. This is called a diffused reflection of light, unlike a homogeneous sample that shows specular reflection.

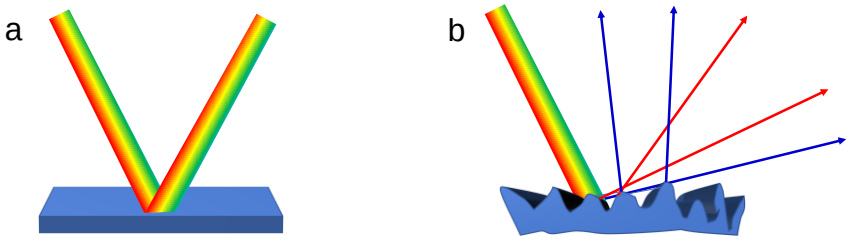


**Figure 7.** a) Specular reflection from a smooth and homogeneous surface, and b) diffuse reflectance from a heterogeneous surface.

To correlate the diffused reflectance with absorbance, two equations were used. One was developed by Tauc *et al.*[9] and later modified by Davis and Mott[10] which shows that absorption strength depends on the difference between photon energy and the bandgap as shown below:

$$(ahv)^{1/n} = A\,(hv - E_g) \qquad \text{( eq. 1)}$$

where h is the planks constant, ν is the frequency of light, α is the absorption coefficient, $E_g$ is the bandgap, and A is the proportionality constant. 1/n takes the value 1/2 for the direct allowed electronic transition. A plot of (αhν) vs hν is called a Tauc plot, and the extrapolation of the linear part of the curve to the x-axis will give the band gap value.

Another model was developed by Kubelka and Munk[11] to transform reflectance into absorbance. The equation for diffused reflectance developed by them is given as shown below:

$$R_\infty = 1 + \frac{k}{s} - \sqrt{\frac{k}{s}\left(2 + \frac{k}{s}\right)}$$

where k is the absorption coefficient of the sample and s is the scattering coefficient. This equation can be solved or k/s to give the K-M transform:

$$\frac{k}{s} = \frac{(1 - R_\infty)^2}{2R_\infty} = F(R_\infty)$$

The scattering coefficient, s, is considered a constant since it is a property of the material and is not affected by the wavelength of excitation. Hence the measured spectroscopic observable, here $R_\infty$, is proportional to the absorption coefficient.

Thus, substituting $F(R_\infty)$ instead of α in equation 1, we get,

$$(F(R_\infty)h\nu)^2 = A\,(h\nu - E_g)$$

After plotting the Kubelka-Munk function, $(F(R_\infty)h\nu)^2$ vs hν, the value of bang-gap can be obtained by drawing a tangent to the point of inflection on the curve to meet the x-axis.

For measuring the bandgap, I fixed the pellet of perovskite or its powder on a glass slide and placed it inside an empty cuvette at a 45° angle. A baseline was taken without the perovskite sample before the measurement. The spectra recorded with perovskite gave directly the transformed Kubelka-Munk plot from which the bandgap was estimated by the above method.

### 2.4.2. Steady-state photoluminescence spectroscopy

The photoluminescence from a perovskite solution corresponding to the radiative relaxation of excited-state charge carriers can be studied by using steady-state PL

spectroscopy. I used the FL-4500 fluorescence spectrophotometer, Hitachi, for this purpose. The optical set up inside the spectrophotometer is shown below:

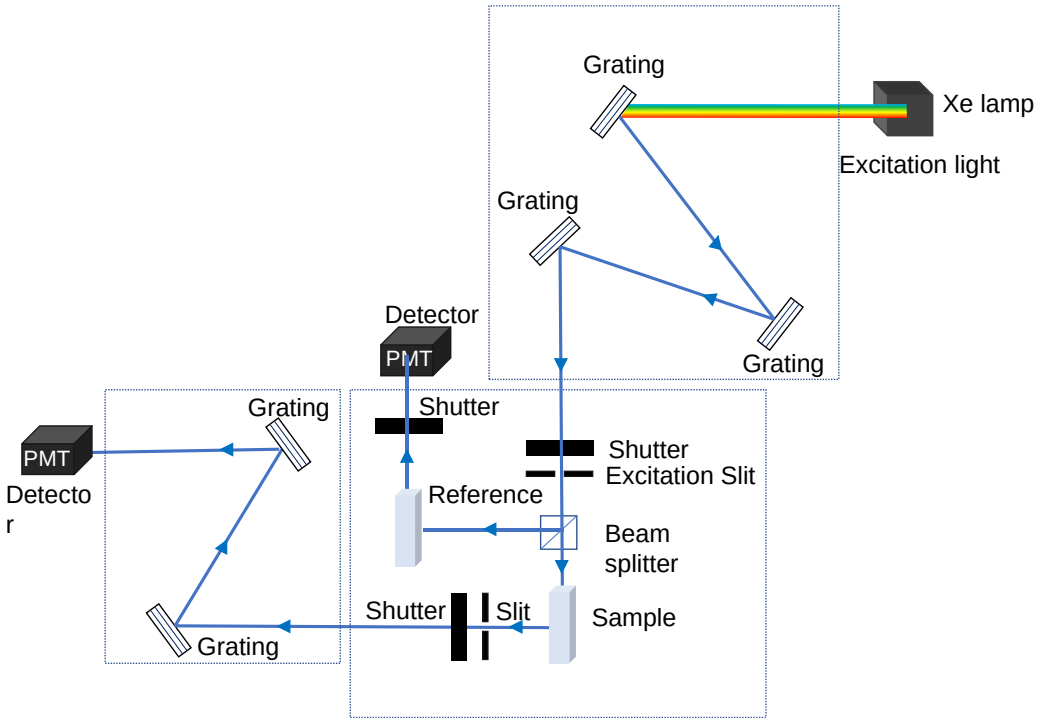


**Figure 8.** The schematic representation of the optical setup inside a spectrophotometer.

The excitation source is a xenon lamp providing a range of wavelengths. A monochromator, which is a diffraction grating, can be used to select the desired wavelength for excitation. The emitted light is collected at right angles so that only the fluorescence enters the detector and not any transmitted light or the excitation light itself. The detector is a photomultiplier tube. The detector collects the emission light, and the signal is an intensity vs wavelength plot.

### 2.3.3. Time-resolved fluorescence spectroscopy

*Femtosecond lifetime system*

I used time-resolved spectroscopy to understand the charge carrier dynamics of perovskites by measuring their photoluminescence lifetime. The general setup used for the PL lifetime measurement is shown below in Figure 9. The 400 nm light suitable for studying perovskite materials is generated by the following method. Coherent Mira 900 mode-locked Ti: Sapphire laser emits 800 nm laser pulses with a 76 MHz repetition rate. The emitted laser light is fed into a Coherent RegA 9000 regenerative amplifier which yields 800 nm laser light with a 200 kHz repetition rate and 150 fs pulse width of

approximately 1W power. This light is then fed to a Coherent optical parametric amplifier (OPA 9400), where the 800 nm laser light gets frequency-doubled to 400 nm by an SHG crystal.

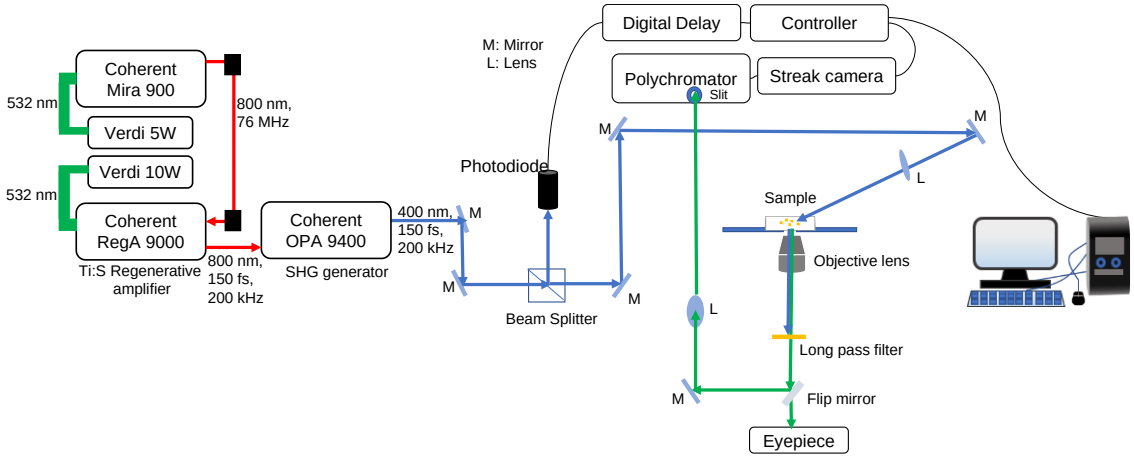


**Figure 9.** Optical setup for time-resolved photoluminescence studies using the ultrafast femtosecond laser pulse generated from the OPA.

The method of studying the emission from the perovskite sample is as follows. The sample was placed on the stage of the inverted optical microscope (Olympus IX70). The 400 nm femtosecond laser pulse of suitable power from the OPA was directed onto the sample from above at an angle using a series of mirrors and lenses. An objective lens (Olympus 40x, NA 0.6, or Olympus 10x) collects the emission light. The emitted light then passes through a long pass filter which cuts the laser light and is directed to the polychromator using a mirror and lens. An iris was set up to study a particular area of interest. The signals are detected by a streak camera (Streak-Scope C4334, Hamamatsu Photonics). A part of the excitation light source is also sent to a digital delay pulse generator using a photodiode. The excitation signal and the signal from the Streak-scope are then processed in a computer. The decay curves thus obtained were fitted with the software and the average lifetimes were calculated based on the equation:

$$\tau_{av} = \frac{\tau_1 A_1 + \tau_2 A_2 + \tau_3 A_3}{A_1 + A_2 + A_3}$$

where τ and A correspond to the lifetime component and amplitudes respectively. The average lifetime ($\tau_{av}$) is a measure of the time that the charge carrier spends in the excited state before being relaxed by radiative and nonradiative events. The PL lifetime is

inversely related to the sum of rate constants of various charge recombination processes like radiative recombination or nonradiative recombination. Hence, from the lifetime values, I extracted different charge carrier recombination processes rates.

*Time-correlated single-photon counting system (TCSPC)*

For studying the PL lifetimes of microcrystals, I utilized a TCSPC system attached with a picosecond laser system (Advanced Laser Diode, 1 MHz). The optical setup is shown in Figure 10. The sample was placed on the stage of a confocal microscope (IX71, Olympus) and is excited by a 465 nm picosecond laser with a 1 MHz repetition rate. A dichroic mirror with 90% transmission in 460 nm- 700 nm was placed on the laser path before exiting the sample. The emission from the sample was acquired by an objective lens (40x, 0.75 NA, UPLanFL N). The detector is an avalanche photodiode (SPCM-AQR, PerkinElmer) and a single-photon counting module (SPC-830, Becker & Hickl GmBH) counts the photons. The obtained photoluminescence decay curve was fitted by using a multiexponential lifetime fit to obtain the average lifetime. An iris was used to study the lifetime of isolated microcrystals.

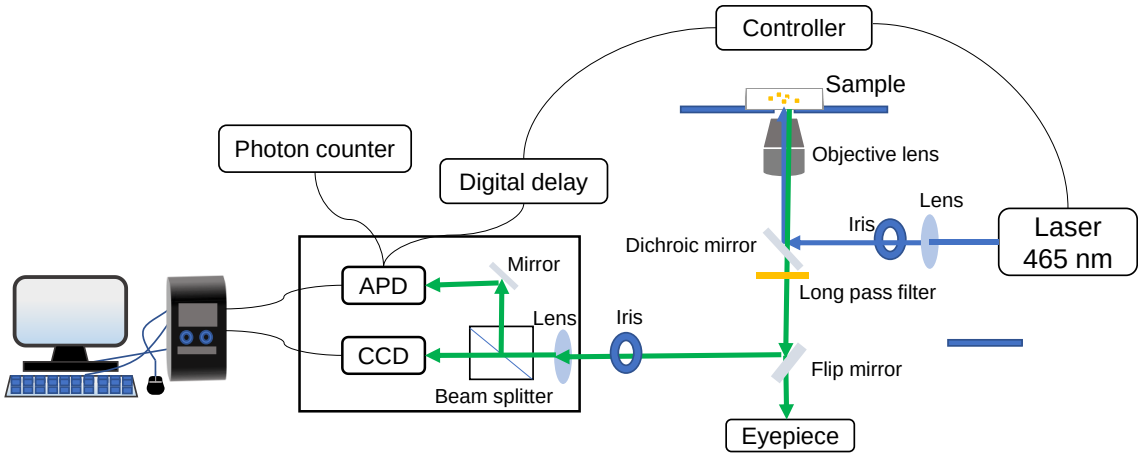


**Figure 10.** Optical setup of a TCSPC lifetime system for studying the PL decay of microcrystals.

### 2.4.4. Single-particle microspectroscopy

Single-particle microspectroscopy is widely used to study single molecules of semiconducting materials and dye molecules. It is used to understand the particle-by-particle heterogeneity in photoluminescence and electroluminescence. The heart of single-molecule imaging I used is an electron-multiplying charge-coupled device

(EMCCD) camera. The sample is excited by photo- or electrical excitation. The structure of the EMCCD sensor is shown below:

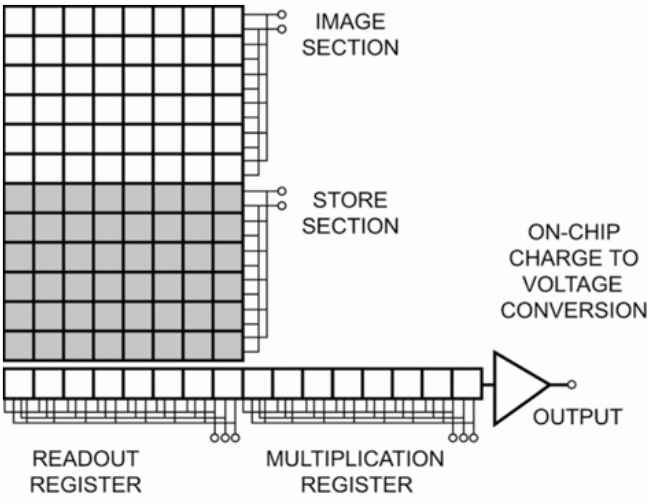


**Figure 11.** Structure of an EMCCD sensor chip.[13]

The emission from the sample is sent to the EMCCD detector which is a silicon-based semiconductor chip. It has a two-dimensional matrix of photo-sensors arranged in rows and columns. This part is called the imaging area. An EMCCD has an additional section called multiplication or gains register. The image area is first exposed to light where the image is captured. Photons from the image are converted to charges and they shift downwards to the storage section. Once sufficient charge is acquired it moves horizontally to the readout register section. The amplification occurs in the multiplication gain register. Processes like impact ionization of charges help in this amplification process. After being amplified, the charges in the amplifier are passed from the analog to the digital converter and the processing is done.

Data acquisition can be modified by using binning and frame transfer techniques. Binning is a process that allows two or more pixels to be combined on the sensor before being read out. But, this may cause the data obtained from other areas of the sensor to be discarded. Frame transfer is a process that can speed up performance. It allows acquiring a new image onto an image area while reading out the masked frame storage area in the sensor. This helps to achieve read-out faster. The signal obtained is viewed through Andor Solis software and gives a time trajectory plot of photo- or electroluminescence. The setup for acquiring the data is shown in Figure 12.

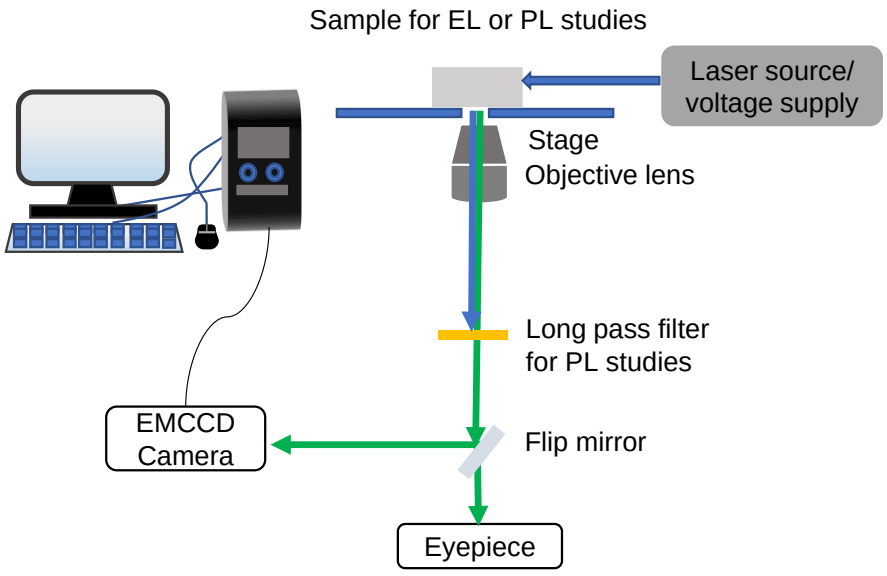


**Figure 12.** Single-particle microspectroscopic setup for studying EL and PL.

The electroluminescence observed under electrical excitation of perovskite sample was collected through an objective lens and sent to the EMCCD camera. Single-particle images and videos are acquired to get EL trajectory from perovskite microcrystals. Instead of electrical excitation, a laser excitation source was used to get photoluminescence from perovskites. Here, an additional long-pass filter was required to filter the emission from the perovskite sample while blocking the laser light passing the objective lens.

Instead of the EMCCD camera, the emission can be sent to a spectrometer camera to get the EL or PL spectra from the microcrystals. The method of collecting data from the perovskite sample involves the following steps. Perovskite microcrystals prepared on ITO-coated glass substrates were used as such for PL measurements. For EL measurements, the perovskite microcrystals prepared on ITO-coated glass substrate were sandwiched with another ITO-coated glass plate, which served as the lead for electrical connections to a power supply. Single-particle PL images were recorded at a 33 ms frame rate in an inverted optical microscope (IX71, Olympus), which was equipped with an objective lens (40 X, NA 0.6, Olympus), a >520 nm long-pass filter, and an EMCCD camera (iXon3, Andor Technology). The excitation light source used for single-molecule PL imaging was a 460 nm continuous wave laser and an electrical excitation from 2-18 V was used for single-particle EL imaging. Several intensity trajectories were collected, which are analyzed statistically to obtain the general behavior of the single particles. EL

and PL spectra from isolated microcrystals were recorded using the setup. The emitted photons were collected using an objective lens (Olympus, 40x, NA=0.6) which were guided to a spectrometer using an optical fiber. The spectra were collected after a background signal correction. The EL and PL spectra were recorded using a fiber optic spectrometer (FLAME, Ocean optics).

### 2.4.5. X-ray diffraction analyses

X-ray diffraction is a non-destructive method to study the crystalline phases of a material. I utilized powder-XRD as well as single crystal XRD to find the phase of the synthesized perovskite materials by comparing the diffraction peaks of the signals collected.

The basic components of an X-ray diffractometer are an X-ray tube, sample holder, and detector. X-rays are generated inside a cathode ray tube. The most common source of X-ray is Cu. Using a monochromator, the X-ray corresponding to the Cu-Kα radiation at 1.5406Å is selected and is collimated. Under an accelerating voltage, the X-rays hit the sample at an angle that excites the electrons in the sample to a higher energy state. Upon relaxation they emit X-rays. The constructive interference of the emitted X-rays by the sample occurs if they satisfy Bragg's law,

$$n\lambda = 2\,d\sin\theta$$

where λ is the wavelength of the X-rays, d is the lattice spacing of the crystal, and θ is the diffraction angle, and n is the order of diffraction and is an integer. The X-ray tube and detector move in a synchronized motion. The detector collects and counts the diffracted X-rays, and the software gives a diffraction spectrum which is a plot of intensity vs 2θ, where θ is the diffraction angle. By comparing peaks with the standard XRD pattern for a particular phase, we can identify the phase of the synthesized crystal.

#### Powder x-ray diffraction

I used Rint 2200, Rigaku X-ray spectrometer to study the powder diffraction. The appropriate amount of sample in powder form was prepared for the studies. It was kept in a vacuum chamber for several hours before data collection. The sample was then placed inside a sample holder and was irradiated with X-rays inside a vacuum chamber. The X-ray source is Cu-$K_\alpha$ radiation at 1.5406Å. The diffracted X-rays then fall on a detector, and the pattern obtained is analyzed.

**Single-crystal x-ray diffraction**

Single-crystal XRD of perovskite microcrystal was measured using Cu-Kα radiation with Rigaku Micromax$^{TM}$- 007HF (40kV, 30mA) at room temperature (20 $^{o}$C).

### 2.4.6 Scanning electron microscopy and energy-dispersive X-ray spectroscopy

I used SU8230, Hitachi, scanning electron microscope for studying the morphology of perovskite pellets and crystals and energy dispersive X-ray spectroscope, QUANTAX EDS, Bruker to perform elemental mapping studies. The perovskite sample was prepared directly on an ITO-coated glass plate. It was mounted on the SEM-EDS substrate (carbon substrate) using copper tapes. I used 1 kV for collecting SEM images and 6 kV for EDS measurements. SEM and EDS measurements have a common set up and as shown below:

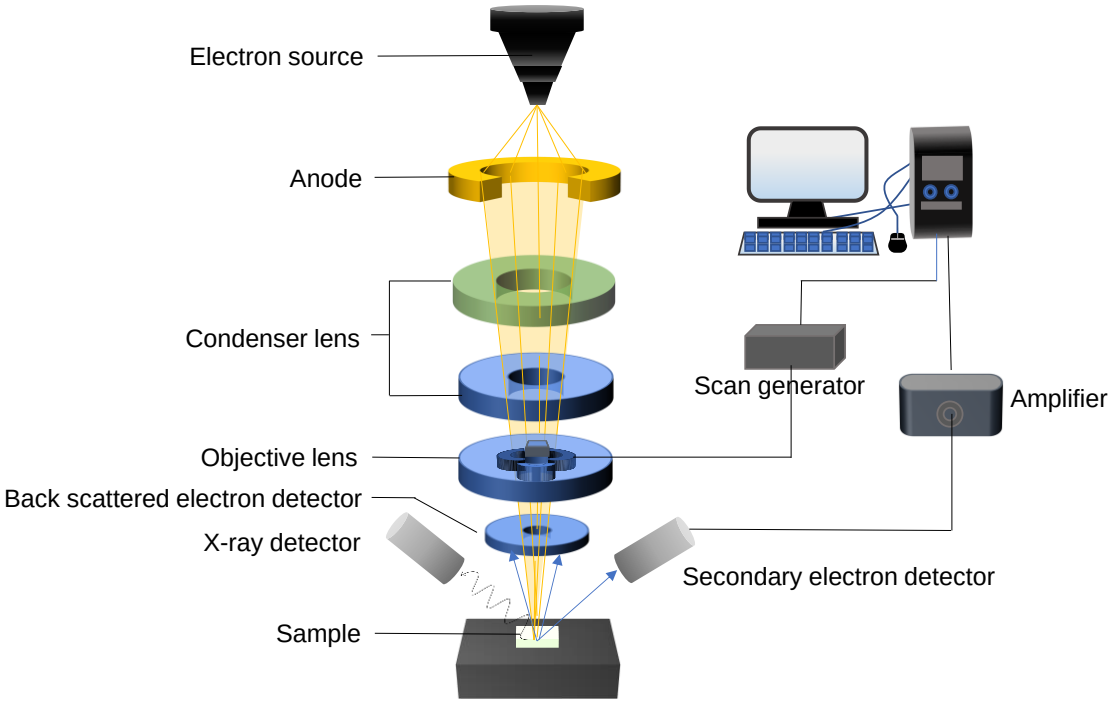


**Figure 13.** A schematic representation of SEM and EDS microscopy.

## References


1. Schmidt, L. C.; Pertegás, A.; Gonzalez-carrero, S.; Malinkiewicz, O.; Agouram, S.; Espallargas, G. M.; Bolink, H. J.; Galian, R. E.; Pérez-prieto, J.; González-carrero, S. Non-Template Synthesis of $CH_3NH_3PbBr_3$ Perovskite Nanoparticles Non-Template Synthesis of $CH_3NH_3PbBr_3$ Perovskite Nanoparticles. *J. Am. Chem. Soc.* **2014**, *136*, 850−853.

2. García-Aboal, R.; Fenollosa, R.; Ramiro-Manzano, F.; Rodríguez, I.; Meseguer, F.; Atienzar, P. Single Crystal Growth of Hybrid Lead Bromide Perovskites Using a Spin-Coating Method. *ACS Omega* **2018**, *3*, 5229–5236.

3. Protesescu, L.; Yakunin, S.; I. Bodnarchuk, M.; Krieg, F.; Caputo, R.; H. Hendon, C.; Xi Yang, R.; Walsh, A.; V. Kovalenko, M. Nanocrystals of Cesium Lead Halide Perovskites ($CsPbX_3$, X = Cl, Br, and I): Novel Optoelectronic Materials Showing Bright Emission with Wide Color Gamut. *Nano Lett.* **2015**, *15*, 3692–3696.

4. Zhang, F.; Zhong, H.; Chen, C.; Wu, X.; Hu, X.; Huang, H.; Han, J.; Zou, B.; Dong, Y. Brightly Luminescent and Color-Tunable Colloidal CH 3 NH 3 PbX 3 (X = Br, I, Cl) Quantum Dots: Potential Alternatives for Display Technology. *ACS Nano* **2015**, *9*, 4533–4542.

5. Ghimire, S.; Takahashi, K.; Takano, Y.; Nakamura, T.; Biju, V. Photon Recycling by Energy Transfer in Piezochemically Synthesized and Close-Packed Methylammonium Lead Halide Perovskites. *J. Phys. Chem. C* **2019**, *123*, 27752–27758.

6. Bhagyalakshmi, S. B.; Ghimire, S.; Takahashi, K.; Yuyama, K. ichi; Takano, Y.; Nakamura, T.; Biju, V. Nonradiative Energy Transfer through Distributed Bands in Piezochemically Synthesized Cesium and Formamidinium Lead Halide Perovskites. *Chem. - A Eur. J.* **2020**, *26*, 2133–2137.

7. García-Aboal, R.; Fenollosa, R.; Ramiro-Manzano, F.; Rodríguez, I.; Meseguer, F.; Atienzar, P. Single Crystal Growth of Hybrid Lead Bromide Perovskites Using a Spin-Coating Method. *ACS Omega* **2018**, *3*, 5229–5236.

8. Tauc, J.; Grigorovici, R.; Vancu, A. Optical Properties and Electronic Structure of Amorphous Germanium. *Phys. Status Solidi B* **1966**, *15*, 627–637.

9. Davis, E. A.; Mott, N. F. Conduction in Non-Crystalline Systems V. Conductivity, Optical Absorption and Photoconductivity in Amorphous Semiconductors. *Philos. Mag.* **1970**, *22*, 0903–0922.

10. Morales, A.E.; Mora, E.S.; Pal, U. Use of Diffuse Reflectance Spectroscopy for Optical Characterization of Un-Supported Nanostructures. *Rev. Mex. Física* **2007**, 53, 18–22.

11. Wahl, M. Technical Notes: Time-Correlated Single Photon Counting. *PicoQuant GmbH* **2014**.

12. Guide, H. IXon Ultra. *Hardw. Guid.* **2013**.

# Chapter 3

# Nonradiative energy transfer and photon recycling in close-packed perovskites

**Abstract**

Perovskite materials show exceptional properties like high rates of radiative recombination, long charge carrier diffusion length, and high photoluminescence quantum yield making them suitable for solar cells, LEDs, and lasers. Also, nonradiative processes occurring in these materials are considered a loss factor in terms of power conversion efficiency. Most synthetic methods use several harmful solvents and ligands to prepare perovskites of different shapes and sizes. Some of them affect the properties of perovskite as well. In this chapter, I use a pressure-induced solid-state method without the use of any solvents or ligands. Although I prepared perovskite pellets of good optical properties, the sample was too thick to be used for electroluminescence studies since a thick perovskite layer leads to inefficient charge transport. This adversely affects the performance of devices like LEDs. However, a thick sample is known to show an intriguing phenomenon called photon recycling. Photon recycling events are known to utilize the emitted photons by a process known as reabsorption-emission. Hence, using the synthesized perovskite in the form of a pellet, I study the role of nonradiative energy transfer in photon recycling. For this purpose, I synthesized closely-packed perovskite crystallites of cesium lead bromide and formamidinium lead bromide in the form of a pellet using a pressure-induced solid-state method. These materials show a distribution of closely spaced energy states as was confirmed from the temporally and spectrally resolved photoluminescence studies. The distribution of closely spaced energy states can act as donor and acceptor states for efficient nonradiative energy transfer. To see the effect of nonradiative energy transfer, I synthesized a mixed halide perovskite composed of bromide and iodide by the same method. The energy transfer from a high bandgap bromide to a low bandgap iodide is indicated by a decrease in the lifetime of bromide rich domain. This observation allows understanding the role of nonradiative energy transfer in photon recycling, often shadowed by radiative energy transfer processes like photon reabsorption.

## 3.1 Introduction

Photon recycling is a process in which a highly absorbing material undergoes repeated self-re-absorption and re-emission of photons. It is a process observed only in high-quality semiconductors with high photoluminescence quantum efficiency, sharp absorption band edge, and relatively small stoke shift. It is commonly observed in thick films and single crystals of perovskites whose dimensions exceed the charge carrier diffusion length or photon propagation length.[1,2,3,4,5,6,7] This process has been found to improve the photovoltaic conversion efficiency in semiconductor-based solar cells by boosting the open-circuit voltage.[3] Friend *et al.* showed that photon recycling could result in increased charge carrier density in lead halide perovskites leading to high photoluminescence quantum yield.[4] Photon recycling is known to propagate the PL emission across long distances which exceed charge carrier diffusion length. However, studies by Huang *et al.* on single-crystal $MAPbI_3$ and $MAPbBr_3$ contradict the above statement. The photon recycling efficiencies accounted for less than 0.5% in these crystals and hence, it was ruled out as the reason for the origin of long carrier diffusion length.[7] Studies on $CsPbBr_3$ microwires showed that photon recycling events assist photon waveguiding and are also useful in photon conversion applications.[8] Photon reabsorption by radiative energy transfer has been facilitated in mixed $CsPbCl_3$:$CsPbI_3$ nanocrystal films where energy transfer occurs from high bandgap chloride perovskite to low bandgap iodide perovskite and resulted in emission solely from iodide.[9] The debate is still ongoing on whether photon recycling or carrier diffusion is the dominant energy transport pathway in perovskites.[10] In all these studies, photon recycling is attributed to a radiative energy transfer process. Although there are one or two reports of energy and charge transfer in $CsPbBr_3$ nanocrystals[11] and $MAPbBr_3$ nanoparticle aggregates,[12] the role of nonradiative energy transfer in photon recycling is seldom studied. This study is very important as photon recycling is an additional route to improve the charge carrier dynamics of perovskite materials in many of its applications like solar cells, LEDs, and lasers.

The study of nonradiative energy transfer calls for donor and acceptor species at proximity. Thus, it was necessary to synthesize close-packed systems. Several wet chemical methods are used to synthesize perovskites.[13,14,15,16] Although these methods are extensively applied in the synthesis of pure and mixed halide perovskites, dissolved oxygen and moisture in solvents such as *N, N*-dimethylformamide (DMF), dimethylsulfoxide (DMSO), γ-butyrolactone (GBL), and dichloromethane used for the

synthesis can adversely affect the performance and durability of perovskite devices.[17] Even though solvents and ligands are inevitable in the synthesis of perovskite nanocrystals, microscopic crystals of perovskite can be synthesized mechanochemically. For example, Miguel *et al.* synthesized hybrid polycrystalline perovskites in 1, 2, and 3 dimensions by the mechanical grinding of precursors, which was followed by annealing at temperatures as high as 250 $^{o}$C.[18] Such mechanochemical and solvent-free methods find applications to the synthesis of perovskites with different chemical compositions and the structural transformation and stabilization of perovskites. For example, Grätzel and co-workers successfully improved the stability of formamidinium lead iodide ($FAPbI_3$) perovskite by the mixing of A-site cation between methylammonium ($MA^+$) and formamidinium ($FA^+$) using MAI and FAI.[19] Although these findings suggest the importance of solvent-less or solvent-free synthesis of perovskites for device technology, the significance of mechanical force is overlooked. In a hand-grinding or ball-milling process, the mechanical force is responsible for the solid-state reaction among precursors.

The above relations between mechanical force and perovskites and the abundance of silicate perovskites in the mantle of earth[20] attracted a pressure-induced solid-state method for the synthesis of high-density $CsPbBr_3$, $FAPbBr_3$, and $FAPb(BrI)_3$ perovskite required for my studies.[21] Also, the required perovskite could be synthesized in ambient temperature and humidity conditions. Here a solid solution of precursors mixed homogeneously was transferred into a chamber, where an optimum pressure is applied using a hydraulic press machine. The pressure allows ionic metathesis between the solid precursors to form the required perovskite crystal structure. The close-packed perovskite crystallites were then studied by various spectroscopic techniques to understand the role of nonradiative energy transfer in photon recycling processes.

### 3.2 Results and discussion

#### 3.2.1 Characterization of $CsPbBr_3$ and $FAPbBr_3$ perovskites pellets

Luminescent crystals of $CsPbBr_3$ and $FAPbBr_3$ perovskites are close-packed in macroscopic pellets, which was by applying a pressure of 2.4 GPa to solid solutions of the corresponding precursors.[21] Here, the applied pressure allows the mixing of the precursors to incorporate various ions to form a perovskite crystal lattice. Using powder-XRD analyses, I characterized both the precursor salts and the resulting perovskite. Below shown is the XRD pattern of CsBr, FABr, $PbBr_2$, $CsPbBr_3$, and $FAPbBr_3$.

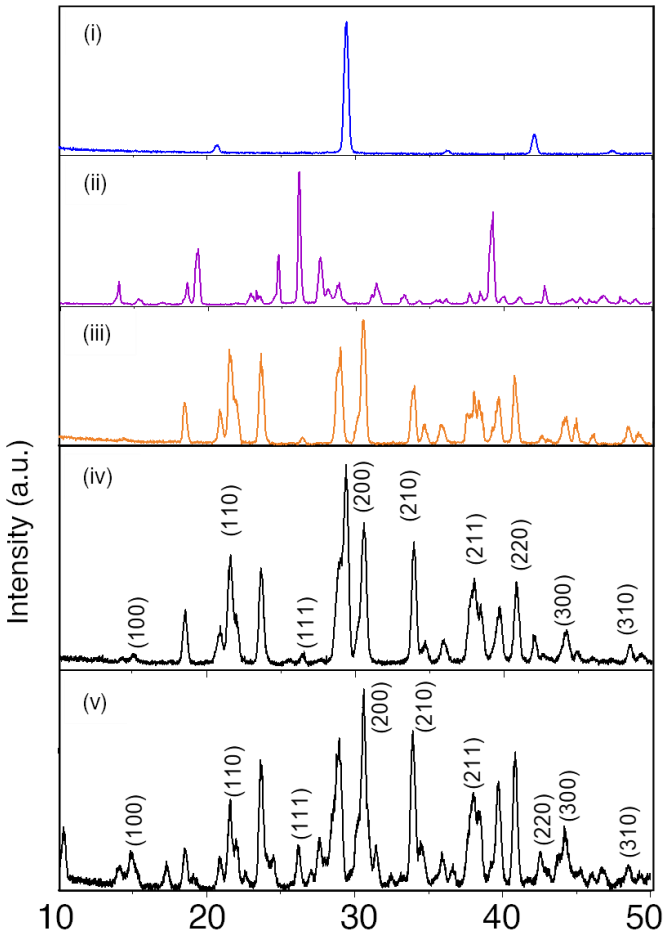


**Figure 1.** The XRD patterns of (i) CsBr, (ii) FABr, (iii) $PbBr_2$, (iv) $CsPbBr_3$, and (v) $FAPbBr_3$ obtained by powder-XRD method.

The XRD patterns of $CsPbBr_3$ (Figure 1(iv)) shows peaks at 15.05°, 21.48°, 30.63°, 33.96°, 37.92°, 44.10° and 48.55° which corresponds (100), (110), (200), (210), (211), (220) and (310) crystal planes, respectively. This helps to assign a cubic *Pm3m* phase for $CsPbBr_3$ by comparing the XRD pattern with literature report[22] and standard ICSD card

no #29073. The diffraction peaks of $FAPbBr_3$ appear at 14.80°, 21.60°, 30.50°, 33.84°, 37.92°, 40.89°, and 44.22°, which are in accordance with the (100), (110), (200), (210), (211), (220), and (300) crystal planes, respectively (Figure 1 (v)). In this case, as well, a cubic phase could be assigned to the crystals. However, in these perovskites, some reminiscent peaks from the precursor salts are also present as can be seen from Figure 1 (i-iii). As references, the XRD patterns of CsBr (Figure 1(i)), FABr (Figure 1 (ii)) and $PbBr_2$ (Figure 1 (iii)) are discussed here. The peaks appearing at 29.27°and 42.00° can be compared with CsBr, those at 29.02°, 30.50°, 33.84°, 44.22° and 55.10° correspond to FABr, and those at 18.40°, 23.58° and 39.65° belong to $PbBr_2$. However, these precursor peaks did not interfere in the characterization of the crystal phases of these perovskites.

I also used SEM microscopy to understand the morphology of the synthesized pellet and crystallites. Figure 2 shows the SEM image of the $FAPbBr_3$ pellet and its crystallites. Figure 2a. is the magnified image of the pellet as such. I crushed the pellet to observe the crystallites, and the SEM images are shown in Figures 2b and 2c.

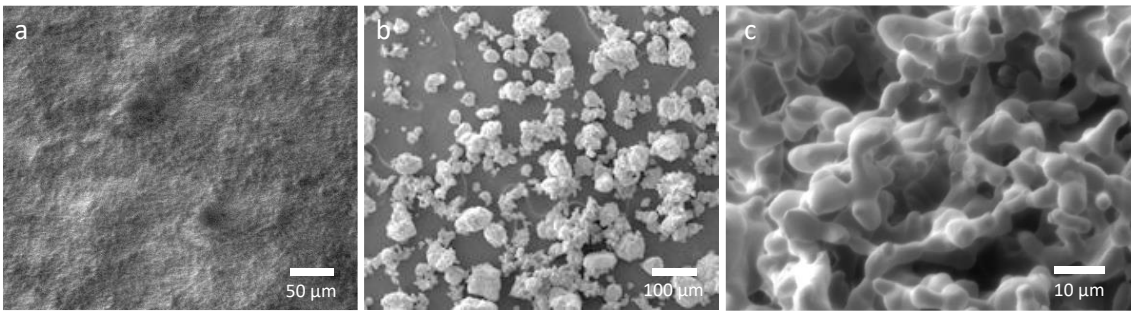


**Figure 2.** SEM images of a) $FAPbBr_3$ pellet, b) $FAPbBr_3$ crystallites, and (c) the zoomed-in image of the crystallite.

### 3.2.2 Optical properties of $CsPbBr_3$ and $FAPbBr_3$ perovskite pellets

I characterized the synthesized crystals using Kubelka-Munk diffused reflectance spectroscopy and PL spectroscopy. Figures 3a and 3b are the Tauc plots obtained for $CsPbBr_3$ and $FAPbBr_3$. The optical band gaps were obtained from the Tauc plot as mentioned in section 2.4.1 and correspond to 2.30 eV and 2.21 eV for $CsPbBr_3$ and $FAPbBr_3$, respectively. The PL maxima are centered around 520 nm for $CsPbBr_3$ and 540 nm for $FAPbBr_3$. The bandgap values and PL maxima are exactly matching with those of wet chemical synthesis based on $CsPbBr_3$ and $FAPbBr_3$ perovskite micro- and nanocrystals.[22,23]

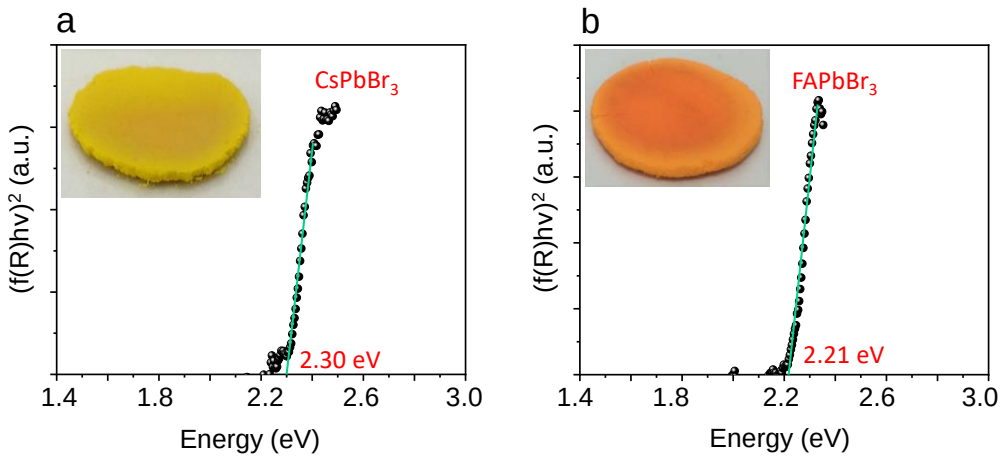


**Figure 3.** a) Tauc plot of $CsPbBr_3$ perovskite pellet (inset shows the as-synthesized $CsPbBr_3$ perovskite pellet), and b) Tauc plot of $FAPbBr_3$ perovskite pellet (inset shows the as-synthesized $FAPbBr_3$ perovskite pellet).

This similarity in the bandgap characteristics brings into the generalization that is already reported that A-site cations seldom contribute towards frontier molecular orbitals, which means that $CsPbBr_3$ and $FAPbBr_3$ will show not much difference in their bandgap. The redshifted emission and long lifetime of $FAPbBr_3$ compared to that of $CsPbBr_3$ as shown in Figures 4a and 4b is seen as the effect of A-site cation or due to the difference in the degree of photon recycling. The difference in the A site cation contributed to the difference in octahedral tilting, which affects the degree of crystal lattice distortion. This leads to strong spin-orbit coupling and hence contributed indirectly to the bandgap variations.[24]

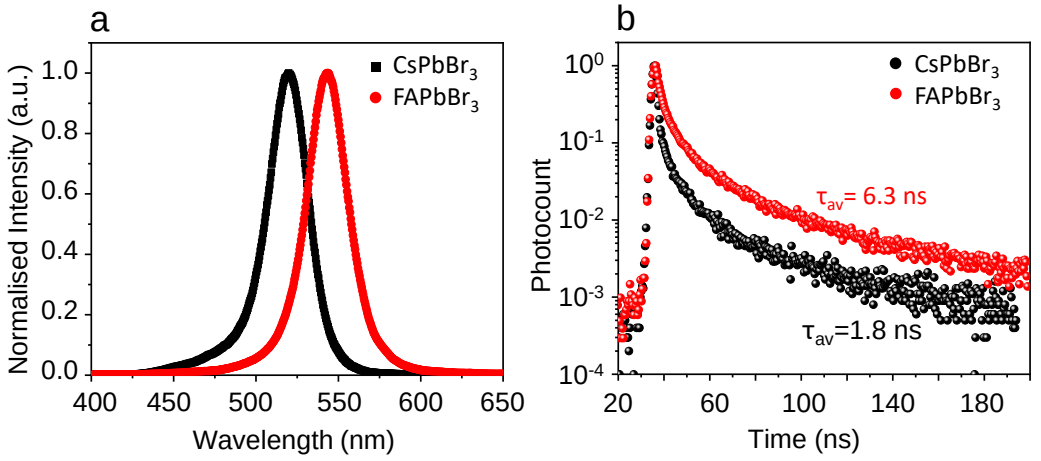


**Figure 4.** (a) PL spectra and (b) PL decay of isolated crystallites of $CsPbBr_3$ and $FAPbBr_3$ perovskites, respectively. 400 nm femtosecond laser was used to excite the sample.

### 3.2.3 Reabsorption emission in pellets

The PL properties showed distinct variation at different parts of the crystal. Towards the edges, the pellet showed green emission, while towards the center, the emission was red-shifted to the yellow region for $CsPbBr_3$ and orange region for $FAPbBr_3$. This is shown in Figure 5. The redshift at the center is attributed to the effect of photon reabsorption. At the edges, the reabsorption effect is low, while at the center, the reabsorption of the emitted photons is seen. Such an observation hints photon recycling phenomenon occurring in the synthesized perovskite pellets.

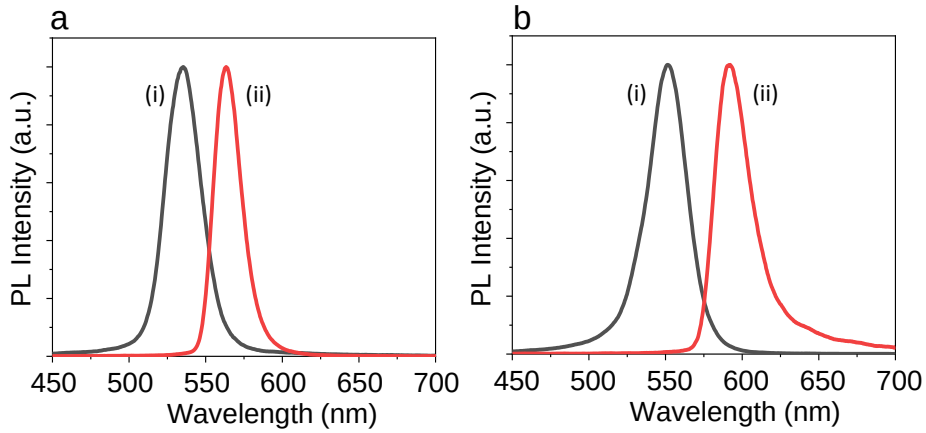


**Figure 5.** a) PL spectra recorded from (i) edge, and (ii) center of the $CsPbBr_3$ pellet, and b) PL spectra recorded from (i) edge, and (ii) center of the $FAPbBr_3$ pellet. Here the sample is excited by a 400 nm femtosecond laser with 0.05 mW power.

### 3.2.4 Distributed energy states in pellets

To understand the phenomenon of photon recycling thoroughly, the pellets were crushed gently, and individual crystallites were studied. It was surprising to observe a distribution of PL maxima from these crystallites, meaning that there is the presence of different bandgaps within the same pellet. The close packing of these crystallites into a pellet allows for closely spaced energy states.

This was further confirmed by the time-resolved PL lifetime studies. It was found that crystallites with blue-shifted emission exhibited a shorter lifetime while the red-shifted emission exhibited a longer lifetime. Such a long lifetime from the crystallites with red-shifted emission together with the existence of closely spaced energy states suggested thinking about the role of nonradiative energy transfer in perovskite pellets.

The PL lifetime was estimated to be 5.7 ns in the case of the $FAPbBr_3$ crystallites which showed red-shifted emission compared to that which showed blue-shifted emission. Figure 6 shows the details.

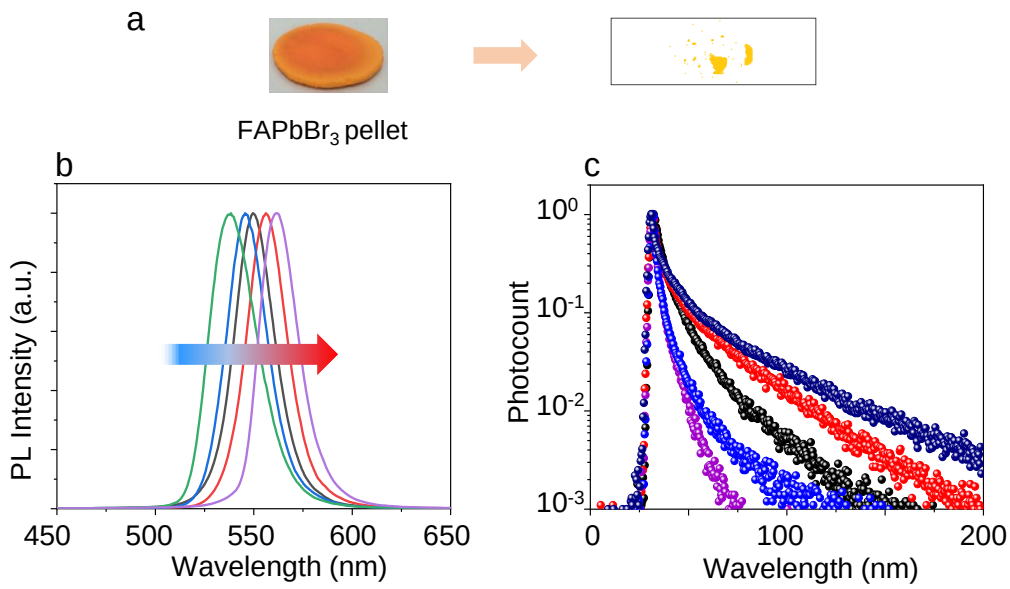


**Figure 6.** a) A scheme showing the $FAPbBr_3$ pellet and the crystallites obtained by gently crushing it for the PL studies, (b) PL spectra, and (c) PL decay curves were obtained in the region 520-600 nm region from random crystallites of $FAPbBr_3$ by exciting using a 400 nm femtosecond laser of 0.05 mW power.

### 3.2.5 Energy transfer in mixed halide perovskite

To clearly see the effect of nonradiative energy transfer in closely packed perovskite crystallites, I purposefully synthesized a mixed halide perovskite, namely, $FAPb(BrI)_3$ using the same pressure-induced solid-state synthesis. From the PL studies as shown in Figure 7a, it is clear that there exist bromide-rich domains and iodide-rich domains within the pellet. For example, in Figure 7a, area 1 shows a PL spectrum with a high-intensity green emission corresponding to the high bandgap bromide rich domain, while in area 2 there is a high-intensity orange emission corresponding to low bandgap iodide rich domain. Some areas showed more or less equal intensity emissions from bromide and iodide parts. The difference can arise either from variations in the bromide-to-iodide ratio or it can be the variations in the efficiency of nonradiative energy transfer occurring at the closely spaced bromide-iodide interface. The energy transfer can be contributed by radiative and nonradiative processes as well as charge carrier migration processes.

However, the nonradiative energy transfer can occur only if the donor and acceptor states are closely spaced. Since I prepare close-packed perovskite crystals, the chance of nonradiative energy transfer is high. To further clarify this, I used PL lifetime measurements with reference to the bromide emitting region, specifically, 500-575 nm region in a mixed halide perovskite sample ($FAPb(BrI)_3$). The results were then compared with that of a pure bromide perovskite sample ($FAPbBr_3$) (i.e., in the presence and absence of iodide species, respectively). The mixed halide showed a comparatively shorter lifetime (2.17 ns) with respect to pure bromide containing $FAPbBr_3$ sample (7. 32 ns) in the 500-575 nm region. This is a clear indication that the presence of iodide is affecting the depopulation of the excited state of bromide species by the most probable route of nonradiative energy transfer.

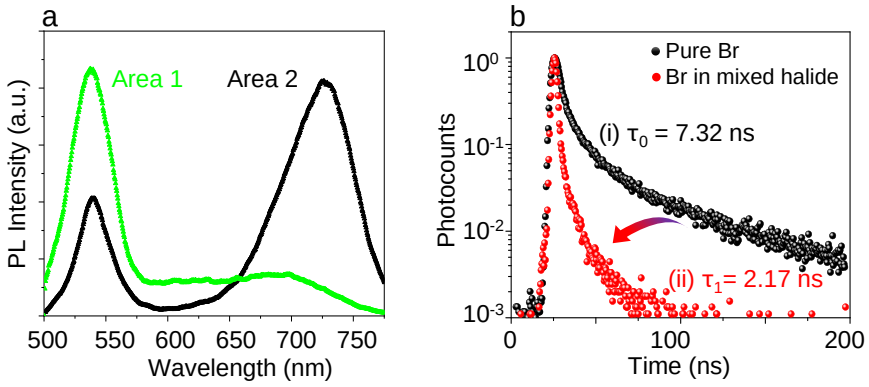


**Figure 7.** a) PL spectra obtained from different areas in a mixed halide $FAPb(BrI)_3$ pellet. (b) PL lifetime of (i) pure $FAPbBr_3$ perovskite and (ii) green-emitting (500-575 nm) region in a $FAPb(BrI)_3$ perovskite. The samples were excited using a 400 nm femtosecond laser of 0.05 mW power.

After excitation, the photoexcited species will undergo various events like diffusion, trapping, surface recombination, radiative and nonradiative recombination at the bulk level, etc. Such events cannot be differentiated from a PL decay curve. However, comparing two samples and studying the decay dynamics of one particular species in the presence and absence of another can give an understanding of a particular relaxation route. I then evaluated the contribution of nonradiative energy transfer among other routes of charge carrier relaxation events like radiative and other nonradiative processes. For this, I compared the rates of relaxation of the excited state of mixed halide perovskite in the 500-575 nm region with that of a pure bromide perovskite (i.e., in the presence and absence of iodide) by solving equations (1) and (2).

$$\tau_0 = \frac{1}{k_r + k_{nr} + k_{ET_1}} = \frac{1}{k_0} \quad (1)$$

$$\tau_1 = \frac{1}{k_0 + k_{ET}} \quad (2)$$

where $\tau_0$ and $\tau_1$ correspond to the average PL lifetime of pure $FAPbBr_3$ and the bromide region (500-575 nm) of the mixed halide, $FAPb(BrI)_3$ perovskite, respectively; $k_r$ and $k_{nr}$ are the rates of radiative and nonradiative relaxations respectively; $k_{ET1}$ is the rate of nonradiative energy transfer occurring in pure bromide perovskite, and $k_{ET}$ is the rate os nonradiative energy transfer occurring in mixed halide perovskite. By inserting the values of $\tau_0$ and $\tau_1$ calculated based on Figure 7b, I found that the rate of energy transfer, $k_{ET}$ is 3.24 $x10^8$ $s^{-1}$. This value is larger than the overall relaxation rate, $k_0$, of a pure $FAPbBr_3$ perovskite which is 1.36 $x10^8$ $s^{-1}$. This proves that the nonradiative energy transfer occurs efficiently in a mixed halide $FAPb(BrI)_3$.

### 3.2.6 The mechanism of energy transfer in close-packed perovskites

In a closed-packed perovskite, several processes can account for the relaxation of excited states. If there is a nearby state that satisfies the conditions for nonradiative energy transfer, the photons can be recycled as shown in the figure in addition to other radiative and nonradiative events. Figure 8 shows the layout of energy states in a closely packed perovskite crystal with distributed band gaps.

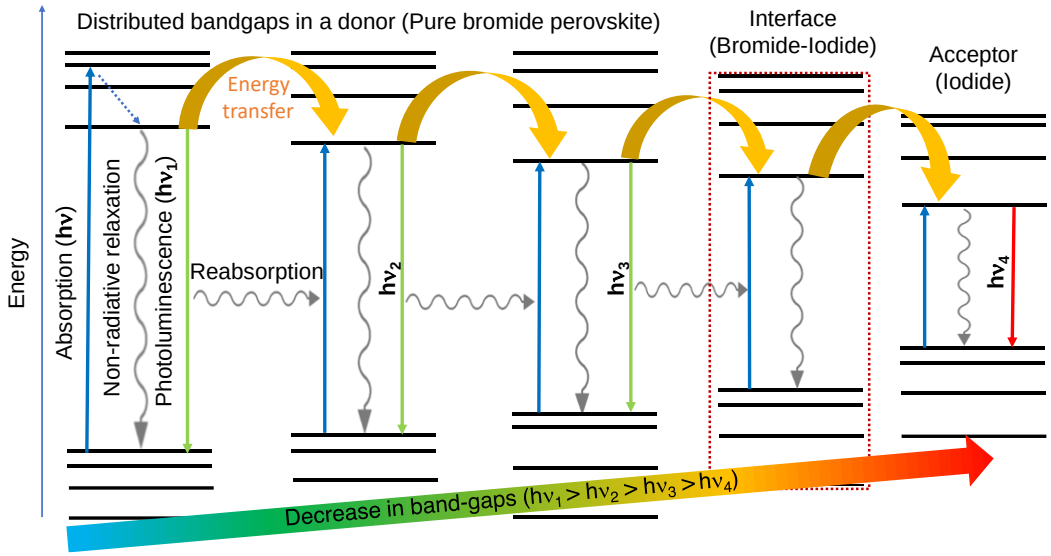


**Figure 8.** A scheme showing the mechanism of photon recycling in a closed-packed perovskite system.

The high bandgap bromide donor states are placed toward the extreme left, and the low bandgap iodide acceptor states are placed to the extreme right. The states with intermediate bandgap assist the transfer of energy either radiatively or nonradiatively. Radiative photon recycling events occur in the bromide, iodide, and intermediate regions. Similarly, nonradiative energy transfer also contributes to photon recycling events.

In the case of a mixed halide perovskite, it was proved by the above rate calculations that the radiative processes could not solely lead to a faster depopulation of excited states of the donor bromide species. A three-fold increase in the rate of relaxation of the donor was seen in the case of mixed halide, $FAPb(BrI)_3$ in comparison to pure $FAPbBr_3$. The presence of intermediate energy states assists the smooth transfer of energy from the high bandgap bromide region to the low bandgap iodide region.

### 3.3 Conclusion

In this chapter, I studied the role of nonradiative energy transfer in photon recycling. For this, I used a simple method for the synthesis of $CsPbBr_3$, $FAPbBr_3$, and $FAPb(BrI)_3$, which is a pressure-induced solid-state method. This method uses pressure as a driving force to synthesize close-packed perovskite crystallites in the form of a pellet. The synthesis was conducted at room temperature with no control on humidity and gave luminescent $CsPbBr_3$, $FAPbBr_3$, and $FAPb(BrI)_3$ pellets. The optical features, crystalline phases, and morphology were in close agreement with that of literature reports. In the case of thick films and single crystals of perovskites, photon recycling is often correlated with reabsorption and emission, masking the contribution of nonradiative energy transfer in this process. From the temporally and spectrally resolved studies, I could understand the contribution of nonradiative processes in photon recycling. Crystallites of pure $FAPbBr_3$ showed the distribution of closely spaced energy states which was seen as different emission maxima in the PL spectra. The PL lifetime studies also indicated the existence of energy states with different bandgaps. The crystallite with a blue-shifted emission showed a shorter lifetime compared to a crystallite showing a red-shifted emission. However, the role of nonradiative transfer was clarified using a close-packed mixed halide perovskite pellet. Such pellets were composed of bromide-rich domains and iodide-rich domains in close proximity as can be seen from PL spectra collected from different areas of the pellet. By comparing the rates of relaxation of an excited state of bromide in a mixed halide perovskite with a pure bromide perovskite, it was found that

radiative energy transfer cannot solely contribute to a decreased lifetime in mixed halide. The excited state of bromide is depopulated by the closely spaced iodide through the nonradiative energy transfer process. In this way, the photons emitted by the bromide are recycled by iodide emission. Apart from the understanding of photon recycling, the above synthesis method and studies have shown that the close-packed perovskite system retains its discrete band gap features and can efficiently undergo photon recycling as well. This will help in applications where multiple bandgaps are required, such as white light LEDs.

## References


1. Yamada, Y.; Yamada, T.; Phuong, L. Q.; Maruyama, N.; Nishimura, H.; Wakamiya, A.; Murata, Y.; Kanemitsu, Y. Dynamic Optical Properties of $CH_3NH_3PbI_3$ Single Crystals as Revealed by One- and Two-Photon Excited Photoluminescence Measurements. *J. Am. Chem. Soc.* **2015**, *137*, 10456–10459.

2. Yamada, T.; Yamada, Y.; Nishimura, H.; Nakaike, Y.; Wakamiya, A.; Murata, Y.; Kanemitsu, Y. Fast Free-Carrier Diffusion in $CH_3NH_3PbBr_3$ Single Crystals Revealed by Time-Resolved One- and Two-Photon Excitation Photoluminescence Spectroscopy. *Adv. Electron. Mater.* **2016**, *2*, 1500290.

3. Pazos-Outon, L. M.; Szumilo, M.; Lamboll, R.; Richter, J. M.; Crespo-Quesada, M.; Abdi-Jalebi, M.; Beeson, H. J.; Vru ini, M.; Alsari, M.; Snaith, H. J.; Ehrler, B.; Friend, R. H.; Deschler, F. Photon Recycling in Lead Iodide Perovskite Solar Cells. *Science* **2016**, *351*, 1430–1433.

4. Richter, J. M.; Abdi-Jalebi, M.; Sadhanala, A.; Tabachnyk, M.; Rivett, J. P. H.; Pazos-Outón, L. M.; Gödel, K. C.; Price, M.; Deschler, F.; Friend, R. H. Enhancing Photoluminescence Yields in Lead Halide Perovskites by Photon Recycling and Light Out-Coupling. *Nat. Commun.* **2016**, *7*, 13941.

5. Kirchartz, T.; Staub, F.; Rau, U. Impact of Photon Recycling on the Open-Circuit Voltage of Metal Halide Perovskite Solar Cells. *ACS Energy Lett.* **2016**, *1*, 731–739.

6. Yamada, T.; Yamada, Y.; Nakaike, Y.; Wakamiya, A.; Kanemitsu, Y. Photon Emission and Reabsorption Processes in $CH_3NH_3PbBr_3$ Single Crystals Revealed by Time-resolved Two-photon-excitation Photoluminescence Microscopy. *Phys. Rev. Appl.* **2017**, *7*, 014001.

7. Fang, Y.; Wei, H.; Dong, Q.; Huang, J. Quantification of Re-Absorption and Re-Emission Processes to Determine Photon Recycling Efficiency in Perovskite Single Crystals. *Nat. Commun.* **2017**, *8*, 14417.

8. Dursun, I.; Zheng, Y.; Guo, T.; De Bastiani, M.; Turedi, B.; Sinatra, L.; Haque, M. A.; Sun, B.; Zhumekenov, A. A.; Saidaminov, M. I.; García de Arquer, F. P.; Sargent, E. H.; Wu, T.; Gartstein, Y. N.; Bakr, O. M.; Mohammed, O. F.; Malko,

A. V. Efficient Photon Recycling and Radiation Trapping in Cesium Lead Halide Perovskite Waveguides. *ACS Energy Lett.* **2018**, *3*, 1492–1498.

9. Davis, N. J. L. K.; de la Peña, F. J.; Tabachnyk, M.; Richter, J. M.; Lamboll, R. D.; Booker, E. P.; Wisnivesky Rocca Rivarola, F.; Griffiths, J. T.; Ducati, C.; Menke, S. M.; Deschler, F.; Greenham, N. C. Photon Reabsorption in Mixed $CsPbCl_3$:$CsPbI_3$ Perovskite Nanocrystal Films for Light-Emitting Diodes. *J. Phys. Chem. C* **2017**, *121*, 3790–3796.

10. Gan, Z.; Wen, X.; Chen, W.; Zhou, C.; Yang, S.; Cao, G.; Ghiggino, K. P.; Zhang, H.; Jia, B. The Dominant Energy Transport Pathway in Halide Perovskites: Photon Recycling or Carrier Diffusion? *Adv. Energy Mater.* **2019**, *9*, 1900185.

11. de Weerd, C.; Gomez, L.; Zhang, H.; Buma, W. J.; Nedelcu, G.; Kovalenko, M. V.; Gregorkiewicz, T. Energy Transfer between Inorganic Perovskite Nanocrystals. *J. Phys. Chem. C* **2016**, *120*, 13310–13315.

12. Bouduban, M. E. F.; Burgos-Caminal, A.; Ossola, R.; Teuscher, J.; Moser, J.-E. Energy and Charge Transfer Cascade in Methylammonium Lead Bromide Perovskite Nanoparticle Aggregates. *Chem. Sci.* **2017**, *8*, 4371–4380.

13. Schmidt, L. C.; Pertegás, A.; González-Carrero, S.; Malinkiewicz, O.; Agouram, S.; Mínguez Espallargas, G.; Bolink, H. J.; Galian, R. E.; Pérez-Prieto, J. Nontemplate Synthesis of $CH_3NH_3PbBr_3$ Perovskite Nanoparticles. *J. Am. Chem. Soc.* **2014**, *136*, 850–853.

14. García-Aboal, R.; Fenollosa, R.; Ramiro-Manzano, F.; Rodríguez, I.; Meseguer, F.; Atienzar, P. Single Crystal Growth of Hybrid Lead Bromide Perovskites Using a Spin-Coating Method. *ACS Omega* **2018**, *3*, 5229–5236.

15. Protesescu, L.; Yakunin, S.; I. Bodnarchuk, M.; Krieg, F.; Caputo, R.; H. Hendon, C.; Xi Yang, R.; Walsh, A.; V. Kovalenko, M. Nanocrystals of Cesium Lead Halide Perovskites ($CsPbX_3$, X = Cl, Br, and I): Novel Optoelectronic Materials Showing Bright Emission with Wide Color Gamut. *Nano Lett.* **2015**, *15*, 3692–3696.

16. Zhang, F.; Zhong, H.; Chen, C.; Wu, X.; Hu, X.; Huang, H.; Han, J.; Zou, B.; Dong, Y. Brightly Luminescent and Color-Tunable Colloidal $CH_3NH_3PbX_3$ (X =

Br, I, Cl) Quantum Dots: Potential Alternatives for Display Technology. *ACS Nano* **2015**, *9*, 4533–4542.

17. Cho, H.; Kim, Y.-H.; Wolf, C.; Lee, H.-D.; Lee, T.-W. Improving the Stability of Metal Halide Perovskite Materials and Light-Emitting Diodes. *Adv. Mater.* **2018**, *30*, 1704587.

18. Jodlowski, A. D., Yépez, A., Luque, R., Camacho, L., de Miguel, G. Benign-by-Design Solventless Mechanochemical Synthesis of Three-, Two-, and One-Dimensional Hybrid Perovskites. *Angew. Chem.***2016,** *55*, 14972-14977.

19. Karmakar, A.; Askar, A. M.; Bernard, G. M.; Terskikh, V. V.; Ha, M.; Patel, S.; Shankar, K.; Michaelis, V. K. Mechanochemical Synthesis of Methylammonium Lead Mixed-Halide Perovskites: Unraveling the Solid-Solution Behavior Using Solid-State NMR. *Chem. Mater.* **2018**, *30*, 2309–2321.

20. Serghiou, G. (Mg, Fe)$SiO_3$-Perovskite Stability Under Lower Mantle Conditions. *Science* **1998**, *280*, 2093–2095.

21. Bhagyalakshmi, S. B.; Ghimire, S.; Takahashi, K.; Yuyama, K.; Takano, Y.; Nakamura, T.; Biju, V. Nonradiative Energy Transfer through Distributed Bands in Piezochemically Synthesized Cesium and Formamidinium Lead Halide Perovskites. *Chem. Eur. J.* **2020**, *26*, 2133–2137.

22. Ghimire, S.; Chouhan, L.; Takano, Y.; Takahashi, K.; Nakamura, T.; Yuyama, K. I.; Biju, V. Amplified and Multicolor Emission from Films and Interfacial Layers of Lead Halide Perovskite Nanocrystals. *ACS Energy Lett.* **2019**, *4*, 133–141.

23. Saidaminov, M. I.; Abdelhady, A. L.; Maculan, G.; Bakr, O. M. Retrograde Solubility of Formamidinium and Methylammonium Lead Halide Perovskites Enabling Rapid Single Crystal Growth. *Chem. Commun.* **2015**, *51*, 17658–17661.

24. Amat, A.; Mosconi, E.; Ronca, E.; Quarti, C.; Umari, P.; Nazeeruddin, M. K.; Grätzel, M.; De Angelis, F. Cation-Induced Band-Gap Tuning in Organohalide Perovskites: Interplay of Spin–Orbit Coupling and Octahedra Tilting. *Nano Lett.* **2014**, *14*, 3608–3616.

# Chapter 4

# Electroluminescence blinking of $MAPbBr_3$ microcrystals


## Abstract

Halide perovskites are extremely capable of optoelectronic applications, especially LEDs, lasers, and other quantum devices. Their direct bandgap nature, bandgap tunability across the wide spectral range, defect tolerance leading to high photoluminescence quantum yield (PLQY), ambipolar charge transport, and cost-effective synthesis are all attractive features making them suitable for photovoltaic and light-emitting applications equally. However, the external quantum efficiency for a perovskite LED (PeLED) has not surpassed the conventional inorganic and organic LEDs. Apart from stability concerns of the perovskite active layer in the optoelectronic device, photoluminescence, and electroluminescence blinking decrease the efficiencies of devices like LED and solar cells. Several reports related to light-induced fluorescence blinking and spectral diffusion have led to deeper insights into charge carrier dynamics in perovskites. However, electroluminescence blinking is seldom studied. In this chapter, I study the electroluminescence blinking in $MAPbBr_3$ perovskite. The real-time observation of quenching and switching of emitting sites under applied voltage has led to the understanding of nonradiative losses in the material. By qualitatively studying the blinking at the ensemble and single-particle level, I model a mechanism of electroluminescence blinking. I find that individual EL emitting centers in a microcrystal show truncated power-law behavior for the ON- and OFF-time duration. This is a characteristic of type-A blinking involving a charging-discharging mechanism. However, an ensemble of microcrystal showed linear power-law behavior for the ON- and OFF-time duration. This is a characteristic of type-B blinking and is due to a charge carrier trapping-de-trapping mechanism. Thus, similar to PL blinking, EL blinking also shows type-A and type-B blinking.

## 4.1 Introduction

The first report of room temperature electroluminescence from perovskite by Friend *et al.* in 2014, showed an external quantum efficiency of 0.76% and 0.1% in the infrared and green regions, respectively.[1] In another 6 years, the research progressed to improve the efficiencies of green, red, and infrared perovskite LEDs (PeLEDs) to over 20%.[2-5] By tailoring perovskite layers in the form of quantum dot (QD) films of different thickness, use of different charge transport layers matching the perovskite valence bands and conduction bands, defect passivation[6,] and post-synthetic modifications,[3,7] the efficiency could be improved for PeLEDs. Apart from the selection of good transport layers or synthesizing good quality quantum dots, and optimizing the thickness of each layer, some external factors also influence the efficiency. The working range of PeLEDs is usually 3-6 V. This high voltage can lead to ion migration.[8,9] In addition, Joule heating can lead to degradation of the perovskite material. Hence, structural stability and thermal stability are affected under high voltage. The optical and electronic properties are hampered by light and moisture apart from the heat.[10] The operational lifetime is far less than that required for commercialization.[11] Most of the studies are directed to solve the above-said issues. However, photoluminescence (PL) and electroluminescence (EL) blinking observed in perovskites are also indirectly contributing to the decrease in efficiency of these materials.[12-23]

The PL blinking phenomenon was first reported by Nirmal *et al.* in 1996 from CdSe QDs.[24] It is a stochastic process in which the emission shows random fluctuations in their intensity with time. It is a result of reversible PL quenching. Since then, several studies were conducted on different types of inorganic quantum dots. Various models were proposed to understand the mechanism of PL blinking. Blinking was classified into type-A and type-B based on the mechanism adopted for intermittent and reversible PL quenching and their correlation with the photoluminescence lifetime.[25-30] Nonradiative Auger process controls charging-discharging events in semiconductor QDs which leads to type-A blinking. Traps act as centers of nonradiative recombination, and their activation and deactivation lead to type-B blinking. Although blinking is a dynamic process, they follow a power law-behavior over decades of the time unit.[25] The breakdown of power-law behavior was noticed in some cases with the appearance of exponential fall-off times.[25] Perovskites are also known to show PL blinking, and so far, they also follow a similar trend as that of other inorganic semiconductor quantum dots.

PL blinking has been reported from perovskite films, microcrystals (MCs), and nanocrystals (NCs).[12-23] In early reports of perovskite blinking, nonradiative Auger processes were not accounted for PL blinking. However, In $CsPbX_3$[15,16] and $FAPbX_3$[19] (X= Cl/Br/I) QDs, the PL blinking is conveniently explained with the help of Auger processes. A diffusion-controlled electron transfer mechanism (DCET) is widely used to explain systems that show truncated power-law behavior with an early cut-off time.[25,26] The OFF-state can be neutralized by many processes like charge carrier tunneling or activated de-trapping, in which case, the linearity in power-law behavior is lost, and a truncation appears. The truncation is also indicative of Auger ionization.

Although PL blinking is extensively studied, EL blinking is seldom noticed or explored. There have been few reports of electroluminescence blinking from perovskites.[31,32,33] EL blinking was seen from $MAPbBr_3$ microcrystal film where the emitting spots shifted with time reversibly, which was accounted for migration of ions under continuous bias.[31] Ngyuen *et al.* also reported EL blinking where the $MAPbBr_3$ single crystals prepared for LED studies showed electroluminescence blinking starting from 2 V.[32] Other than accounting for it due to differences in the rates of radiative and nonradiative processes at the crystal edges, no study was followed up. Vacha *et al.* studied EL blinking from $CsPbBr_3$ aggregates.[33] The charges are funneled and accumulated at a large nanocrystal based on the bandgap energy differences and lead to a particle selective carrier recombination. The origin and understanding of EL blinking remain unexplored. In this chapter, I study electroluminescence blinking from $MAPbBr_3$ microcrystals. The microcrystals prepared were sandwiched between two ITO glass plates which take the shape of an LED consisting of bare $MAPbBr_3$ as the emitting material. The observation of electroluminescence blinking in these crystals at voltages ranging from 3 V- 18 V allowed for an extensive study. Statistical analysis at the ensemble and single-particle level allowed me to clarify the blinking mechanism within these perovskites. Like PL blinking, EL blinking could also be described as type-A or type-B based on their power-law behavior. Understanding electroluminescence blinking and their suppression can help achieve greater efficiencies from perovskite-based LEDs in the future.

## 4.2 Results and discussion

### 4.2.1. Synthesis and characterization of perovskite microcrystals

The $MAPbBr_3$ microcrystals for photoluminescence (PL) and electroluminescence (EL) studies were prepared using the antisolvent vapor-assisted crystallization method (AVC), and inverse temperature crystallization method (ITC) on glass or ITO-coated glass substrate.[34,35,36] For the AVC method, a stoichiometric precursor solution was prepared using lead bromide and methylammonium hydrobromide. An appropriate amount of this solution was dropped on a glass/ ITO-coated glass substrate kept inside a chamber filled with dichloromethane as antisolvent. The crystals grown from this method were larger crystals of size greater than 100 μm.

To obtain smaller size crystals, an additive called *N*-cyclohexyl pyrrolidone (CHP) was added to the precursor solution before growing it by the ITC method. In the ITC method, an appropriate amount of precursor was dropped on a pre-heated glass/ ITO-coated glass substrate on a hot plate. Within minutes, uniform-sized smaller crystals grew with the assistance of CHP. Several additives can be used for controlling crystal size. CHP, on account of its high-boiling point, low vapor pressure, and apolar ring structure, helps to achieve crystal size control. Isolated $MAPbBr_3$ crystals could be obtained for PL and EL studies. PL properties were studied directly from the glass or ITO-coated glass containing the crystals. The crystals showed bright green luminescence on account of band-edge recombination. Figure 1 shows a PL image of the synthesized microcrystals of various crystal sizes under a 400 nm cw laser irradiation.

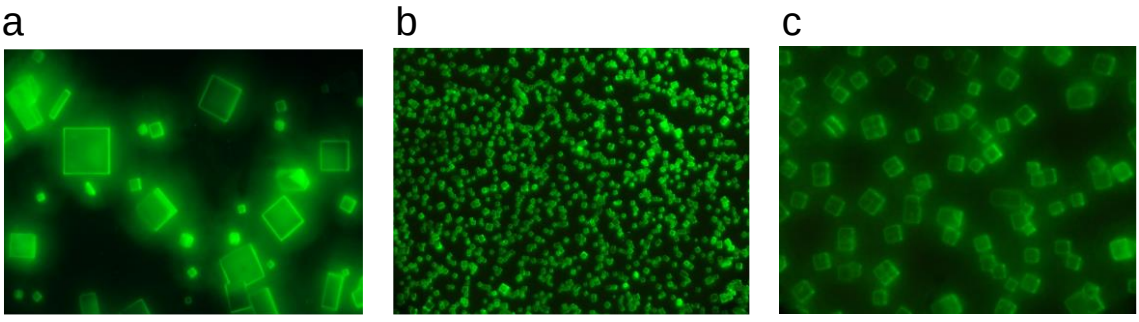


**Figure 1.** PL images of $MAPbBr_3$ MCs under 460 nm laser excitation. a) Larger microcrystals synthesized by AVC method, b) smaller microcrystals synthesized by ITC method using CHP additive (10x objective lens), and c) PL image of microcrystals in b under a 40x objective lens. Image size of (a,b) is 320x 240 $\mu m^2$, and (c) 80 x 60 $\mu m^2$.

For EL studies, $MAPbBr_3$ microcrystals synthesized on one ITO glass were sandwiched using another ITO glass, and the two ITOs were connected to a power supply through electrical leads. Polybutadiene was used as a spacer between the ITO plates to prevent short-circuiting. The crystals started showing EL from voltages as low as 3 V. However, the intensity was so low at lower voltages. With the increase in voltage, the intensity of EL emission increased, and also, more and more crystals started showing electroluminescence. Crystals also show many emitting sites within the center, which was characterized by blinking. The number of such emitting sites also increased with applied voltage. Figure 2 shows an EL image of microcrystals at various voltages. The crystals show multiple emitting centers within them. This can be seen in Figure 2a. Figure 2 (b,c) shows EL images collected from the same area under different voltage conditions. It could be seen that the number of emitting sites increased with an increase in voltage. Such an increase in the number of emitting centers can be attributed to the filling of energy states, preferably by the externally injected electrons and their radiative recombination with the holes.

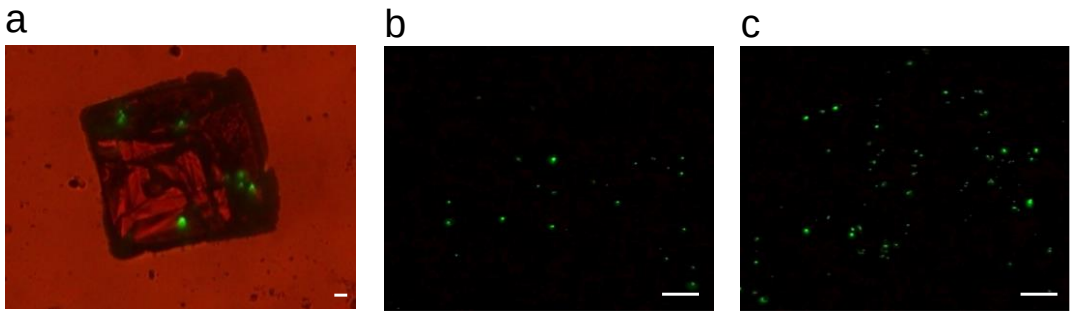


**Figure 2.** EL images of $MAPbBr_3$ microcrystals. a) a microcrystal showing EL at 10 V, multiple emitting centers within the crystal can be noticed (Scale bar corresponds to 10 μm). (b,c) EL image of the same area containing $MAPbBr_3$ microcrystals at 15 V and 18 V, respectively (the scale bar corresponds to 40 μm).

To assign the crystal structure for the synthesized $MAPbBr_3$ microcrystal, I carried out single-crystal XRD at room temperature. The single-crystal XRD pattern (Figure 3) shows diffraction peaks at $14.90^0$, $21.20^0$, $30.10^0$, $33.80^0$, $37.10^0$, $43.10^0$, $45.90^0$, and $48.60^0$. Using the diffraction angles in the Braggs law, the crystal planes were assigned as (100), (110), (200), (210), (211), (220), (300), and (310) respectively. Comparing these values with the XRD patterns of $MAPbBr_3$ in different literature suggested a cubic Pm3m phase for the as-synthesized $MAPbBr_3$ microcrystal.[13,37] The lattice parameter of the crystal was read from the software as 5.92Å.

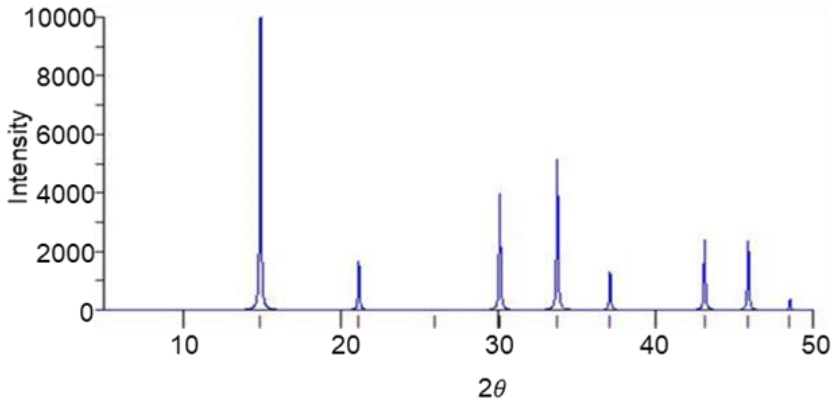


**Figure 3.** Single-crystal XRD pattern of the as-synthesized $MAPbBr_3$ microcrystal at 20 ℃.

### 4.2.2 Photoluminescence and electroluminescence properties of microcrystals

In order to understand the photoluminescence properties of the perovskite microcrystals synthesized by the AVC or ITC methods, first I collected PL spectra from them. The $MAPbBr_3$ microcrystals were excited by a 400 nm laser. The emission coming from the sample is passed through an objective lens followed by a long pass filter to isolate the PL from laser light. The PL was then sent to a fibreoptic spectrometer. The signal obtained is a background corrected spectrum of $MPAbBr_3$ microcrystal. An iris was used to collect the emission solely coming from the isolated microcrystal. The optical setup used is discussed in Chapter 2 of the thesis. Figure 4a shows the PL spectrum collected from a $MAPbBr_3$ microcrystal.

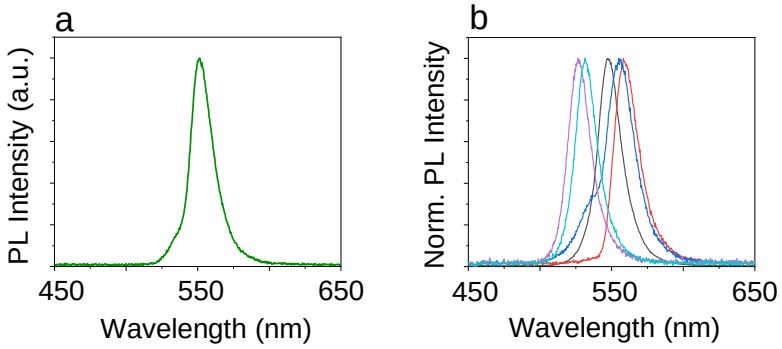


**Figure 4.** a) A PL spectrum of $MAPbBr_3$ MC showing emission centered at 550 nm, and b) PL spectra of $MAPbBr_3$ MCs of different sizes under 460 nm laser irradiation. The integration time used is 1s.

A PL maximum of about 550 nm accounts for the radiative recombination of charge carriers at the band edge. However, particle to particle differences in PL maxima was

seen. The PL spectra red-shifted with crystal size. Such a kind of red-shifting is noticed in larger crystals whose dimensions exceed light penetration depth of approximately 100nm limited by the one-photon excitation. This is shown in studies by Diab *et al.*[36] In crystals with dimensions larger than the light penetration depth, the emission from one end of the crystal can be reabsorbed before being collected as low-energy emissions from the other parts of the same crystal. Hence larger crystals always tend to show slightly red-shifted emissions in comparison to the smaller crystals. In figure 4b, such a red-shifting can be noticed with the increase in the size of $MAPbBr_3$ crystals.

Next, I studied the electroluminescence from the synthesized microcrystals by sandwiching the microcrystals synthesized on ITO glass with another ITO glass and applying a bias. $MAPbBr_3$ crystals showed 'blinking' EL under an applied voltage of 3 V- 18 V for hours. The applied voltage is sufficient to inject the charge carriers (the electrons and holes) into the perovskite active layer. The EL corresponds to the radiative recombination of the excited charge carriers. The EL from an isolated microcrystal is collected by an objective lens which is sent to a fibreoptic spectrometer. The EL spectra of $MAPbBr_3$ microcrystal showed continuous fluctuations in the emission signal both in intensity, spectral maximum as well as the full width at half maxima (FWHM) in the range of 540- 560 nm. Figure 5a shows the EL spectra collected from an isolated $MAPbBr_3$ microcrystal at an integration time of 1s. Figures 5b and 5c show a plot of PL spectral maxima and FWHM obtained from the crystal studied in Figure 5a against voltage starting from 9 to 18 V, respectively. As can be seen, the spectral maxima and FWHM shows extreme fluctuations with respect to voltage.

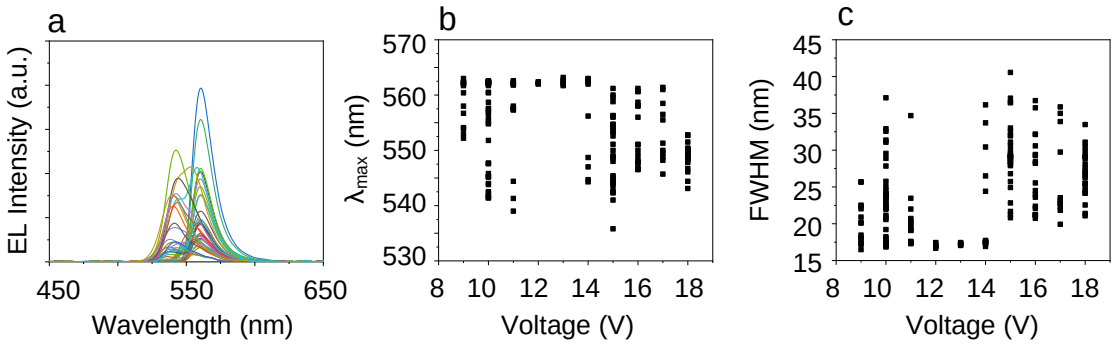


**Figure 5.** a) EL spectra collected from a large single $MAPbBr_3$ MC at 10 V. b) EL spectra collected from a small $MAPbBr_3$ microcrystal at 10 V. Fluctuations in spectral intensity can be seen. An integration time of 100 ms was used.

The reason for spectral fluctuations can be many. One of the reasons can be the photon-reabsorption-emission phenomenon. In large crystals of perovskites, emissions coming from one end of the crystal can be reabsorbed at other parts and will be later emitted with lower energy. Studies performed on $MAPbBr_3$ single crystals by depth-resolved cathodoluminescence spectroscopy show evidence for the photon-reabsorption phenomenon.[38] In the above experiments, I use large microcrystals. I also collect the emission from the bottom side of the device. Hence the emission coming from the crystals from various distances can undergo reabsorption events before being collected. Another possibility is that there can be several closely spaced energy states within the crystal. The recombination coming from these energy states can be different in energy and thus can exhibit closely spaced spectra. Apart from this, it is proven that Joule heating due to long operational time can lead to red-shifting. The associated material degradation can also lead to spectral shifting.[39] In the above sample, I observe dynamic spectral shifting. The reasons for EL spectral shifts observed in $MAPbBr_3$ microcrystals can be the combined effects of processes like re-absorption emission, Joule heating, or material degradation. Trap state emission EL has also been discussed in some reports accounting for a shoulder in the broad EL spectrum of $CsPbBr_3$ perovskite.[11] Apart from spectral shifts, intensity fluctuations are also seen in the above sample. Such a fluctuation can come from the difference in the density of nonradiative centers surrounding various emitting centers within a perovskite. I also observed that smaller $MAPbBr_3$ microcrystals of size ~10 µm also showed such spectral and intensity fluctuations. This is shown in Figures 6a and 6b. Figure 6 shows the EL collected from small $MAPbBr_3$ microcrystal at 10 V, and Figure 6b shows the EL spectra collected from the same microcrystal at 13 V.

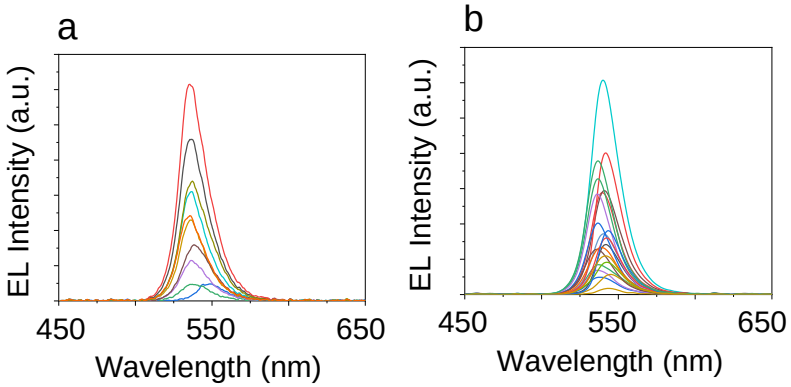


**Figure 6.** EL spectra collected from smaller $MAPbBr_3$ microcrystals of size ~ 10 µm at a) 10 V and b) 13 V. An integration time of 1s is used to record the spectrum.

Such a fluctuating nature of EL spectra can be associated with the excitation of only particular energy states at a time when it is locally excited by the applied voltage. On the other hand, the absence of any fluctuations in the PL spectrum of the $MAPbBr_3$ microcrystal comes from the fact that the PL spectrum obtained is averaged as the emission occurs from a globally excited crystal.

### 4.2.3 Single-particle photoluminescence and electroluminescence studies of $MAPbBr_3$ microcrystals

The observation of blinking EL from the $MAPbBr_3$ microcrystals led me to utilize the single-particle micro spectroscopy method to further study its details. PL blinking is widely known in metal halide perovskite, and several models were proposed to explain its origin. However, there are no studies done so far to understand the origin of EL blinking. Here, similar to single-particle PL blinking analysis, I study the $MAPbBr_3$ microcrystals for EL and PL blinking. The $MAPbBr_3$ microcrystals are excited either by light or an applied voltage. The emission coming out is collected through an objective lens passes through a >500 nm long-pass filter, and was sent to an EMCCD camera. A video is recorded for a fixed time at 33 ms exposure time. From the video, a single microcrystal is studied, and a time-dependent PL or EL intensity profile is collected.

First of all, I studied the microcrystals for PL blinking. I used $MAPbBr_3$ microcrystals synthesized on a glass slide by the AVC method for single-particle studies. The microcrystal was excited by a 400 nm laser. The emission collected by the objective lens passed through a > 500 nm filter was sent to the EMCCD camera. The video was analyzed, and the PL trajectory was collected from the whole microcrystal by fixing the region of interest (ROI). PL blinking from a $MAPbBr_3$ microcrystal of size >10 μm so did not show any blinking profile.

Figure 7 shows a PL trajectory collected from a $MAPbBr_3$ microcrystal excited by a 400 nm laser. The red line corresponds to the background signal, and the black line corresponds to the PL intensity profile. As is seen in the figure, there were no temporal fluctuations observed in PL intensity. Thus, the single-particle analysis of a large microcrystal did not give much information regarding PL blinking. Surprisingly, the single-particle studies on the $MAPbBr_3$ microcrystals of sizes in the micrometer scale showed EL blinking features. The experimental setup was the same. The $MAPbBr_3$

microcrystals were synthesized on an ITO glass slide by AVC or ITC method to get larger and smaller microcrystals, respectively. The $MAPbBr_3$ containing ITO glass was sandwiched with another ITO glass. The leads were connected to a voltage supply, and an appropriate voltage was applied across the ITO glass plates, which served as electrodes. The sample shows EL at a very low voltage starting from 3 V. The emission was collected by an objective lens and was directly sent to the EMCCD camera. The single-particle video was acquired for one minute at 33ms exposure time. Using a 10x objective lens, several microcrystals were seen in the selected area in the video. Such video was collected for several voltages. After the video was collected, the ROI was fixed for one whole microcrystal. The EL trajectories collected from the microcrystal as a whole showed a blinking phenomenon. Figure 7b shows an EL trajectory collected from a single $MAPbBr_3$ microcrystal at 10 V.

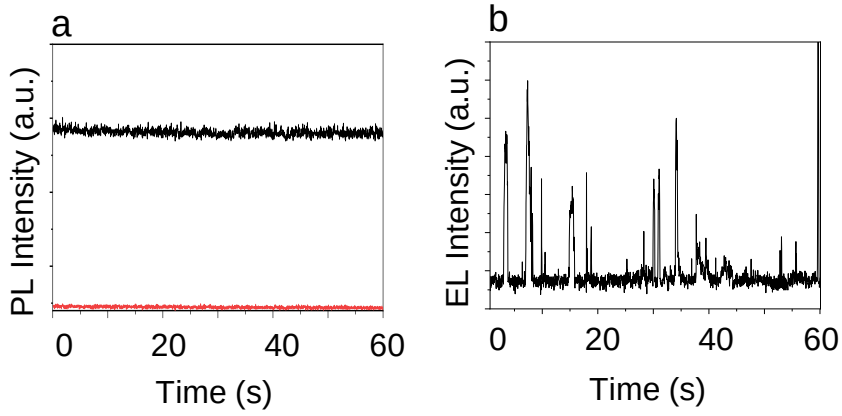


**Figure 7.** a) a PL trajectory of a single $MAPbBr_3$ MC excited by a 460 nm cw laser. The red line corresponds to background noise, and b) an EL intensity trajectory of a single $MAPbBr_3$ MC at 10 V.

The EL trajectories show blinking with high-intensity EL states and low-intensity EL states fluctuating with time. The high-intensity EL states had a very short time period, while low-intensity EL states remained for a long-time scale. These states were differentiated as ON- and OFF-states based on a threshold value above which they are termed ON, below which they are termed OFF-state. It is seen that crystal remains most of the time in OFF-state. Blinking is a result of competing radiative and nonradiative recombination processes, which are occurring repeatedly and reversibly. The difference in the rates of these recombination processes can be the cause of such temporal and intensity fluctuations. The burst occurrence of intensity can be associated with the

accumulation of charge carriers, which suddenly recombine at a particular site, while low-intensity occurrences are coming radiative recombination events occurring at a uniform rate.

### 4.2.4 Comparison of electroluminescence blinking and photoluminescence blinking

Although a single $MAPbBr_3$ microcrystal did not show any blinking features, $MAPbBr_3$ nanocrystals (NCs) in the sample showed PL blinking. The PL blinking trajectory of $MAPbBr_3$ nanocrystals excited with a 460 nm laser is shown in Figure 8(a,b) below. Also shown in Figure 8c is an EL trajectory of a small blinking $MAPbBr_3$ microcrystal (size of ca 7 μm) at around 10 V.

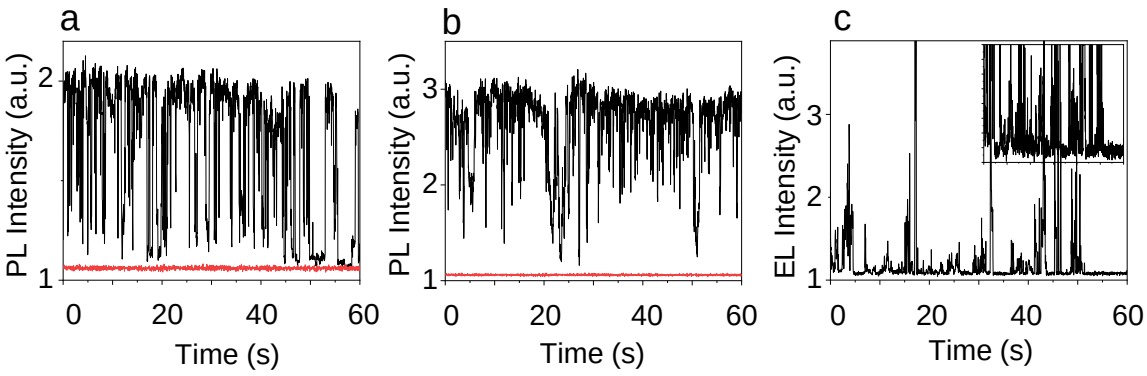


**Figure 8.** (a,b) PL trajectories of $MAPbBr_3$ NCs under 460 nm laser irradiation. The red line corresponds to background noise. c) EL trajectory of a single $MAPbBr_3$ MC at 10 V. Zoomed-in image of the trajectory is shown in the inset.

The PL trajectories show blinking, which clearly distinguishes the ON- and OFF-states. The GREY state or intermediate intensity states have been seen in some NCs and suggest the presence of multiple emitting states in them. PL blinking in nanocrystals is mostly accounted as type-A blinking associated with a charging-discharging mechanism. An EL trajectory obtained from a small $MAPbBr_3$ microcrystal also shows temporal intensity fluctuation similar to that of a larger microcrystal. However, the mechanism associated with EL blinking is still unknown.

Hence, in the following sections, I attempt to understand the origin of electroluminescence blinking in $MAPbBr_3$ perovskite by collecting single-particle trajectories and performing a statistical analysis; and also deduce a mechanism for the electroluminescence blinking phenomenon.

### 4.2.5 Electroluminescence blinking within a single $MAPbBr_3$ microcrystal

I found that a larger $MAPbBr_3$ microcrystal of 100 μm or more showed multiple emitting centers within them that were blinking as well. Using the single-particle instrument, I collected a video of a large microcrystal showing multiple emitting spots in them. Figure 9 shows single-particle images of one such crystal showing multiple emitting centers. The images extracted from the single-particle video are shown in Figure 9(a-e). An overlaid image is developed from these images and is shown in Figure 9f. The crystal showed at least one emitting center in a time frame of 33 ms. There was particle-to-particle variation in the number of these emitting sites. An important observation was that the emitting sites continuously switched their positions.

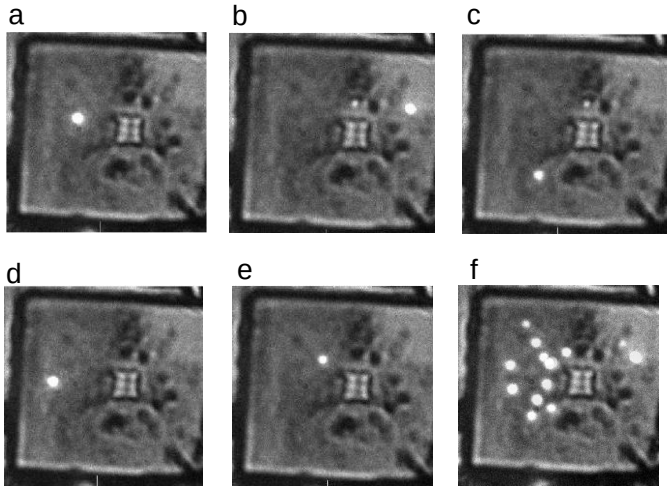


**Figure 9. (**a-f) single-particle images of a microcrystal showing multiple emitting centers, b) the overlaid image of the single microcrystal. A temporal fluctuation in intensity of one of the emitting sites is shown alongside and, c) EL trajectory of one of the emitting centers shown in 'b'. (Image size is 160 x 160 $\mu m^2$)

Figure 10 shows the single-particle images of frames showing temporal fluctuations in the intensity of an emitting center. One frame corresponds to 33 ms.

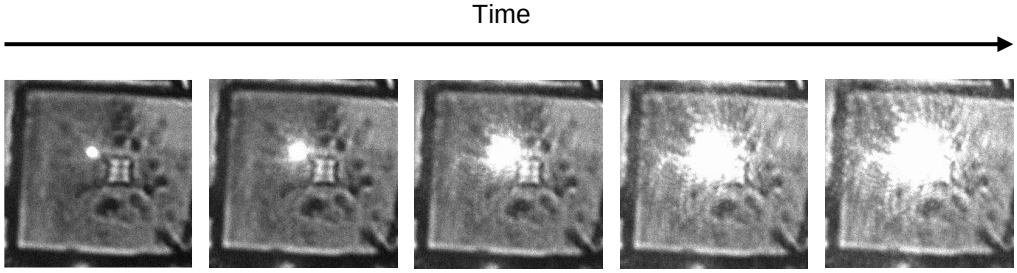


**Figure 10.** A temporal fluctuation in intensity of one of the emitting sites

Next, I analyzed each of these emitting sites within the microcrystal shown in the above figures. EL trajectories of each of these emitting centers were collected, and the EL blinking trajectory of one of the emitting centers is shown in Figure 11. The blinking phenomena are associated with ON and OFF processes where the ON-state corresponds to the radiative recombination at the emitting center, and the OFF-state corresponds to the quenching of radiative processes by processes like trapping of charge carrier and other nonradiative processes. The EL trajectories are characterized by high-intensity EL periods and low-intensity EL periods, as shown in the figure below.

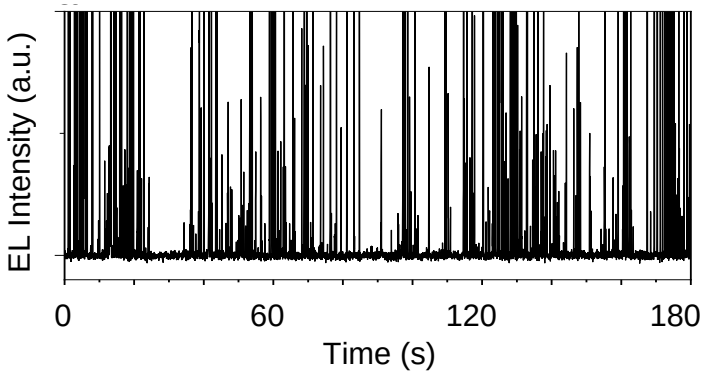


**Figure 11.** EL intensity trajectory collected from an emitting center within a large $MAPbBr_3$ microcrystal at 16V.

It was found that EL trajectories showed center-to-center variations in blinking features. The random fluctuating behavior from one emitting center alone cannot give a general conclusion about the origin or mechanism of EL blinking. Hence a statistical analysis was performed as follows. EL trajectories were collected from several centers within a single microcrystal. A threshold intensity was determined for each trajectory, and the events were classified as either ON or OFF based on it. The events with a value greater than the threshold are termed as ON, and smaller than the threshold is termed as OFF. Following this, the ON- and OFF-time of a particular event were calculated by adding the time for consecutive events occurring. A probability density distribution for ON- and OFF-time ($P(\tau_{ON/OFF})$ was calculated from occurrences of respective events based on the following equation. $P(\tau_{ON/OFF}) = \frac{N(\tau_{ON/OFF})}{N^{tot}_{ON/OFF}} \frac{1}{\delta\tau_{ON/OFF}}$. To get the probability distribution, the number of occurrences of one particular event i.e., ON or OFF ($N(\tau_{ON/OFF}$)) is divided by the total number of events ($N^{tot}_{ON/OFF}$) and also the average time duration between preceding and succeeding events ($\delta\tau_{ON/OFF}$).

In the case of conventional semiconductor QD blinking, a power law, $P(\tau_i) \propto \tau_i^{-m}$ is used to describe the probability ($P(\tau_i)$) of an ON- or OFF- time, where m is the power-law exponent.[25-30] The OFF-time probability usually follows a linear power-law on a long timescale, whereas the ON-time probability follows an exponentially truncated power-law, $P(\tau_i) \propto \tau_i^{-m} e^{-\tau_i/\tau_c}$, where $\tau_c$ is the truncation time. If the probability density plot shows a truncated power-law behavior, they show type-A blinking that occurs by a charging-discharging process. In a charging-discharging type of blinking, an ON event is resulted due to the radiative recombination of charge carriers. However, excess charge in the QD leads to its ionization, and several fast nonradiative recombination processes like Auger recombination leads to switching off the ON-state. Only a charge neutralization can bring the QD back to the ON-state. The truncated nature of a particular process, be it ON or OFF, implies multiple events associated with different rates. Another type of blinking is called type-B blinking. Such a type of blinking is characterized by a linear power-law behavior for ON and OFF-time probability distribution. The linearity of the power-law distribution implies that an event with a single rate constant sufficiently describes the ON and OFF process. In type-B blinking, the trapping and de-trapping of charge carriers lead to OFF and ON events, respectively. After the photo-excitation, if the charges get trapped, the QD goes to OFF-state. Only the de-trapping of charge carriers can bring them back to ON-state.

Similar to QDs, I plotted a probability distribution plot for the ON- and OFF-times collected from the EL trajectories of multiple emitting sites in the large $MAPbBr_3$ microcrystal studied above. The probability distribution plots for ON- and OFF-times are shown in Figures 12a and 12b, respectively.

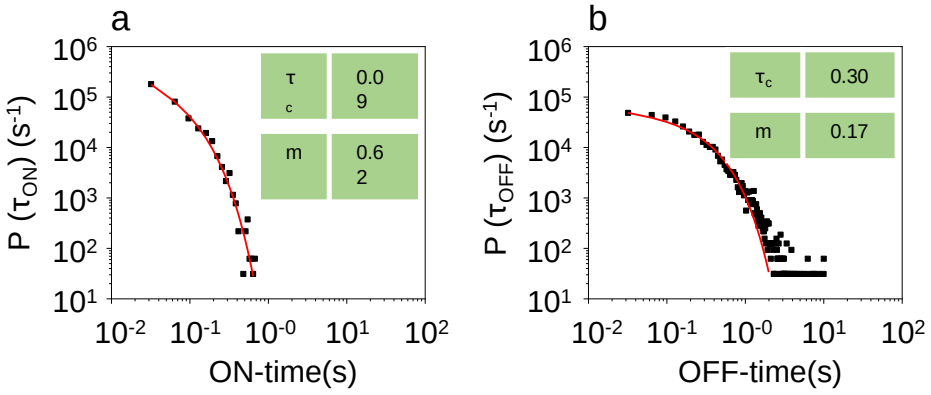


**Figure 12.** a) ON-time and b) OFF-time probability distribution plots for multi-emitting centers in a large microcrystal. The red curves correspond to the fitting. Fitting constants are shown in the insets.

The ON-time and OFF-time probability distribution curves plotted for multiple emitting centers shown in Figure 12 showed a truncated power-law behavior with a very early cut-off time for ON and OFF-time durations. The fall-off was seen at 0.06s s for the ON-time and 0.17s for the OFF-time probability distribution curves. Based on the above observation, a type-A blinking is seen, which is due to charging-discharging processes.

### 4.2.6 Electroluminescence blinking in an ensemble of $MAPbBr_3$ microcrystals

I also performed EL studies on smaller $MAPbBr_3$ microcrystals at various voltages. The smaller crystals of dimensions approximately 10 µm were synthesized using the ITC method. The details of the synthesis are mentioned in chapter 2. Using the single-particle set-up described in the above sections, I studied the EL blinking. An area containing several microcrytsals showing EL blinking was chosen for ensemble studies. I collected EL trajectories from several small microcrystals by fixing the ROI (region of interest) on a whole crystal at various voltages. This is shown in Figure 13.

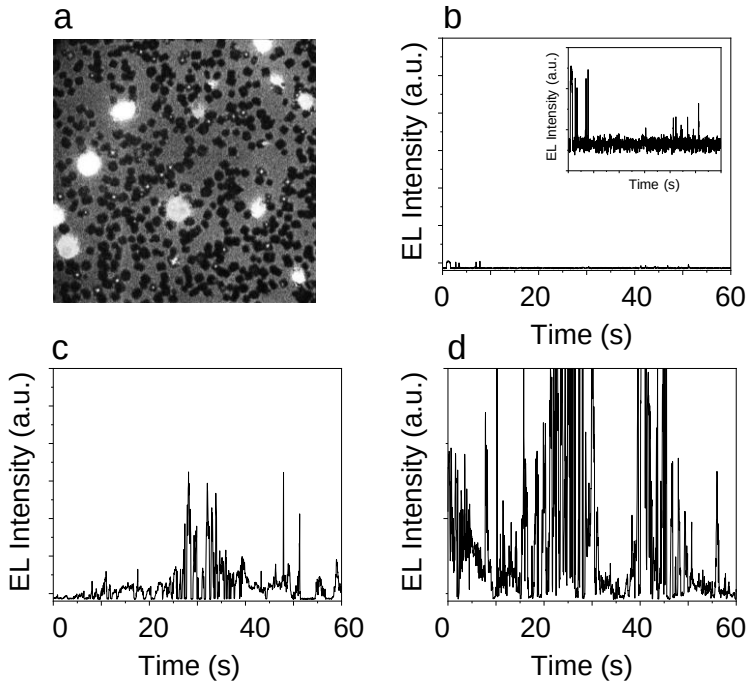


**Figure 13.** a) A single particle image showing several small $MAPbBr_3$ showing EL blinking, image size is 335x 335 $\mu m^2$, b) EL blinking trajectory of a small $MAPBbr_3$ microcrystal at b) 5 V, c) 10 V, and d) 15 V, respectively. The inset in (b) is a zoomed-in image of the EL trajectory.

Figure 13a shows the single-particle image containing several $MAPbBr_3$ microcrystals, which showed blinking starting from a very low voltage. It was seen that with the increase

in voltage, more and more crystals started showing EL. Also, the intensity of EL blinking increased with voltage. The EL trajectories collected for a particular microcrystal at 5 V, 10 V, and 15 V are shown in Figure 13b, c, and d, respectively. The increase in the intensity with an increase with voltage is because of an increase in the number of externally injected charge carriers and their radiative recombination.

Several such trajectories were collected from different crystals at various voltages from 5-15 V. But all of them showed particle-to-particle differences. Hence a statistical analysis was performed to understand the blinking behavior. I used namely 5 V, 10 V, and 15 V for the analysis. A probability distribution plot for ON- and OFF-times are plotted for EL trajectories collected for each voltage and is shown in Figure 14.

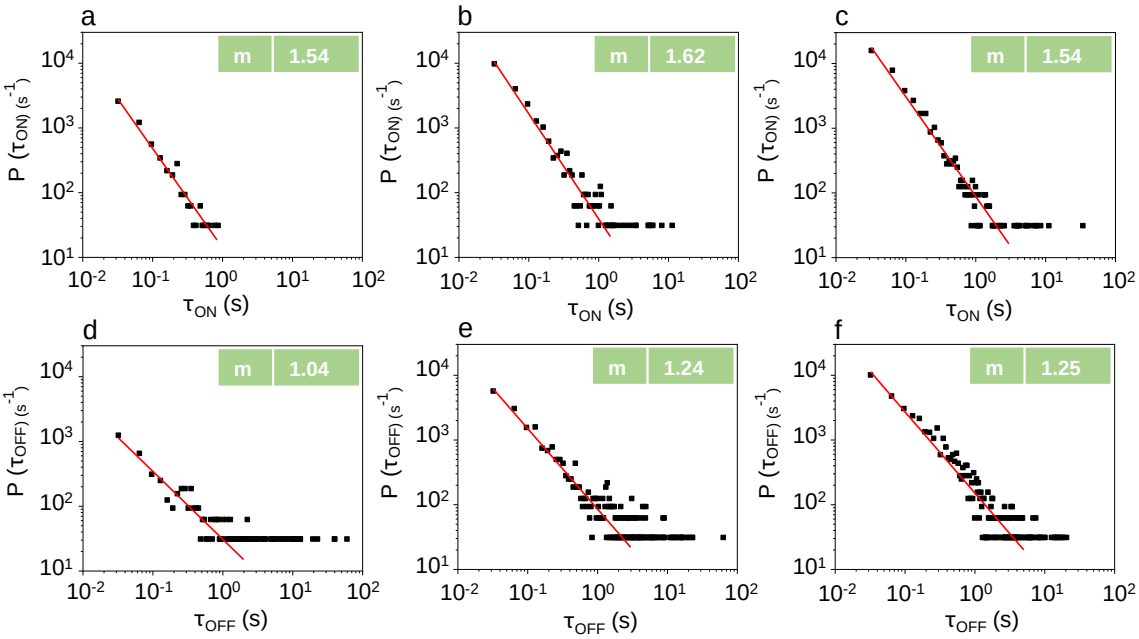


**Figure 14.** (a-c) ON-time probability distribution plots at 5 V, 10 V, and 15 V, and (d-f) OFF-time probability distribution plots at 5 V, 10 V, and 15 V, respectively, for an ensemble of $MAPbBr_3$ microcrystals.

In stark contrast, the ON-time and OFF-time probability distribution curves of an ensemble of crystals for all voltages studied as shown in Figure 14, fit with a linear power-law. The power-law exponents for the ensemble level single-particle EL blinking studies fit with a linear power-law exponent, m, in the range -0.9 to -1.6. This value is similar to the reported nanocrystal PL blinking power-law exponents.[30] As can be seen from Figure 14, it is also noticeable that the ON-times is shorter by a decade unit of time than the OFF-times at all voltages. A short ON-time is suggestive of a higher probability of the

charging process leading to nonradiative recombination. The fitting of ON-time and OFF-time curves by linear power-law behavior is suggestive of type-B blinking. Type-B blinking follows a trapping-de-trapping mechanism. I believe that the halide vacancies in the perovskite act as traps that can quench emitting sites. Sheblykin *et al.* had proposed a super-trap model for the PL blinking in large $MAPbI_3$ crystals.[40,41] The super-trap can act as a donor-acceptor pair which can trap electrons as well as the hole. Such a super-trap exists anywhere within the large crystal. When a super trap switches between active and passive states, blinking results. Such traps can lead to spontaneous quenching and hence results in short ON-time. This OFF-state then continues as long as the super trap is passivated or relocated.

### 4.2.7 The mechanism of electroluminescence blinking in $MAPbBr_3$ microcrystals

It was seen that the blinking observed from a crystal with multi-emitting centers and an ensemble of microcrystal showed differences in the type of EL blinking as noticed from the power-law distributions of their ON- and OFF-times. The next question is how to correlate the different blinking mechanisms observed in the same microcrystals, i.e., a type-A blinking for individual emitting centers within a crystal and type-B blinking for an ensemble of microcrystals. In a large microcrystal with multi-emitting centers, I observe a random switching of emitting centers. Such a random switching of emitting centers can be thought of as redistribution of the trap states. This is similar to 'super traps' observed in large $MAPbI_3$ perovskites, which act as mobile PL quenchers as reported by Scheblykin *et al.*[40,41] But with the truncated nature observed in the power-law behavior of a crystal with multiple emitting centers, different processes with different rate constants are necessary to account for the ON-and OFF-states.

However, in a single microcrystal, the processes with several rate constants are expressed as a single rate constant leading to a power-law behavior. Thus, an averaging process leads to the linear power behavior that became prominent in the case of the study from different emitting centers within a crystal. In both cases, the migrating trap act as the EL quencher. The single-particle study has thus clearly helped in understanding the mechanism of EL blinking in $MAPbBr_3$ perovskite microcrystals. Figure 15 shows a scheme for type-B blinking shown in $MAPbBr_3$ microcrystal in which a migrating trap like halogen vacancy quenching an EL emitting center. The type-A blinking is a process similar to the charging-discharging mechanism occurring by the Auger process. Here, the

excess charge injected into the conduction levels of $MAPbBr_3$ causes the charging of the particular state by creating a negative trion state. The Auger type recombination of this state leads to nonradiative recombination or the OFF-state. In Figure 15b (i) and (ii), I represent the type-A and type-B blinking mechanisms suitable for the EL blinking in $MAPbBr_3$ microcrystal.

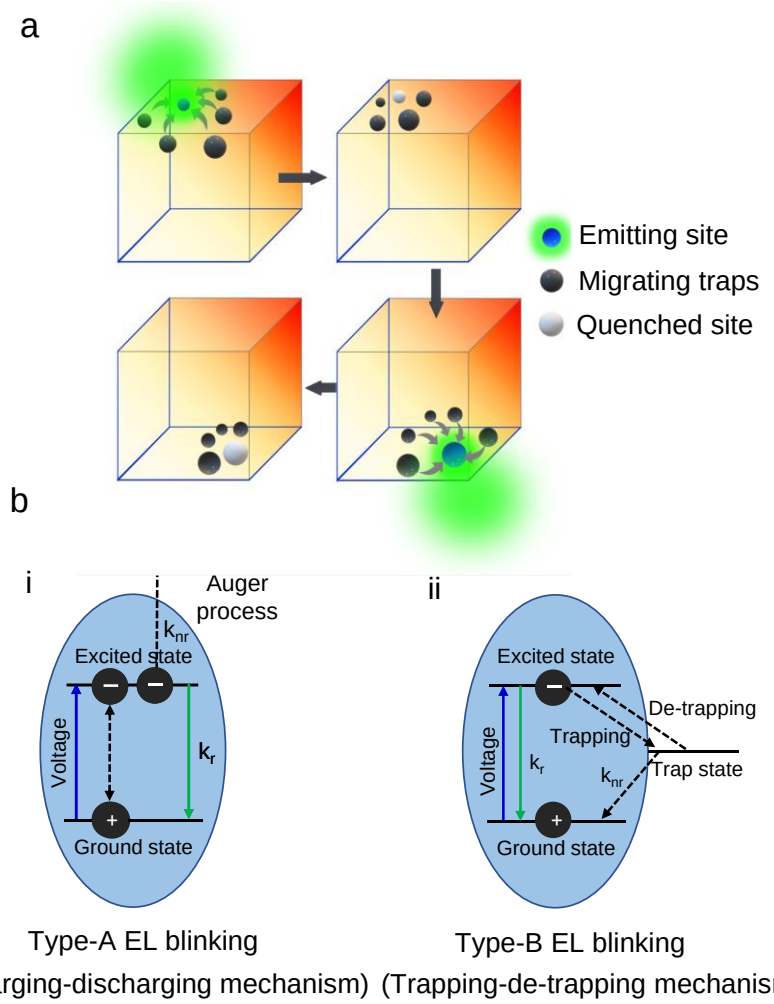


**Figure 15.** a) A scheme showing the role of migrating traps in random switching of emitting centers, and b) (i) type-A mechanism for EL blinking and (ii) type-B mechanism for EL blinking.

### 4.3 Conclusion

In this chapter, I studied electroluminescence blinking in $MAPbBr_3$ microcrystals. Methylammonium lead bromide ($MAPbBr_3$) perovskite microcrystals were synthesized on an ITO-coated glass substrate by using antisolvent vapor-assisted crystallization and inverse temperature crystallization. The samples for EL studies were prepared by sandwiching the ITO-coated glass plate containing $MAPbBr_3$ microcrystals with another

ITO-coated glass substrate. These crystals show well-defined ON-OFF EL blinking under 3-18 V. The EL and PL spectra were recorded from individual microcrystals. The EL and PL trajectories of these microcrystals were obtained by using a single particle microspectroscopy system. I observed EL blinking in the case of $MAPbBr_3$ microcrystal. However, no such blinking was observed in PL from these microcrystals. The EL blinking was completely different from a nanocrystal PL blinking. Blinking is a result of nonradiative losses during carrier recombination processes. I verify the origin of such a loss in an EL device to be blinking by switching carrier recombination between the emitting and quenching sites. I detect randomly switching multiple EL centers within a $MAPbBr_3$ perovskite single particle. The EL intensity trajectories and spectra of single particles reveal that the switching of blinking between a bright and a dark center is associated with changes to the radiative and nonradiative rates of injected charge carriers. The ON-time and OFF-time probability distributions for the individual emitting centers show a truncated power-law behavior with an early cut-off time, suggesting multiple charge recombination processes. However, the ON-time and OFF-time probability distributions of a particle as a whole fit with the linear power-law behavior. The EL images, spectra, intensity trajectories, and ON- and OFF-time probability distributions show that the EL blinking of the individual emitting centers is due to the charging-discharging mechanism, whereas the random switching of the emitting centers is due to the trapping- de-trapping mechanism. Electroluminescence (EL) and photoluminescence (PL) blinking of perovskite crystals is a bottleneck to achieving high-efficiency LEDs, lasers, and quantum optical devices. Hence the mechanism of EL blinking I proposed, and its understanding can help enhance the efficiency of optical device applications like LEDs, lasers, and photodetectors.

## References


1. Tan, Z. K.; Moghaddam, R. S.; Lai, M. L.; Docampo, P.; Higler, R.; Deschler, F.; Price, M.; Sadhanala, A.; Pazos, L. M.; Credgington, D.; Hanusch, F.; Bein, T.; Snaith, H. J.; Friend, R. H. Bright Light-Emitting Diodes Based on Organometal Halide Perovskite. *Nat. Nanotechnol.* **2014**, *9*, 687–692.

2. Lin, K.; Xing, J.; Quan, L. N.; de Arquer, F. P. G.; Gong, X.; Lu, J.; Xie, L.; Zhao, W.; Zhang, D.; Yan, C.; Li, W.; Liu, X.; Lu, Y.; Kirman, J.; Sargent, E. H.; Xiong, Q.; Wei, Z. Perovskite Light-Emitting Diodes with External Quantum Efficiency Exceeding 20 percent. *Nature* **2018**, *562*, 245–248.

3. Cao, Y.; Wang, N.; Tian, H.; Guo, J.; Wei, Y.; Chen, H.; Miao, Y.; Zou, W.; Pan, K.; He, Y.; Cao, H.; Ke, Y.; Xu, M.; Wang, Y.; Yang, M.; Du, K.; Fu, Z.; Kong, D.; Dai, D.; Jin, Y.; Li, G.; Li, H.; Peng, Q.; Wang, J.; Huang, W. Perovskite Light-Emitting Diodes Based on Spontaneously Formed Submicrometre-Scale Structures. *Nature* **2018**, *562*, 249–253.

4. Chiba, T.; Hayashi, Y.; Ebe, H.; Hoshi, K.; Sato, J.; Sato, S.; Pu, Y.-J.; Ohisa, S.; Kido, J. Anion-Exchange Red Perovskite Quantum Dots with Ammonium Iodine Salts for Highly Efficient Light-Emitting Devices. *Nat. Photonics* **2018**, *12*, 681–687.

5. Zhao, B.; Bai, S.; Kim, V.; Lamboll, R.; Shivanna, R.; Auras, F.; Richter, J. M.; Yang, L.; Dai, L.; Alsari, M.; She, X.-J.; Liang, L.; Zhang, J.; Lilliu, S.; Gao, P.; Snaith, H. J.; Wang, J.; Greenham, N. C.; Friend, R. H.; Di, D. High-Efficiency Perovskite–Polymer Bulk Heterostructure Light-Emitting Diodes. *Nat. Photonics* **2018**, *12*, 783–789.

6. Xu, W.; Hu, Q.; Bai, S.; Bao, C.; Miao, Y.; Yuan, Z.; Borzda, T.; Barker, A. J.; Tyukalova, E.; Hu, Z.; Kawecki, M.; Wang, H.; Yan, Z.; Liu, X.; Shi, X.; Uvdal, K.; Fahlman, M.; Zhang, W.; Duchamp, M.; Liu, J.-M.; Petrozza, A.; Wang, J.; Liu, L.-M.; Huang, W.; Gao, F. Rational Molecular Passivation for High-Performance Perovskite Light-Emitting Diodes. *Nat. Photonics* **2019**, *13*, 418–424.

7. Bohn, B. J.; Tong, Y.; Gramlich, M.; Lai, M. L.; Döblinger, M.; Wang, K.; Hoye, R. L. Z.; Müller-Buschbaum, P.; Stranks, S. D.; Urban, A. S.; Polavarapu, L.; Feldmann, J. Boosting Tunable Blue Luminescence of Halide Perovskite Nanoplatelets through Postsynthetic Surface Trap Repair. *Nano Lett.* **2018**, *18*, 5231–5238.

8. Birkhold, S. T.; Precht, J. T.; Liu, H.; Giridharagopal, R.; Eperon, G. E.; Schmidt-Mende, L.; Li, X.; Ginger, D. S. Interplay of Mobile Ions and Injected Carriers Creates Recombination Centers in Metal Halide Perovskites under Bias. *ACS Energy Lett.* **2018**, *3*, 1279–1286.

9. Yuan, Y.; Wang, Q.; Shao, Y.; Lu, H.; Li, T.; Gruverman, A.; Huang, J. Electric-Field-Driven Reversible Conversion Between Methylammonium Lead Triiodide Perovskites and Lead Iodide at Elevated Temperatures. *Adv. Energy Mater.* **2016**, *6*, 1501803.

10. Cho, H.; Kim, Y.-H.; Wolf, C.; Lee, H.-D.; Lee, T.-W. Improving the Stability of Metal Halide Perovskite Materials and Light-Emitting Diodes. *Adv. Mater.* **2018**, *30*, 1704587.

11. Wei, Z.; Xing, J. The Rise of Perovskite Light-Emitting Diodes. *J. Phys. Chem. Lett.* **2019**, *10*, 3035–3042.

12. Tian, Y.; Merdasa, A.; Peter, M.; Abdellah, M.; Zheng, K.; Ponseca, C. S.; Pullerits, T.; Yartsev, A.; Sundström, V.; Scheblykin, I. G. Giant Photoluminescence Blinking of Perovskite Nanocrystals Reveals Single-Trap Control of Luminescence. *Nano Lett.* **2015**, *15*, 1603–1608.

13. Zhu, F.; Men, L.; Guo, Y.; Zhu, Q.; Bhattacharjee, U.; Goodwin, P. M.; Petrich, J. W.; Smith, E. A.; Vela, J. Shape Evolution and Single Particle Luminescence of Organometal Halide Perovskite Nanocrystals. *ACS Nano* **2015**, *9*, 2948–2959.

14. Wen, X.; Ho-Baillie, A.; Huang, S.; Sheng, R.; Chen, S.; Ko, H. C.; Green, M. A. Mobile Charge-Induced Fluorescence Intermittency in Methylammonium Lead Bromide Perovskite. *Nano Lett.* **2015**, *15*, 4644–4649.

15. Tachikawa, T.; Karimata, I.; Kobori, Y. Surface Charge Trapping in Organolead Halide Perovskites Explored by Single-Particle Photoluminescence Imaging. *J. Phys. Chem. Lett.* **2015**, *6*, 3195–3201.

16. Hu, F.; Zhang, H.; Sun, C.; Yin, C.; Lv, B.; Zhang, C.; Yu, W. W.; Wang, X.; Zhang, Y.; Xiao, M. Superior Optical Properties of Perovskite Nanocrystals as Single Photon Emitters. *ACS Nano* **2015**, *9*, 12410–12416.

17. Park, Y. S.; Guo, S.; Makarov, N. S.; Klimov, V. I. Room Temperature Single-Photon Emission from Individual Perovskite Quantum Dots. *ACS Nano* **2015**, *9*, 10386–10393.

18. Swarnkar, A.; Chulliyil, R.; Ravi, V. K.; Irfanullah, M.; Chowdhury, A.; Nag, A. Colloidal CsPbBr3 Perovskite Nanocrystals: Luminescence beyond Traditional Quantum Dots. *Angew. Chemie - Int. Ed.* **2015**, *54*, 15424–15428.

19. Yuan, H.; Debroye, E.; Caliandro, G.; Janssen, K. P. F.; Van Loon, J.; Kirschhock, C. E. A.; Martens, J. A.; Hofkens, J.; Roeffaers, M. B. J. Photoluminescence Blinking of Single-Crystal Methylammonium Lead Iodide Perovskite Nanorods Induced by Surface Traps. *ACS Omega* **2016**, *1*, 148–159.

20. Trinh, C. T.; Minh, D. N.; Ahn, K. J.; Kang, Y.; Lee, K. G. Organic-Inorganic $FAPbBr_3$ Perovskite Quantum Dots as a Quantum Light Source: Single-Photon Emission and Blinking Behaviors. *ACS Photonics* **2018**, *5*, 4937–4943.

21. Seth, S.; Ahmed, T.; Samanta, A. Photoluminescence Flickering and Blinking of Single $CsPbBr_3$ Perovskite Nanocrystals: Revealing Explicit Carrier Recombination Dynamics. *J. Phys. Chem. Lett.* **2018**, *9*, 7007–7014.

22. Pathoor, N.; Halder, A.; Mukherjee, A.; Mahato, J.; Sarkar, S. K.; Chowdhury, A. Fluorescence Blinking Beyond Nanoconfinement: Spatially Synchronous Intermittency of Entire Perovskite Microcrystals. *Angew. Chemie* **2018**, *130*, 11777–11781.

23. Gibson, N. A.; Koscher, B. A.; Alivisatos, A. P.; Leone, S. R. Excitation Intensity Dependence of Photoluminescence Blinking in $CsPbBr_3$ Perovskite Nanocrystals. *J. Phys. Chem. C* **2018**, *122*, 12106–12113.

24. Nirmal, M.; Dabbousi, B. O.; Bawendi, M. G.; Macklin, J. J.; Trautman, J. K.; Harris, T. D.; Brus, L. E. Fluorescence Intermittency in Single Cadmium Selenide Nanocrystals. *Nature* **1996**, *383*, 802–804.

25. Galland, C.; Ghosh, Y.; Steinbrück, A.; Sykora, M.; Hollingsworth, J. A.; Klimov, V. I.; Htoon, H. Two Types of Luminescence Blinking Revealed by Spectroelectrochemistry of Single Quantum Dots. *Nature* **2011**, *479*, 203–207.

26. Efros, A. L.; Nesbitt, D. J. Origin and Control of Blinking in Quantum Dots. *Nat. Nanotechnol.* **2016**, *11*, 661–671.

27. Peterson, J. J.; Nesbitt, D. J. Modified Power Law Behavior in Quantum Dot Blinking: A Novel Role for Biexcitons and Auger Ionization. *Nano Lett.* **2009**, *9*, 338–345.

28. Kim, T.; Jung, S. Il; Ham, S.; Chung, H.; Kim, D. Elucidation of Photoluminescence Blinking Mechanism and Multiexciton Dynamics in Hybrid Organic-Inorganic Perovskite Quantum Dots. *Small* **2019**, *15*, 1900355.

29. Trinh, C. T.; Minh, D. N.; Ahn, K. J.; Kang, Y.; Lee, K. G. Verification of Type-A and Type-B-HC Blinking Mechanisms of Organic–Inorganic Formamidinium Lead Halide Perovskite Quantum Dots by FLID Measurements. *Sci. Rep.* **2020**, *10*, 1–8.

30. Han, X.; Zhang, G.; Li, B.; Yang, C.; Guo, W.; Bai, X.; Huang, P.; Chen, R.; Qin, C.; Hu, J.; Ma, Y.; Zhong, H.; Xiao, L.; Jia, S. Blinking Mechanisms and Intrinsic Quantum-Confined Stark Effect in Single Methylammonium Lead Bromide Perovskite Quantum Dots. *Small* **2020**, *16*, 2005435.

31. Yu, J. C.; Kim, D. W.; Kim, D. Bin; Jung, E. D.; Park, J. H.; Lee, A.-Y.; Lee, B. R.; Di Nuzzo, D.; Friend, R. H.; Song, M. H. Improving the Stability and Performance of Perovskite Light-Emitting Diodes by Thermal Annealing Treatment. *Adv. Mater.* **2016**, *28*, 6906–6913.

32. Nguyen, V. C.; Katsuki, H.; Sasaki, F.; Yanagi, H. Single-Crystal Perovskite $CH_3NH_3PbBr_3$ Prepared by Cast Capping Method for Light-Emitting Diodes. *Jpn. J. Appl. Phys.* **2018**, *57*, 04FL10.

33. Sharma, D. K.; Hirata, S.; Vacha, M. Single-Particle Electroluminescence of CsPbBr3 Perovskite Nanocrystals Reveals Particle-Selective Recombination and Blinking as Key Efficiency Factors. *Nat. Commun.* **2019**, *10*, 4499.

34. García-Aboal, R.; Fenollosa, R.; Ramiro-Manzano, F.; Rodríguez, I.; Meseguer, F.; Atienzar, P. Single Crystal Growth of Hybrid Lead Bromide Perovskites Using a Spin-Coating Method. *ACS Omega* **2018**, *3*, 5229–5236.

35. Schmidt, L. C.; Pertegás, A.; González-Carrero, S.; Malinkiewicz, O.; Agouram, S.; Mínguez Espallargas, G.; Bolink, H. J.; Galian, R. E.; Pérez-Prieto, J. Nontemplate Synthesis of $CH_3NH_3PbBr_3$ Perovskite Nanoparticles. *J. Am. Chem. Soc.* **2014**, *136*, 850–853.

36. Saidaminov, M. I.; Abdelhady, A. L.; Murali, B.; Alarousu, E.; Burlakov, V. M.; Peng, W.; Dursun, I.; Wang, L.; He, Y.; MacUlan, G.; Goriely, A.; Wu, T.; Mohammed, O. F.; Bakr, O. M. High-Quality Bulk Hybrid Perovskite Single Crystals within Minutes by Inverse Temperature Crystallization. *Nat. Commun.* **2015**, *6*, 1–6.

37. Wang, K. H.; Li, L. C.; Shellaiah, M.; Sun, K. W. Structural and Photophysical Properties of Methylammonium Lead Tribromide ($MAPbBr_3$) Single Crystals. *Sci. Rep.* **2017**, *7*, 1–14.

38. Diab, H.; Arnold, C.; Lédée, F.; Trippé-Allard, G.; Delport, G.; Vilar, C.; Bretenaker, F.; Barjon, J.; Lauret, J. S.; Deleporte, E.; Garrot, D. Impact of Reabsorption on the Emission Spectra and Recombination Dynamics of Hybrid Perovskite Single Crystals. *J. Phys. Chem. Lett.* **2017**, *8*, 2977–2983.

39. Kim, H.; Zhao, L.; Price, J. S.; Grede, A. J.; Roh, K.; Brigeman, A. N.; Lopez, M.; Rand, B. P.; Giebink, N. C. Hybrid Perovskite Light Emitting Diodes under Intense Electrical Excitation. *Nat. Commun.* **2018**, *9*, 4893.

40. Merdasa, A.; Tian, Y.; Camacho, R.; Dobrovolsky, A.; Debroye, E.; Unger, E. L.; Hofkens, J.; Sundström, V.; Scheblykin, I. G. "supertrap" at Work: Extremely Efficient Nonradiative Recombination Channels in $MAPbI_3$ Perovskites Revealed by Luminescence Super-Resolution Imaging and Spectroscopy. *ACS Nano* **2017**, *11*, 5391–5404.

41. Eremchev, I. Y.; Tarasevich, A. O.; Li, J.; Naumov, A. V.; Scheblykin, I. G. Lack of Photon Antibunching Supports Supertrap Model of Photoluminescence Blinking in Perovskite Sub-Micrometer Crystals. *Adv. Opt. Mater.* **2021**, *9*, 2001596.

# Chapter 5

## The role of halide vacancies in electroluminescence blinking of $MAPbBr_3$ microcrystals

**Abstract**

Metal halide perovskites are prone to light, electric field, and heat-induced modulations in their optical and electronic properties. Apart from intrinsic defects formed during crystal growth and formation, defects are also generated by light and electric fields in perovskites. Some of these defects are reversible, while others cause irreversible damage to the material. Defects, energetically called trap states, affect the stability and the efficiency of the light-harvesting, emitting, and amplifying ability of perovskite materials. As discussed in the previous chapter, electroluminescence blinking is one of the reasons for efficiency loss from perovskites. Blinking is caused by nonradiative losses, which are mostly trap-mediated. The role of migrating halide ions in reversible quenching of the EL was disclosed in Chapter 4. In this chapter, I further study the role of halide vacancies or associated defects in determining the EL blinking mechanism. Using precursor solution consisting of under-stoichiometric, stoichiometric, and over-stoichiometric MABr: $PbBr_2$ solution, I vary the bromide composition in the formed perovskite crystals. By studying the blinking from the microcrystals and conducting statistical analysis, a change in the blinking behavior could be noticed. The under-stoichiometric sample shows a linear power-law blinking behavior, characteristic of type-B blinking due to trapping-de-trapping of charge carriers. However, the blinking follows a truncated power-law behavior for stochiometric and over-stoichiometric samples. This confirms that halide vacancies act as trap states and dominate the trapping-de-trapping mechanism of blinking in an under-stoichiometric sample, while other mechanisms control blinking in stoichiometric and over-stoichiometric samples. I also post-treat perovskite crystals with MABr solution to study changes in blinking behavior. Time-resolved photoluminescence studies, energy dispersive X-ray spectroscopic studies are also performed to corroborate the results. These studies have shown that MABr addition has improved the PL and EL properties of $MAPbBr_3$ perovskites.

## 5.1. Introduction

Lead halide perovskites are rapidly emerging as new materials for optoelectronic applications. However, they suffer from stability-related issues that hinder their commercialization. Defects in perovskite are one reason for their low stability. Defects in perovskite can be intrinsic, associated with crystal formation; or induced by light, electric field, heat, or moisture.[1-6] Such defects control the photo- or electroluminescence responses of perovskite materials which can be reversible or irreversible.[7] Electric field is known to cause irreversible phenomena like current-voltage hysteresis,[7,8,9] luminescence quenching,[1,4,7] phase changes,[6] or even material degradation.[5,10] Reversible responses occur due to ion migration under an applied field which will recover when the field is removed. For example, Deng *et al.* showed that in an Au/FTO/$CH_3NH_3PbI_3$/FTO/Au sample, PL quenching with morphology change was noticed near the electrodes, which were reversible within a range of applied field but became irreversible above a limit.[7] These changes were caused by ion migration in conjunction with humidity variations. It was also found that perovskites produce gaseous products under external electrical bias.[5,10] Perovskites like $MAPbBr_3$ and $MAPbI_3$ are known to degrade in the presence of moisture.[5]

All such effects are the reasons for decreased efficiency and a low operational lifetime of perovskite-based devices compared to conventional semiconductor LEDs. The maximum efficiency of perovskite-based LED to date is just a little above 20 percent.[12-15] Solar cell efficiency has reached only around 25%.[16] The operational stability of perovskite-based LED is limited to few hours as compared to thousands of hours for other semiconductor-based LEDs.[11] The role of sub-bandgap defects in limiting open-circuit voltage by allowing nonradiative Shockley-Read- Hall emission is well known in the case of perovskite solar cells.[17] Perovskite lasing threshold is also affected by defects.[6] Joule heating is another reason for perovskite material degradation, thus limiting the high radiance and operational lifetime of perovskite-based LEDs.[17,18] Yet another very important phenomenon associated with defects is PL blinking. Several strategies are undertaken to prevent defects induced by light, heat, electric field, or moisture. Encapsulation can prevent moisture-assisted perovskite degradation under the applied field.[7,19] Self-passivation techniques by employing smaller grains on larger $MAPbBr_3$ grains have led to achieving high-performance LED.[20] Using pulsed electrical excitation instead of continuous biasing has shown to increase the efficiency of perovskite LEDs.[18]

Efficient thermal management by using layers that can act as heat sinks can reduce Joule heating-induced damages.[18] Operating perovskite LED under alternating electric field over a constant electric field has shown to suppress PL blinking and lead to significant PL enhancement.[21,22]

Several studies are carried out to understand the nature of the defects in lead halide perovskites. Some classify them as point defects.[23,24,25] The presence of charged cations like $MA^+$ in the interstitials affects the radiative recombination efficiency in perovskite.[4] Halide vacancies or halide ions at the interstitials also lead to the formation of defect states. Distortion of the crystal structure at the grain boundaries results in neutral state defects.[4] Some defects are localized, while some are extremely mobile. Vacancies and interstitial defects are classified as mobile defects, while the crystal imperfections and lattice distortions are localized in nature. The localized traps form a distribution of energy states within the bandgap. The role of organic cations in forming these localized trap states is also discussed using $MAPbBr_3$ perovskites through low temperature and power-dependent PL studies.[6] The sub-bandgap defects can be deep traps or shallow traps. Halide defects in the form of vacancies, interstitials, or anti-sites are known to form deep trap levels in the perovskite band structure.[4,25] For e.g., it was understood that the bromide ion vacancies and interstitials are known to form deep defect levels leading to nonradiative recombination seen as PL blinking.[26] Theoretical DFT calculations have shown that the main defect under halide rich conditions is the lead vacancy, lead anti-sites, and halide vacancy, all have a deep trap character.[25]

Perovskite blinking is a sign of defect-mediated charge carrier recombination processes. Single-particle studies reveal the mechanism of charge carrier recombination in perovskite materials. Similar to quantum dots, two types of blinking are common for perovskite.[27,28,29] One is type-A blinking which is due to charging and discharging of charge carriers by Auger processes. Another is type-B blinking which is characterized as a trapping-de-trapping mechanism. Perovskite blinking was first observed from large nanocrystals and microcrystals where trap assisted mechanism was suggested over commonly known charging-discharging mechanism.[30-33] Here, dynamic traps controlled the blinking. Blinking observed in nanocrystals was attributed mainly to the type-A mechanism where photoionization results in OFF-state and a consecutive charge re-neutralization event can bring it back to the PL active or ON-state.[34-36] In larger crystals, super-trap acts as PL quenching sites within the crystal. These super-traps can migrate all

over the crystal.[37,38] Although trap-assisted recombination is considered nonradiative, some studies reveal that there can be photo-emissive trap states, as in the case of a $CsPbBr_3$ sample which showed broad emission with a shoulder.[11]Here, they also report emissive trap state in EL as well. However, they are a sign of degradation of the perovskite material. There are reports which show the type-A and type-B blinking co-existing in the perovskite crystal.[34,39] Several studies are meant to understand photoinduced blinking in perovskites. However, EL blinking is seldom looked upon. There are only a handful of reports mentioning EL blinking.[40,41,42] Blinking under an applied bias is an interesting phenomenon. The role of migrating halide vacancies in blinking could be understood in the studies shown in chapter 4.

In this chapter, I further study the role of halogen in the EL blinking mechanism. It is known that fractional variations in the stoichiometry of the precursor solution used for synthesizing perovskite can cause non-negligible changes in optoelectronic behavior.[43,44] Hence, excess or deficiency of halide ions will mediate charge carrier recombination in perovskite. The switching of blinking behavior from type-B in perovskite crystals synthesized from an under-stoichiometric sample to type-A in a stoichiometric sample, and an over-stoichiometric sample helps us to further clarify the EL blinking mechanism in perovskite microcrystals. A post-synthetic MABr treatment on $MAPbBr_3$ microcrystal has revealed that filling of halide vacancies improves charge-carrier dynamics like PL lifetime, PL intensity, EL emission, and generation of new EL emitting centers in the microcrystals.

## 5.2 Results and discussions

### 5.2.1 Synthesis of perovskite microcrystals

To understand the role of halide vacancies in the EL blinking phenomenon in $MAPbBr_3$ perovskite, I synthesized $MAPbBr_3$ perovskite microcrystals of varying bromide composition by simply varying the precursor ratio (MABr: $PbBr_2$). I used the AVC method to grow the crystals on an ITO-coated glass substrate.[45] Essentially, I drop-cast 20 µL of the precursor solution on an ITO glass substrate kept inside a chamber filled with DCM as the antisolvent. The crystals nucleate immediately and grow overnight. Details of synthesis are mentioned in Chapter 2 of the thesis. The table below shows a scheme for the concentration of precursor solution used to prepare an under-stoichiometric, stoichiometric, and over-stoichiometric perovskite precursor solution for $MAPbBr_3$ microcrystals.

| MABr content | $PbBr_2$ content | Precursor solutions |
|---|---|---|
| 1 mL 0.20 M MABr | 1 mL 0.20 M $PbBr_2$ | Stoichiometric |
| 1 mL 0.18 M MABr | 1 mL 0.20 M $PbBr_2$ | Under- stoichiometric |
| 1 mL 0.22 M MABr | 1 mL 0.20 M $PbBr_2$ | Over- stoichiometric |

Table 1. Scheme for preparing $MAPbBr_3$ microcrystals of varying bromide composition.

For the post-treatment studies, the MABr solution was prepared as follows. 0.01M MABr was prepared in 5 mL methyl alcohol. About 100 µL was taken and mixed with 2.5 mL toluene. This resulted in ~ 400 µM MABr solution. An appropriate amount is used for post-treatment studies.

### 5.2.2 Photoluminescence and electroluminescence properties

Following the synthesis of $MAPbBr_3$ microcrystals of varying bromide composition, I studied their PL and EL characteristics by exciting the crystals with light and applied electric fields. The sample for PL studies was prepared by growing the microcrystals on a glass slide using the AVC method. The photoluminescence image was collected by exciting the sample using a 460 nm laser. The crystals showed green luminescence on account of band-edge charge carrier recombination.

Next, I observed EL blinking from perovskite microcrystals by sandwiching the crystals prepared on one ITO glass by a second ITO glass and applying a bias. Starting

from a very low voltage, the EL blinking could be noticed. With the increase in voltage, the number of EL blinking spots increased. I used 8 V to study EL blinking characteristics in $MAPbBr_3$ microcrystals made from under-stoichiometric, stoichiometric, and over-stoichiometric precursor solutions. At this voltage, a considerable number of EL emitting centers required for statistical analysis were observed.

Below, I show the details of my study, dividing it into three parts. Observations from a) under-stoichiometric, b) stoichiometric, and c) over-stoichiometric precursor solutions.

a) An under-stoichiometric sample:

I prepared an under-stoichiometric precursor solution using 0.18 M MABr and 0.20 M $PbBr_2$ using deoxidized DMF as the solvent. Although precursor nature is called under-stoichiometric because of less MABr, based on simple dissociation of precursors into ions, this sample will have an excess of $Br^-$ and $Pb^{2+}$ ions after the formation of $MAPbBr_3$. Figure 1 below shows the PL and EL characteristics of the synthesized microcrystals under light and electric field excitation respectively.

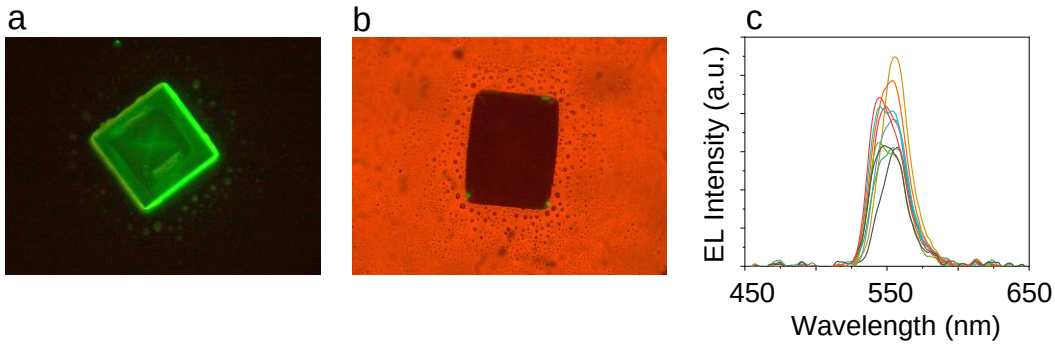


**Figure 1.** PL and EL properties of $MAPbBr_3$ microcrystals prepared from an under-stoichiometric precursor solution (0.18 M MABr + 0.20 M $PbBr_2$ in DMF). a) PL image of a microcrystal excited by 460 nm cw laser, b) EL image of a microcrystal at 8 V (the image size of (a) and (b) is 320x 240 $\mu m^2$), and c) EL spectra obtained from microcrystal shown in (b) at an integration rate of 1s at 8 V.

Figure 1a shows the PL image of a $MAPbBr_3$ microcrystal under 460 nm cw laser excitation. The green luminescence is characteristic of the band edge recombination of photogenerated charge carriers in $MAPbBr_3$. Figure 1b shows the image of the $MAPbBr_3$ microcrystal showing blinking EL at 8 V. Several $MAPbBr_3$ crystals showed blinking EL observed at several emitting spots within them as can be seen as green spots within the one such crystal in Figure 1b. Such emitting spots changed their location over time or continued to blink at the same spot. This can be accounted for migrating halide ions as

understood from studies done in Chapter 4. The EL spectra collected from the corresponding crystal are shown in Figure 1c. The emission from the crystals was collected through an objective lens and using a fiber spectrometer, and the EL spectra are generated after substrating the background signal. An integration time of 1s was used to record one spectrum. The crystal showed fluctuation in intensity temporally and spectrally. In the above case, peaks were observed at 544, 548, 553, and 556 nm.

Such spectral and intensity fluctuations can be accounted for for many reasons. One of the reasons can be the photon-reabsorption-emission phenomenon. It is known that in large crystals of perovskites, emissions coming from one end of the crystal can be reabsorbed at other parts before being emitted again. This is explained in studies performed on photoluminescence of $MAPbBr_3$ single crystals by depth-resolved cathodoluminescence spectroscopy.[46] Such emissions will be lower in energy than the previous emission. Since I use large microcrystals and collect the EL using an objective lens placed below the LED device, the same phenomenon can cause spectral shifts in electroluminescence. Since I observe many spectral maxima, it can also imply that there exist several closely spaced energy states within the crystal. Studies under high-intensity electrical excitation have shown that Joule heating and associated material degradation can cause red-shifting of the spectrum.[47] However, since dynamic spectral shifting is observed in my studies, the reasons for spectral shifts can be combined effects of processes like re-absorption emission, Joule heating, or material degradation. Trap state emission EL has also been discussed in some reports accounting for a shoulder in the broad EL spectrum of $CsPbBr_3$ perovskite.[11] The fluctuations in EL intensity can be due to a difference in the density of the nonradiative recombination centers surrounding each emitting center, as is discussed in Chapter 4.

The EL blinking behavior was observed at several emitting spots within the $MAPbBr_3$ crystal was studied using single-particle imaging and micro-spectroscopy. The emission coming out from the crystal is collected through an objective lens and passes through a >500 nm long-pass filter, and is received by an EMCCD camera. The setup for single-particle studies is described in Chapter 2 of the thesis. A single-particle video is recorded for one minute at 33 ms exposure time. From the video, a single microcrystal showing several EL blinking spots is studied, and a time-dependent EL intensity profile is generated. Figure 2 (a-g) shows examples of EL trajectories collected from different emitting centers within a microcrystal at 8 V.

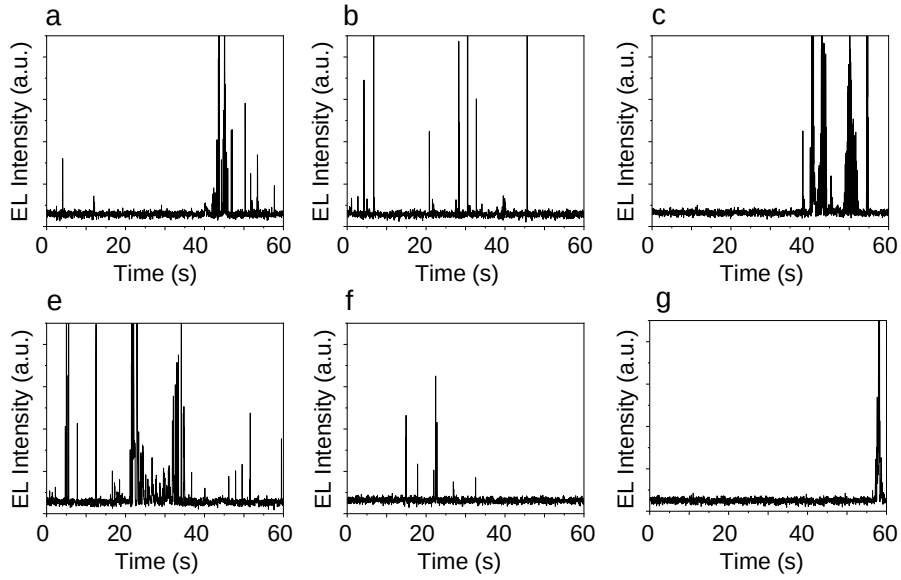


**Figure 2.** (a-g) EL trajectories collected at 8 V from six emitting centers within a single $MAPbBr_3$ microcrystal prepared from an under-stoichiometric precursor solution (0.18 M MABr + 0.20 M $PbBr_2$ in DMF).

The blinking can be seen as fluctuations in the EL intensity between high and low levels. The nature of the blinking varied from center-to-center, and hence a statistical analysis was performed to understand the blinking behavior. Based on a threshold intensity value, ON- and OFF- times were estimated, and their probability distribution plots were obtained. The method of calculating the probability distribution is explained in Chapter 4. Figure 3 shows the ON- and OFF-time probability density plots.

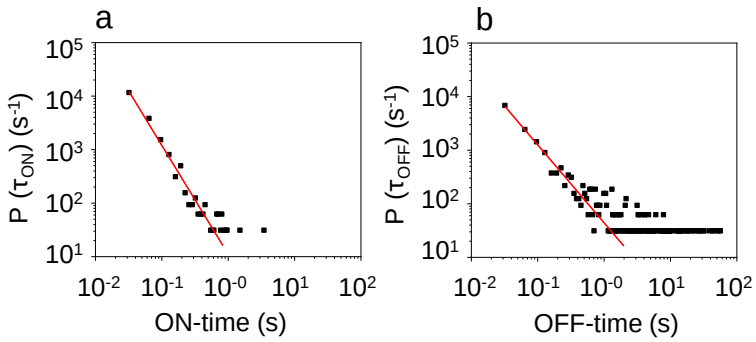


**Figure 3.** a) ON- and b) OFF-time probability density plots of EL trajectories collected at 8 V from a single $MAPbBr_3$ crystal prepared from the under-stoichiometric precursor solution (0.18 M MABr+ 0.20 M $PbBr_2$ in DMF).

The ON- and OFF-times showed a linear power-law behavior. This is characteristic of type-B blinking that is associated with a trapping-de-trapping mechanism. I believe that the $MAPbBr_3$ microcrystals prepared from an under-stoichiometric sample will have an excess of halide vacancies. These halide vacancies can act as migrating traps and

dominate the type-B blinking behavior in the above sample. The halide vacancies migrate under the electric field and quench the EL emitting center by nonradiative recombination. The linear nature of the OFF-state shows that the recovery of the OFF process is limited to a single-rate process which is by the de-trapping mechanism.

a) A stoichiometric sample:

Next, I prepared $MAPbBr_3$ microcrystals by using a stoichiometric precursor solution: 0.20 M MABr and 0.20 M $PbBr_2$ using deoxidized DMF as the solvent. Based on the nature of the precursor solution, the resulting perovskite microcrystal should be a perfect one with no defects. However, it is certain that not only the nature of precursor solution but also other factors like time for crystallization will also affect the crystal formation and defect generation. Below are shown the PL and EL features of the synthesized crystals.

The PL image under a 460 nm laser irradiation shows green emission due to band-edge charge carrier recombination (Figure 4a). The microcrystals showed blinking EL starting from a very low voltage. An EL image of the microcrystal collected at 8 V is shown in Figure 4b. The EL showed temporal fluctuations in spectral maxima and intensity. It is represented in Figure 4c. The reason for spectral fluctuations can be accounted for photon-reabsorption, Joule heating, material degradation, or emissive trap-states.[46,47] The intensity fluctuation is a result of the difference in the density of the nonradiative recombination centers surrounding each emitting center, similar to the discussion in Chapter 4. The major EL peaks were observed at 554, 557, and 560 nm.

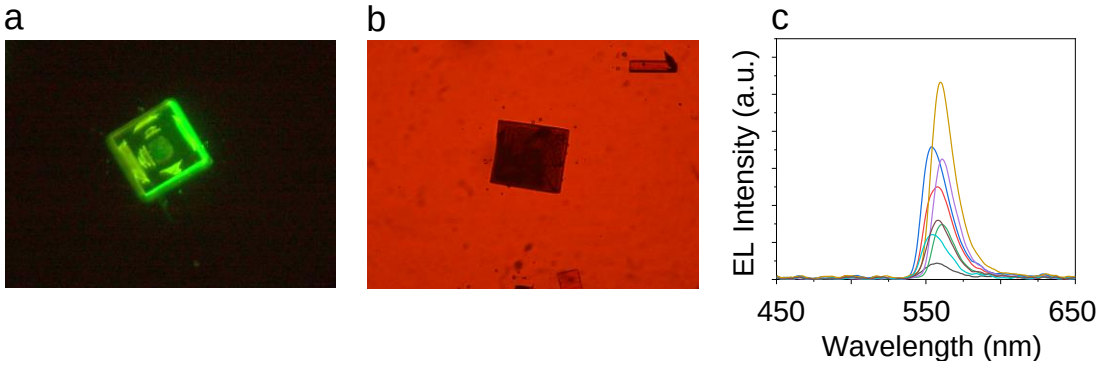


**Figure 4.** PL and EL properties of $MAPbBr_3$ microcrystals prepared from a stoichiometric precursor solution (0.20 M MABr + 0.20 M $PbBr_2$ in DMF). a) PL image of a microcrystal excited by 460 nm cw laser, b) EL image of a microcrystal at 8 V (the image size of a) and b) is 320x 240 $\mu m^2$), and c) EL spectra obtained from microcrystal shown in b) at an integration rate of 1s at 8 V.

I collected the EL trajectories from various emitting centers within the $MAPbBr_3$ perovskite microcrystal prepared from the stoichiometric precursor samples showing EL at 8 V by using the single-particle instrument. The procedure for data collection is the same as mentioned in the case of the under-stoichiometric sample. Some of the trajectories are shown in Figure 5(a-g).

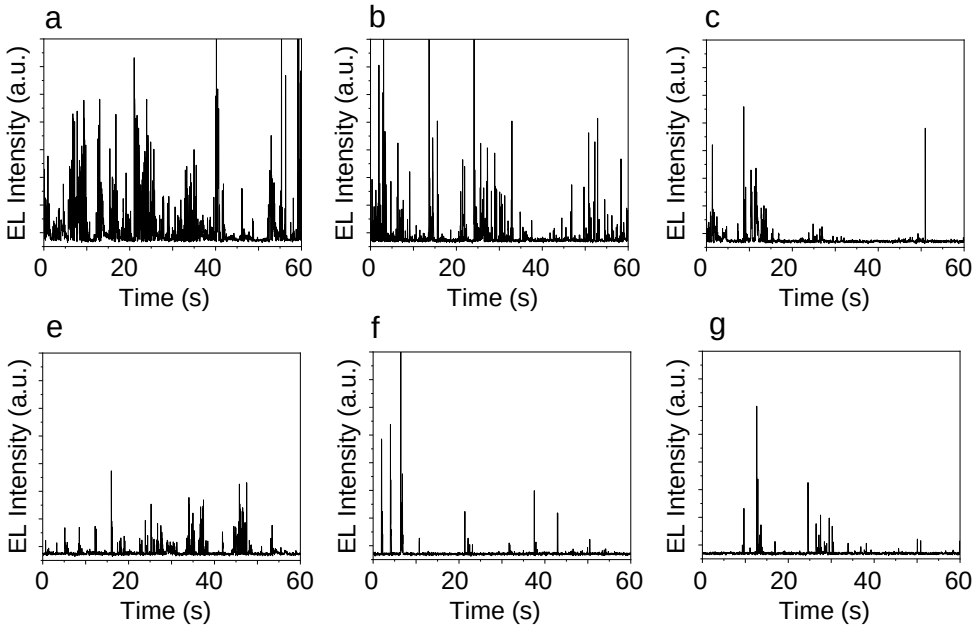


**Figure 5.** (a-g) EL trajectories collected at 8 V from six emitting centers within a single $MAPbBr_3$ microcrystal prepared from a stoichiometric precursor solution (0.20 M MABr + 0.20 M $PbBr_2$ in DMF).

The EL trajectories obtained from various emitting centers were characterized by spectral and temporal intensity fluctuations. The blinking varies from the center-to-center. And hence the data obtained from these trajectories were subjected to statistical analysis to understand how the ON- and OFF-time varied within a crystal. Figure 6 shows the ON- and OFF-time probability density distribution plots for the $MAPbBr_3$ crystals prepared from the stoichiometric precursor solution. The blinking behavior of these microcrystals showed a truncated power-law behavior for both ON- and OFF-time probabilities. This is unlike the blinking behavior shown by $MAPbBr_3$ microcrystal prepared from an under-stoichiometric precursor solution which showed a linear power-law blinking behavior. The truncation of ON- and OFF- time represents multiple recombination pathways opened for OFF-state recovery. In a stoichiometric sample, where I believe that the density of halide vacancy will be less than that in an under-stoichiometric sample, the blinking is contributed not only by migrating halide vacancies but also by other pathways

whose origin is still not clear. Thus, there should be several ways for nonradiative recombination within the $MAPbBr_3$ perovskite prepared from a stoichiometric precursor solution. The migrating halogen vacancy-assisted EL quenching is only one such route.

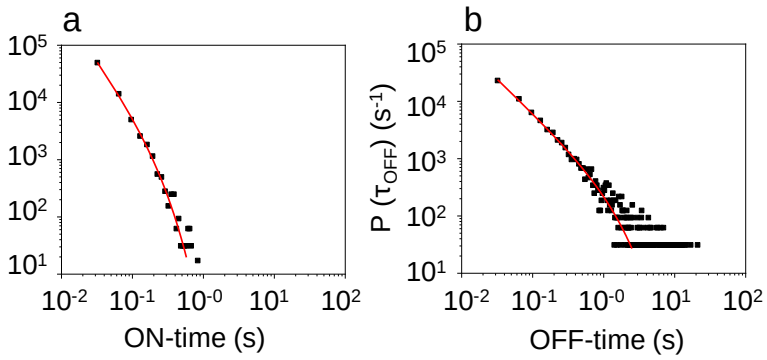


**Figure 6.** a) ON- and b) OFF-time probability density plots of EL trajectories collected at 8 V from a single $MAPbBr_3$ microcrystal prepared from the stoichiometric precursor solution (0.20 M MABr+0.20 M $PbBr_2$ in DMF).

b) An over-stoichiometric sample:

I prepared $MAPbBr_3$ microcrystal using an over-stochiometric precursor solution using the AVC method. I used 0.22 M MABr and 0.20 M $PbBr_2$ in deoxidized DMF as a solvent for making the precursor solution. Here the excess $Br^-$ ions are thought to fill the halide vacancies present during crystal formation itself. Figure 7 shows the PL and EL properties of the synthesized microcrystals.

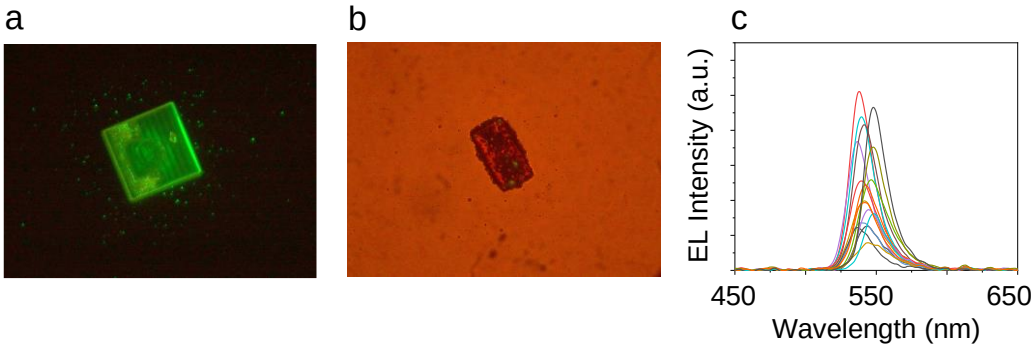


**Figure 7.** PL and EL properties of $MAPbBr_3$ microcrystals prepared from an over-stoichiometric precursor solution (0.22 M MABr + 0.20 M $PbBr_2$ in DMF). a) PL image of a microcrystal excited by 460 nm cw laser, b) EL image of a microcrystal at 8 V (the image size of a) and b) is 320x 240 $\mu m^2$), and c) EL spectra obtained from microcrystal shown in b) at an integration rate of 1s at 8 V.

The microcrystal showed green luminescence and is due to the band-edge carrier recombination, as shown in Figure 7a. The microcrystals showed EL (Figure 7b) starting from a very low voltage; however, 8 V was fixed for the studies as at this voltage, a good number of emitting spots could be seen and used for studies. Fluctuations were seen in EL spectra. It is shown in Figure 7c. An integration time of 1s was used to record the spectra. EL peaks were observed at 536- 549 nm with even a 1 nm difference in peak wavelength. Like in the discussion made for under-stoichiometric and stoichiometric samples, the dynamic shifts in the spectral maxima and intensity can be due to combined effects of photon reabsorption-emission, Joule heating material degradation, or emissive trap states.

The EL trajectories collected from several emitting centers in a single $MAPbBr_3$ microcrystal prepared from an over-stoichiometric sample at 8 V from a single-particle video are shown below. Based on center-to-center differences in blinking behavior, statistical analysis was performed to understand the nature of EL blinking from these crystals. Figure 8(a-g) shows examples of EL blinking trajectories collected from the microcrystal.

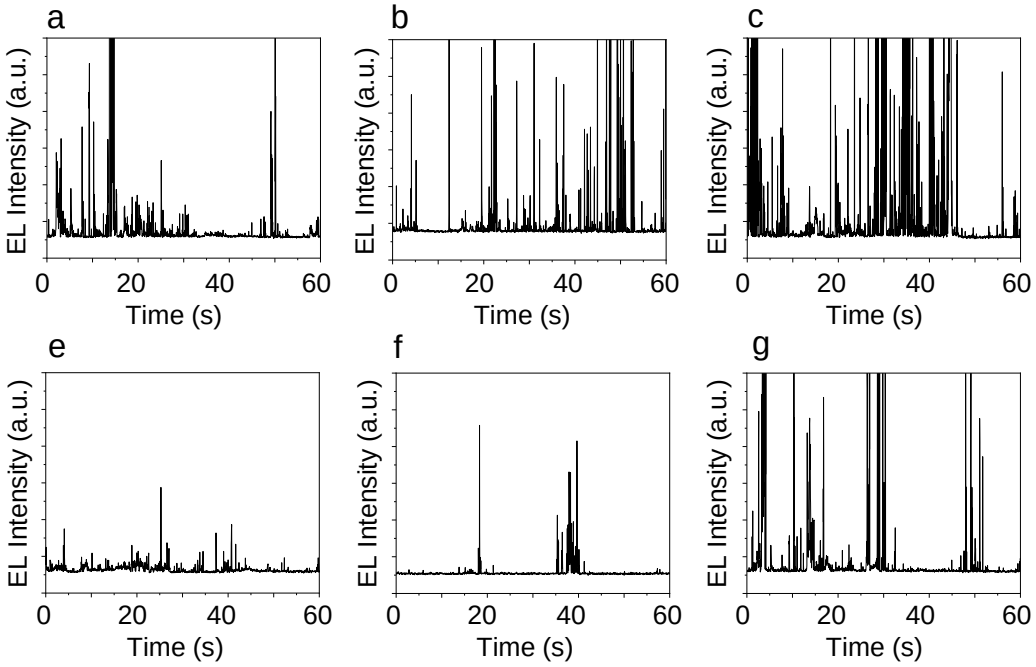


**Figure 8.** (a-g) EL trajectories collected at 8 V from six emitting centers within a single $MAPbBr_3$ microcrystal prepared from an over-stoichiometric precursor solution (0.22 M MABr + 0.20 M $PbBr_2$ in DMF).

A statistical analysis shows that similar to a stoichiometric sample, and the blinking showed a truncated power-law dependence for both ON- and OFF-time probabilities, as shown in Figure 9.

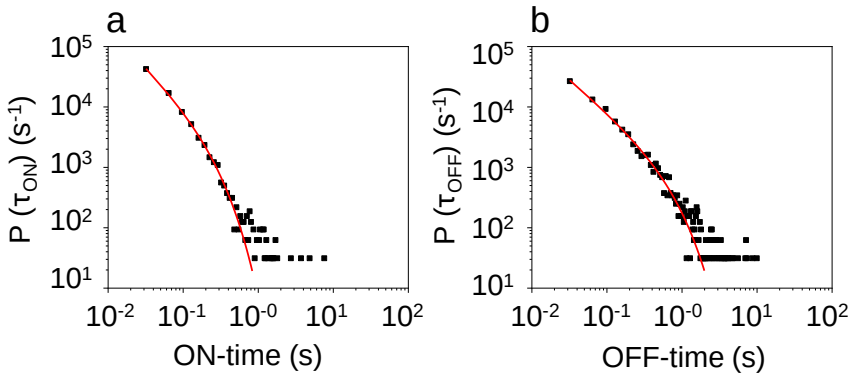


**Figure 9.** a) ON-time, and b) OFF-time probability density plots of EL trajectories collected at 8 V from a single $MAPbBr_3$ microcrystal prepared from the under-stoichiometric precursor solution (0.22 M MABr + 0.20 M $PbBr_2$ in DMF).

The studies performed on under-stoichiometric, stoichiometric, and over-stoichiometric samples showed that the density of halide vacancy could affect the nature of the blinking mechanism. In an under-stoichiometric sample, where the density of halide vacancy is the highest, the blinking is dominated by the trapping-de-trapping mechanism, as seen by the type-B blinking characteristics. However, in a stoichiometric sample, such halide vacancies are reduced, and hence the contribution of halide vacancy-assisted blinking is also reduced. Other nonradiative relaxation pathways cause blinking in samples prepared using stoichiometric and over-stoichiometric samples. The EL spectral and intensity fluctuations existed in all samples irrespective of their nature. This means that spectral fluctuations are not contributed by the density of halide vacancies alone, but also by other factors like the inner filtering effect where emissions from one part of the crystal are reabsorbed at other parts before being emitted, Joule heating, and material degradation due to continuous device operation or trap state emissions contributed by reasons other than halide vacancies. To follow up, I performed post-MABr treatment studies, as is discussed in the next section.

### 5.2.3 MABr treatment studies

It is certain that not all the crystals are formed perfectly devoid of any defects. Most of them are having different kinds of defects, be they intrinsic or extrinsic. In lead halide

perovskite, there exist several point defects like ion vacancies, interstitials, antisites, or even crystal imperfections.[48,49,50] However, one can control the formation of these defects by carefully arranging conditions like providing an optimum temperature condition for crystal growth, controlling precursor solution concentration, setting up a moisture-free environment, and so on. All these are pre-synthesis methods for getting good quality crystals. However, post-synthetic treatments also exist to passivate any defects generated Here, I use excess MABr solution and post-treat the $MAPbBr_3$ microcrystal with this solution. I observed the changes occurring in the PL and EL properties of these microcrystals. The studies done are as follows.

Firstly, $MAPbBr_3$ crystals were prepared from stoichiometric precursor solution (0.20 M MABr + 0.20M $PbBr_2$ in DMF) on ITO glass substrate. I performed PL lifetime studies on untreated $MAPbBr_3$ microcrystals as well as MABr treated $MAPbBr_3$ microcrystals. The $MAPbBr_3$ microcrystal was selectively excited using a 460 nm picosecond pulsed laser with a 1 MHz repetition rate. The selected crystal was isolated from other crystals by using an iris. The PL decay profile was recorded for 2 minutes in a nanosecond time window (Figure 10 a(i)). The PL decayed with multiexponential kinetics, which was fitted with a multiexponential lifetime fitting equation, and the average lifetime of the sample was calculated. Similarly, many such crystals were studied, and PL decay was recorded. Later, the microcrystals on the glass slide were treated with approximately 20 µL of MABr solution. The preparation of the MABr solution is mentioned in the synthesis section. After the MABr solution was dried, the PL decay was recorded again from the same crystals. PL decay after a certain time of laser irradiation was also collected. Both these decays also showed multiexponential decay kinetics and were also fitted to obtain the average lifetime value. The results obtained from one of the crystals are shown below in Figure 10. The average lifetime increased from 3 ns in an untreated $MAPbBr_3$ microcrystal to 4.4 ns in MABr treated microcrystal (Figure 10 a(ii)). Also, with laser irradiation for two minutes, the lifetime further increased to 5 ns (Figure 10 a(iii)). With the addition of MABr, we can see that the initial fast decay became slower, meaning that the fast decay caused by nonradiative relaxation assisted by halide vacancies was suppressed by filling such vacancies with the addition of MABr solution. With laser irradiation, the lifetime has further increased. This is because laser irradiation helps the migration of added halide ions and helps in filling the vacancies at distant sites.

In addition to lifetime studies, the changes in PL intensity before and after MABr addition was also studied. $MAPbBr_3$ crystals were prepared from a stoichiometric precursor solution on a glass slide using the AVC method. The microcrystals formed were excited using a 460 nm cw laser, and the PL spectrum of an isolated $MAPbBr_3$ crystal was collected. It is shown in Figure 10 b(i). About 20 µL of MABr solution was added to the sample. After the solution was dried, the PL spectrum was acquired from the same crystal Figure 10 b(ii). It was found that the PL intensity also increased. This also confirms the filling of defect states, mostly the bromide vacancy defects, which helps to improve the PL properties of the sample. Such trap filling associated with photoluminescence enhancement is reported in various literature.

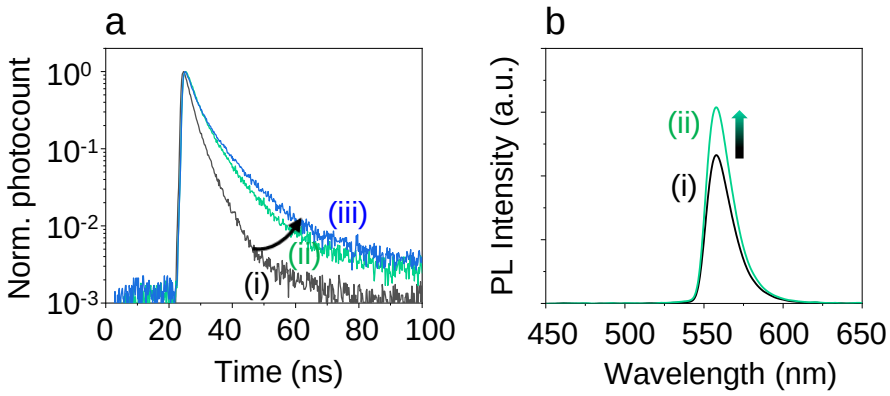


**Figure 10.** a) PL lifetime studies on $MAPbBr_3$ microcrystals prepared from a stoichiometric precursor solution. (i) shows the PL decay of untreated $MAPbBr_3$ sample, (ii) shows the PL decay of MABr treated $MAPbBr_3$ crystal, and (iii) shows the PL decay of MABr treated $MAPbBr_3$ sample after 2 minutes of laser irradiation. The samples were excited by a 460 nm laser of 1 MHz repetition rate under the same power. b) PL spectra collected from (i) untreated and (ii) MABr treated $MAPbBr_3$ crystal. 460 nm laser was used to irradiate the sample, and the integration time used to record the spectra was 10 ms.

Next, I also studied the changes in EL blinking behavior after MABr treatment. For this, I synthesized $MAPbBr_3$ crystals from a stoichiometric precursor solution on an ITO glass using the AVC method. The crystals grew overnight. It was then treated with approximately 80 µL of the MABr solution. After the solution was dried, the electroluminescence was observed by sandwiching the crystals with another ITO glass and connecting it to a voltage supply. Although the electroluminescence turned on at lower voltages, the studies were performed at 8 V, at which a lot of emitting centers were seen. Multicentre EL blinking was observed from microcrystals. Blinking trajectories

were acquired from several emitting centers from different microcrystals. Some of the trajectories collected from the emitting centers within the crystals are shown in Figure 11(a-g).

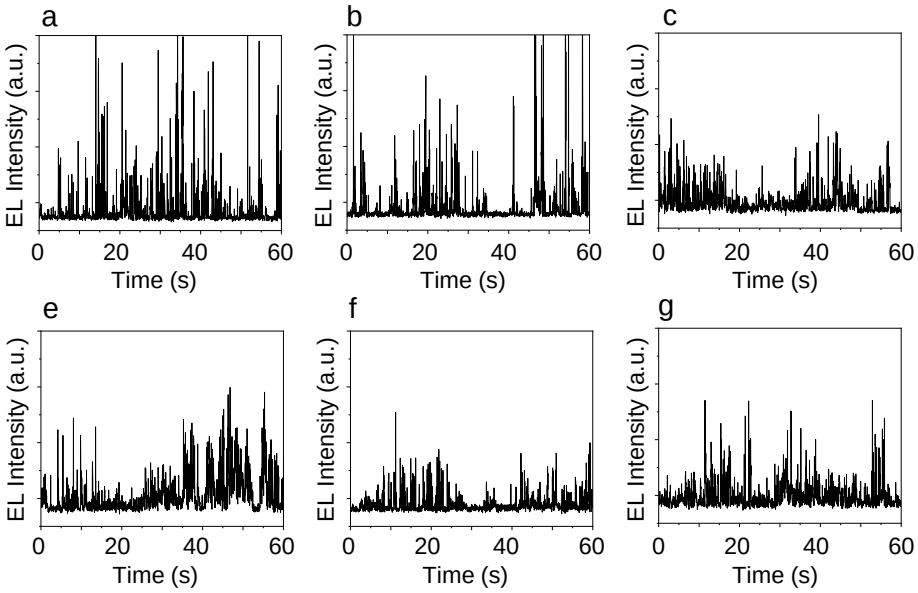


**Figure 11.** (a-g) EL trajectories collected at 8 V from six emitting centers from $MAPbBr_3$ microcrystals after MABr treatment.

From the EL trajectories, it can be seen that the number of ON- events increased. Since there exists particle to particle variation in EL blinking, a statistical analysis was performed to study the EL blinking behavior. Using the threshold method to distinguish ON and OFF events, the probability distribution for ON- and OFF-time duration was plotted and is shown in Figure 12.

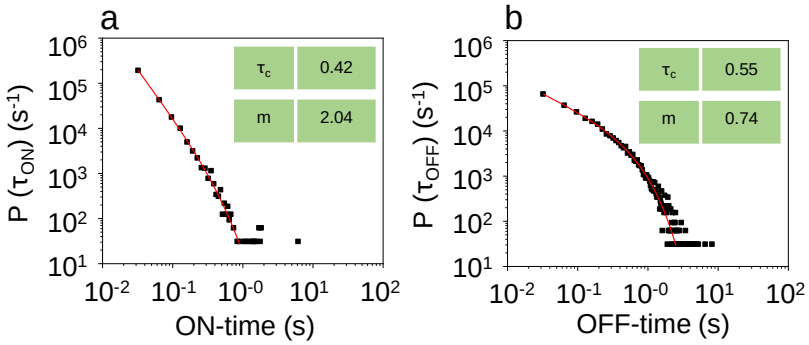


**Figure 12.** a) ON-time, and b) OFF-time probability distribution plot obtained for MABr treated $MAPbBr_3$ sample. Studies were performed at 8 V.

It was seen the cut-off for ON-time improved considerably from an untreated $MAPbBr_3$ sample observed in Chapter 4. The cut-off value for ON-time increased by approximately 5-fold under a voltage half of that used for untreated $MAPbBr_3$ sample in Chapter 4.

I also conducted SEM-EDS analysis to understand changes in the bromine composition after MABr addition by comparing the EDS-spectra collected before and after MABr addition. I prepared the $MAPbBr_3$ microcrystals on ITO glass by AVC method, which grew overnight. After keeping the crystals for hours in a vacuum chamber, it was used for SEM-EDS analysis. The sample on ITO was attached to a carbon substrate using copper tapes. The EDS spectra and elemental mapping images of several microcrystals were recorded at 6 kV for about 5 minutes. From the spectra and images, the elemental mapping was performed to understand the distribution of Pb and Br in the crystal. Using the software, the composition of Pb and Br was also quantified. The SEM-EDS image, elemental mapping images for Pb and Br, and EDS spectra collected before MABr treatment is shown in Figure 13.

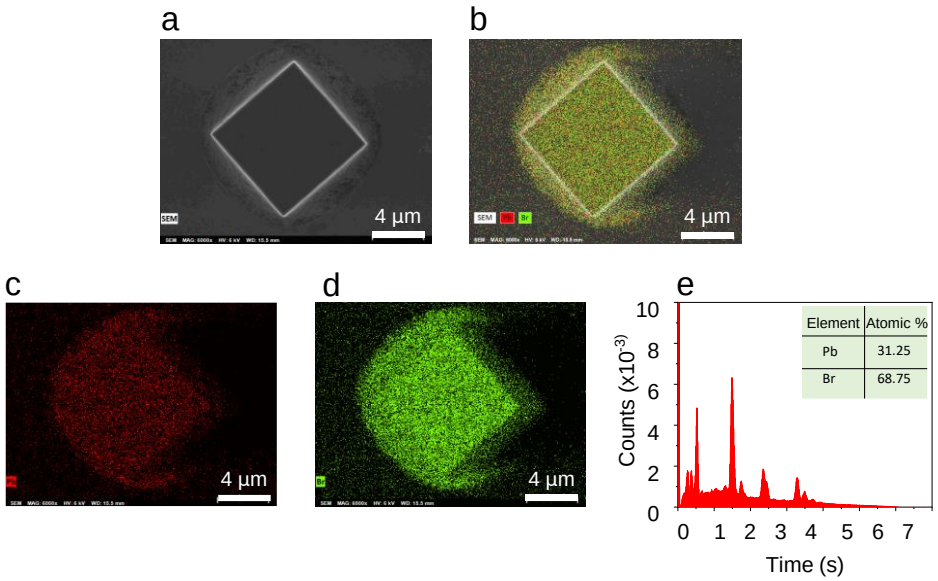


**Figure 13.** SEM-EDS analysis of untreated $MAPbBr_3$ microcrystal prepared from a stoichiometric precursor solution. a) SEM-EDS image of the microcrystal collected at 6kV, b) elemental mapping image showing overlaid images of SEM, Pb composition, and Br composition, c) elemental mapping image for Pb composition, d) elemental mapping image for Br composition (scale bar shows 4 µm), and e) EDS-spectra collected for untreated $MAPbBr_3$ sample at 6 kV for 5 minutes.

The elemental mapping of Pb and Br suggests that these elements are uniformly distributed over the entire crystal. The ratio Br/Pb for the untreated $MAPbBr_3$ microcrystal is around 2.20 that is less than the expected value of 3. This is proof that even samples prepared from stoichiometric precursor solution have ionic vacancies predominantly that of bromide. Hence the post-treatment of these crystals with a bromide-

rich salt solution should help in filling these vacancies. After the studies, the same crystals were treated with approximately 50 µL of MABr solution. After the solution was dried, it was vacuum dried before performing the EDS studies. The EDS spectra and images were recorded for the same crystal, and the composition of Pb and Br was quantified in the same way as before and is shown in Figure 14.

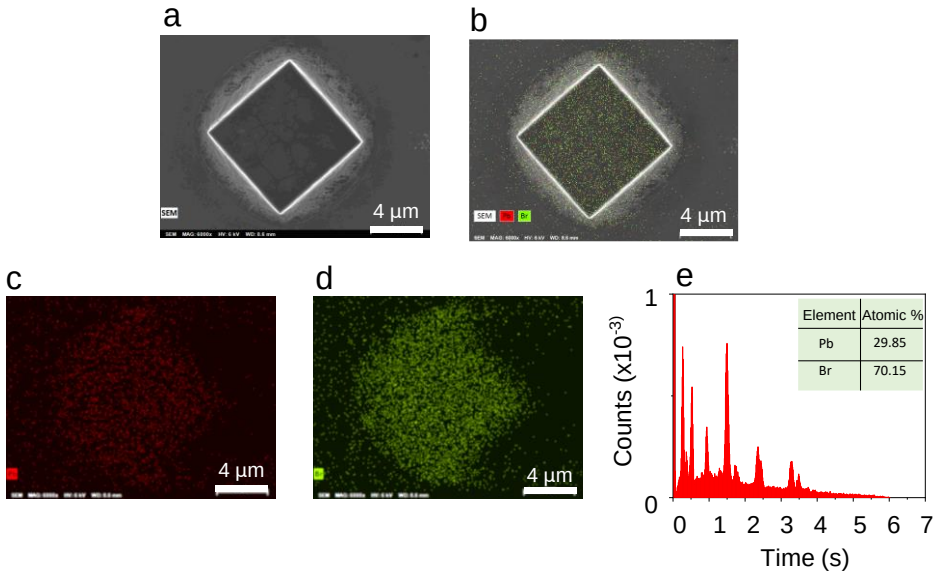


**Figure 14.** SEM-EDS analysis of MABr-treated $MAPbBr_3$ microcrystal prepared from a stoichiometric precursor solution. a) SEM-EDS image of the microcrystal collected at 6kV, b) elemental mapping image showing overlaid images of SEM, Pb composition and Br composition, c) elemental mapping image for Pb composition, d) elemental mapping image for Br composition (scale bar shows 4 µm), and e) EDS-spectra collected for MABr treated $MAPbBr_3$ sample at 6 kV for 5 minutes.

From the EDS spectra, the ratio of Br/Pb was quantified. The ratio increased from 2.20 for an untreated $MAPbBr_3$ microcrystal to 2.35 for MABr treated $MAPbBr_3$ microcrystal. The percentage of bromide composition increased by 15 percent.

After understanding that the MABr treated samples show improved EL and PL properties, I further performed MABr treatment to under-stoichiometric samples with more bromide vacancies. The studies performed show that the MABr addition improved the EL and PL properties in an under-stoichiometric sample. For example, a microcrystal named MC 1 (Figure 15 a), showed improvement in EL intensity upon MABr treatment. Also, a slight blue shift in the spectra could be noticed, which might be the emission coming from states after de-trapping of the charges. The EL spectra collected before and after the MABr treatment is shown in Figure 15 b and 15c, respectively.

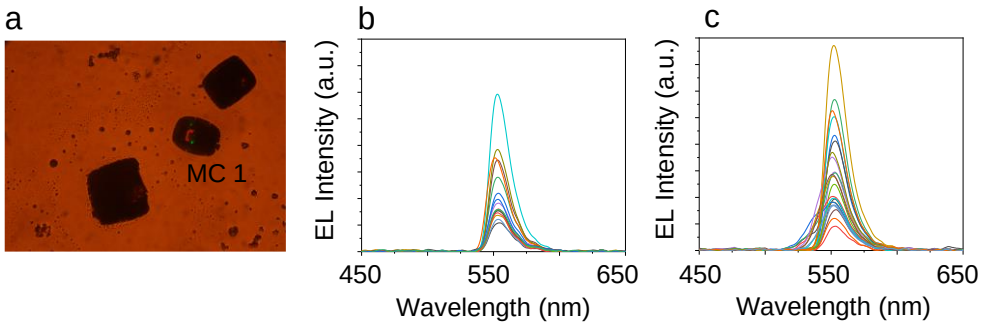


**Figure 15.** EL properties of untreated $MAPbBr_3$ and MABr treated $MAPbBr_3$ sample prepared from under-stoichiometric precursor solution. a) camera image of isolated microcrystals which shows EL blinking (size of the image is 320x240 $\mu m^2$), b) the EL spectra collected from $MAPbBr_3$ microcrystals before MABr treatment under 8 V, and c) EL spectra collected from MABr-treated $MAPbBr_3$ micro crystals under 8 V. The integration time for recording spectra is 1 s.

The MABr addition was seen to improve EL emission from various emitting centers within the $MAPbBr_3$ microcrystal, MC 1. A single-particle video was collected before and MABr addition. By fixing the region of interest (ROI) coordinates at the same place in both the videos, I studied the before and after MABr addition changes in the blinking profile. The change in the blinking profile of a particular emitting center within the crystal is shown in Figure 16.

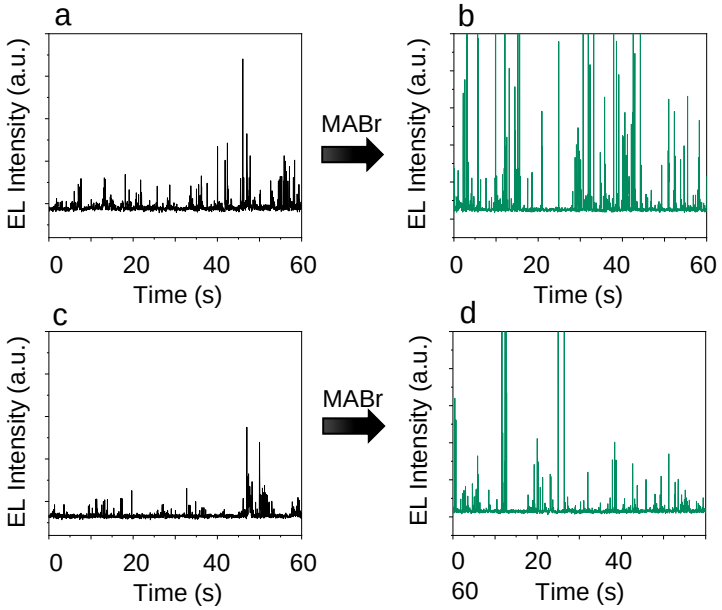


**Figure 16.** (a,b) EL intensity trajectory of an emitting center in a $MAPbBr_3$ microcrystal prepared from an under-stoichiometric precursor solution before and after MABr addition. (c,d) EL intensity trajectory of another emitting center before and after MABr addition. The experiment was performed at 8 V.

The emission intensity and the number of ON events of a particular emitting center increased, as can be seen in figure16 a to Figure 16 b and in Figure 16 c to Figure 16 d.

In the same set of a sample prepared from under-stoichiometric solution, new crystals started showing intense EL blinking after the MABr addition. For e.g., MC 3 and MC 4, as shown in Figure 17 (a,b), show intense EL at 8 V condition after MABr addition.

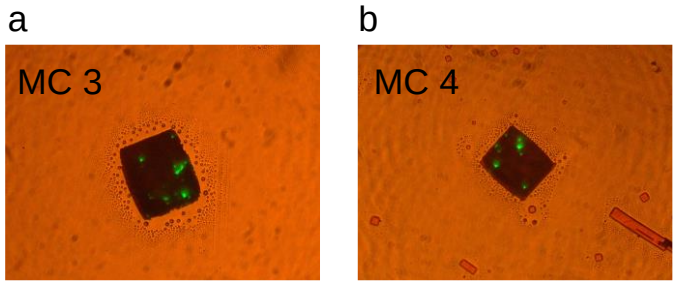


**Figure 17.** The camera images of microcrystals a) MC 3, and b) MC 4 showing intense EL blinking post-MABr treatment at 8 V. Image size is 320 x 240 $\mu m^2$.

The EL blinking trajectories collected from MC 3 exhibiting intense EL blinking after MABr treatment is shown in Figure 18. As can be noticed, the ON-time events increased considerably.

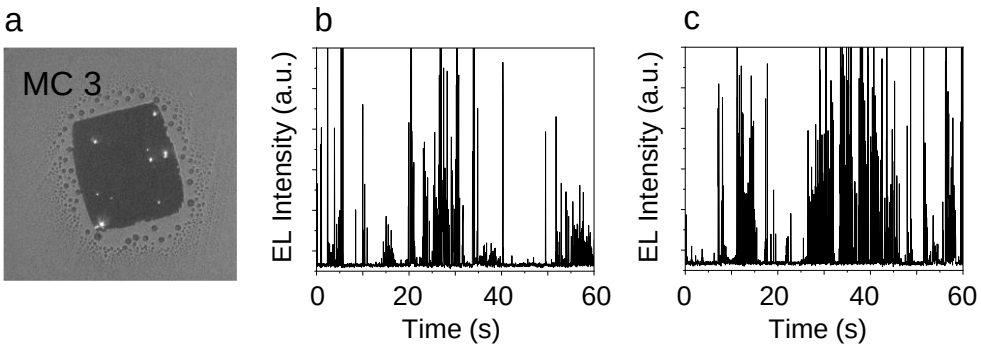


**Figure 18.** a) Single-particle camera of a MABr treated $MAPbBr_3$ microcrystal showing blinking EL at 8 V (image size is 335 x 335 $\mu m^2$), (b,c) EL trajectories of two emitting centers within the microcrystal post-MABr treatment at 8 V.

It was also interesting to notice that in a different sample prepared from under-stoichiometric precursor solution, some new emitting sites with good EL emission were seen from microcrystal named MC 4 with the addition of MABr solution. Hence centers that were non-emissive became emissive after the addition of MABr. The EL trajectories obtained from the new emitting centers from MC 4 is shown in Figure 19 below:

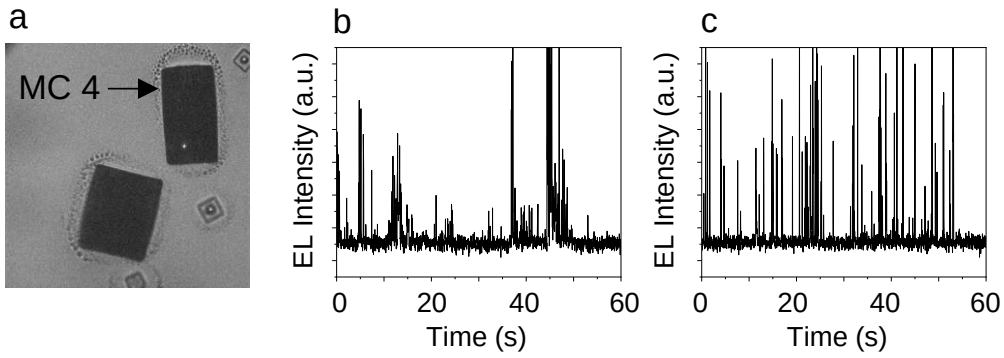


**Figure 19.** a) Single-particle image showing the microcrystals showing EL blinking at 8 V (image size is 335 x 335 $\mu m^2$). (b,c) EL trajectories collected from the new emitting sites that appeared after MABr addition collected at 8 V.

### 5.2.4 The mechanism of electroluminescence blinking in $MAPbBr_3$ microcrystals of varying bromide composition

The mechanism of EL blinking in perovskite microcrystals of varying halide composition can be described as follows. In an under-stoichiometric $MAPBbr_3$ sample, the halide vacancies act as traps, opening the dominant pathway for nonradiative relaxation. The OFF-state recovery mostly depends on the de-trapping of these charge carriers and revert them to ON-state. Thus, a type-B blinking associated with the charge carrier trapping-de-trapping process can be assigned to an under-stoichiometric sample that has a high concentration of halide vacancies. The linear power-law behavior seen for both ON- and OFF-time duration in the probability distribution plots also confirms the type-B blinking assignment.

In the case of $MAPbBr_3$ crystals prepared from stoichiometric and over-stoichiometric precursor solutions, the density of halide vacancy is less than that in the under-stoichiometric sample. Hence other pathways are responsible for nonradiative processes leading to EL blinking. A truncated power-law behavior is noticed for stoichiometric and over-stoichiometric samples, implying that there exist several processes leading to both ON- and OFF-states. Since the ON- and OFF-time probability distribution fits a truncated power-law equation characteristic of type-A blinking, the charging-discharging mechanism is assigned for EL blinking in a stoichiometric and under-stoichiometric sample. Here the excess charge from electrical charge injection may have a role in causing charging of perovskites and lead to Auger-type nonradiative recombination processes mostly by the formation of a negative trion. This process leads

to the OFF-state. Figure 20 shows a scheme for type-A and type-B EL blinking mechanisms in perovskite microcrystals with varying bromide compositions. Under the applied voltage, the excitation of charge carriers from the ground state (i.e., the valence band maximum) to the excited state (i.e., the conduction band minimum) is facilitated. In a type-A mechanism (Figure 20a), an additional electron injected into the conduction band under the applied voltage can cause charging of the perovskite by the formation of a negative trion. This trion can undergo Auger recombination leading to EL quenching with a rate constant, $k_{nr}$. The re-neutralization of the charges can allow for its radiative recombination with a rate constant, $k_r$. This is the charging-discharging mechanism seen in the case of the stoichiometric and over-stoichiometric $MAPbBr_3$ samples. In the type-B mechanism (Figure 20b), after the electrical excitation, the excited state charge carriers can be trapped in a sub-bandgap trap state formed by halide vacancies leading to no emission. The rate constant of this trapping can be expressed at $k_{nr}$ as it is a nonradiative process. The de-trapping of the charge carriers can allow for radiative recombination with a rate constant, $k_r$. This is the type of blinking seen in the case of under-stoichiometric $MAPbBr_3$ samples.

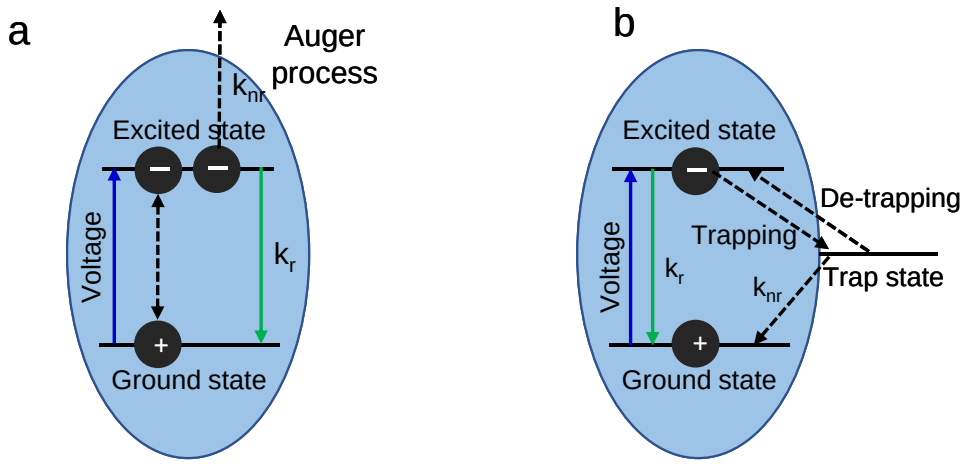


**Figure 20.** Scheme for EL blinking mechanism. a) Type-A mechanism observed in the case of stoichiometric and over-stoichiometric $MAPbBr_3$ samples assisted by the charging-discharging mechanism, and b) type-B mechanism observed in the case of under-stoichiometric $MAPbBr_3$ sample assisted by the trapping-de-trapping mechanism

### 5.2.5 Conclusion

In this chapter, I studied the role of halogen in the EL blinking mechanism. For this, I synthesized $MAPbBr_3$ microcrystals of varying bromide composition by preparing an

under-stoichiometric, stoichiometric, and over-stoichiometric precursor solution using MAB and $PbBr_2$. I varied the concentration of MABr to bring the changes in bromide composition within the formed microcrystal. The PL and EL properties of these three samples were studied. It was found that an under-stoichiometric sample showed a type-B blinking behavior which was characterized by a linear power-law behavior. However, stoichiometric and over-stoichiometric precursor samples showed a type-A blinking behavior characterized by a truncated power-law behavior. Type-B blinking is associated with a trapping-de-trapping mechanism. In an under-stoichiometric sample, the halide vacancies are thought to be a dominant factor causing the nonradiative losses in EL. Thus, the type-B blinking behavior noticed also supports the role of halide vacancies in EL blinking. However, type-A in the case of stoichiometric and over-stoichiometric samples is characterized by the truncated-power law fitting. This truncated behavior implies a distributed kinetics involved in both ON and OFF processes in the EL blinking. Thus, not only halogen vacancy-assisted blinking but other nonradiative processes also lead to EL blinking. The externally injected charge carriers can lead to an excited state trion formation favoring a charging-discharging type of blinking. I also studied the effect of MABr addition on $MAPbBr_3$ photoluminescence and electroluminescence. Such post-treatment studies reveal improvement in PL lifetime and PL intensity and are a result of halide vacancy filling, which otherwise quenches the PL. This was also confirmed by SEM-EDS analysis. The EDS spectral analysis and elemental mapping studies show an increase in the percentage composition of Br after the addition of MABr. In the case of EL, MABr added $MAPbBr_3$ sample showed a ~5-fold improvement in ON-time cut-off. MABr addition studies performed on an under-stoichiometric $MAPbBr_3$ sample showed that the EL properties had improved greatly. The EL intensity increased, the occurrence of ON-events increased, the blinking spots showed enhanced EL emissions, and even new emitting sites appeared in the crystal with the addition of MABr. Thus, the role of bromide ions in the enhancement of PL and EL properties and also in the blinking mechanism was understood from the above studies.

## References


1. Li, C.; Guerrero, A.; Huettner, S.; Bisquert, J. Unravelling the Role of Vacancies in Lead Halide Perovskite through Electrical Switching of Photoluminescence. *Nat. Commun.* **2018**, *9*, 5113.

2. Sharma, D. K.; Hirata, S.; Biju, V.; Vacha, M. Stark Effect and Environment-Induced Modulation of Emission in Single Halide Perovskite Nanocrystals. *ACS Nano* **2019**, *13*, 624–632.

3. Lee, S.; Kim, D. Bin; Yu, J. C.; Jang, C. H.; Park, J. H.; Lee, B. R.; Song, M. H. Versatile Defect Passivation Methods for Metal Halide Perovskite Materials and Their Application to Light-Emitting Devices. *Adv. Mater.* **2019**, *31*, 1805244.

4. Knight, A. J.; Patel, J. B.; Snaith, H. J.; Johnston, M. B.; Herz, L. M. Trap States, Electric Fields, and Phase Segregation in Mixed-Halide Perovskite Photovoltaic Devices. *Adv. Energy Mater.* **2020**, *10*, 1903488.

5. Prakasam, V.; Tordera, D.; Bolink, H. J.; Gelinck, G. Degradation Mechanisms in Organic Lead Halide Perovskite Light-Emitting Diodes. *Adv. Opt. Mater.* **2019**, *7*, 1900902.

6. Fu, J.; Jamaludin, N. F.; Wu, B.; Li, M.; Solanki, A.; Ng, Y. F.; Mhaisalkar, S.; Huan, C. H. A.; Sum, T. C. Localized Traps Limited Recombination in Lead Bromide Perovskites. *Adv. Energy Mater.* **2019**, *9*, 1803119.

7. Deng, X.; Wen, X.; Lau, C. F. J.; Young, T.; Yun, J.; Green, M. A.; Huang, S.; Ho-Baillie, A. W. Y. Electric Field Induced Reversible and Irreversible Photoluminescence Responses in Methylammonium Lead Iodide Perovskite. *J. Mater. Chem. C* **2016**, *4*, 9060–9068.

8. Zhao, Y.; Liang, C.; Zhang, H.; Li, D.; Tian, D.; Li, G.; Jing, X.; Zhang, W.; Xiao, W.; Liu, Q.; Zhang, F.; He, Z. Anomalously Large Interface Charge in Polarity-Switchable Photovoltaic Devices: An Indication of Mobile Ions in Organic-Inorganic Halide Perovskites. *Energy Environ. Sci.* **2015**, *8*, 1256–1260.

9. Choi, H.; Jeong, J.; Kim, H.-B.; Kim, S.; Walker, B.; Kim, G.-H.; Kim, J. Y. Cesium-Doped Methylammonium Lead Iodide Perovskite Light Absorber for Hybrid Solar Cells. *Nano Energy* **2014**, *7*, 80–85.

10. Leijtens, T.; Hoke, E. T.; Grancini, G.; Slotcavage, D. J.; Eperon, G. E.; Ball, J. M.; De Bastiani, M.; Bowring, A. R.; Martino, N.; Wojciechowski, K.; McGehee, M. D.; Snaith, H. J.; Petrozza, A. Mapping Electric Field-Induced Switchable Poling and Structural Degradation in Hybrid Lead Halide Perovskite Thin Films. *Adv. Energy Mater.* **2015**, *5*, 1500962.

11. Warby, J. H.; Wenger, B.; Ramadan, A. J.; Oliver, R. D. J.; Sansom, H. C.; Marshall, A. R.; Snaith, H. J. Revealing Factors Influencing the Operational Stability of Perovskite Light-Emitting Diodes. *ACS Nano* **2020**, *14*, 8855–8865.

12. Xiao, Z.; Kerner, R. A.; Zhao, L.; Tran, N. L.; Lee, K. M.; Koh, T. W.; Scholes, G. D.; Rand, B. P. Efficient perovskite light-emitting diodes featuring nanometre-sized crystallites. *Nat. Photonics* **2017**, *11*, 108–115.

13. Cao, Y.; Wang, N.; Tian, H., Guo, J.; Wei, Y.; Chen, H.; Miao, Y.; Zou, W.; Pan, K.; He, Y.; Cao, H.; Ke, Y.; Xu, M.; Wang, Y.; Yang, M.; Du, K.; Fu, Z.; Kong, D.; Dai, D.; Huang, W. Perovskite light-emitting diodes based on spontaneously formed submicrometre-scale structures. *Nature* **2018**, *562*, 249–253.

14. Chiba, T.; Hayashi, Y.; Ebe, H.; Hoshi, K.; Sato, J.; Sato, S.; Pu, Y.-J.; Ohisa, S.; Kido, J. Anion-Exchange Red Perovskite Quantum Dots with Ammonium Iodine Salts for Highly Efficient Light-Emitting Devices. *Nat. Photonics* **2018**, *12*, 681–687.

15. Zhao, B.; Bai, S.; Kim, V.; Lamboll, R.; Shivanna, R.; Auras, F.; Richter, J. M.; Yang, L.; Dai, L.; Alsari, M.; She, X.-J.; Liang, L.; Zhang, J.; Lilliu, S.; Gao, P.; Snaith, H. J.; Wang, J.; Greenham, N. C.; Friend, R. H.; Di, D. High-Efficiency Perovskite–Polymer Bulk Heterostructure Light-Emitting Diodes. *Nat. Photonics* **2018**, *12*, 783–789.

16. NREL 2021 PCE efficiency chart

17. Kim, H.; Zhao, L.; Price, J. S.; Grede, A. J.; Roh, K.; Brigeman, A. N.; Lopez, M.; Rand, B. P.; Giebink, N. C. Hybrid Perovskite Light Emitting Diodes under Intense Electrical Excitation. *Nat. Commun.* **2018**, *9*, 4893.

18. Zhao, L.; Roh, K.; Kacmoli, S.; Al Kurdi, K.; Jhulki, S.; Barlow, S.; Marder, S. R.; Gmachl, C.; Rand, B. P. Thermal Management Enables Bright and Stable Perovskite Light-Emitting Diodes. *Adv. Mater.* **2020**, *32*, 1–7.

19. Lv, W.; Li, L.; Xu, M.; Hong, J.; Tang, X.; Xu, L.; Wu, Y.; Zhu, R.; Chen, R.; Huang, W. Improving the Stability of Metal Halide Perovskite Quantum Dots by Encapsulation. *Adv. Mater.* **2019**, *31*, 1900682.

20. Qin, J.; Zhang, J.; Bai, Y.; Ma, S.; Wang, M.; Xu, H.; Loyd, M.; Zhan, Y.; Hou, X.; Hu, B. Enabling Self-Passivation by Attaching Small Grains on Surfaces of Large Grains toward High-Performance Perovskite LEDs. *iScience* **2019**, *19*, 378–387.

21. Chen, R.; Li, J.; Dobrovolsky, A.; González-Carrero, S.; Gerhard, M.; Messing, M. E.; Chirvony, V.; Pérez-Prieto, J.; Scheblykin, I. G. Creation and Annihilation of Nonradiative Recombination Centers in Polycrystalline Metal Halide Perovskites by Alternating Electric Field and Light. *Adv. Opt. Mater.* **2020**, *8*, 1901642.

22. Xia, S.; Wang, Z.; Ren, Y.; Gu, Z.; Wang, Y. Unusual Electric Field-Induced Optical Behaviors in Cesium Lead Bromide Perovskites. *Appl. Phys. Lett.* **2019**, *115*, 201101.

23. Ball, J. M.; Petrozza, A. Defects in Perovskite-Halides and Their Effects in Solar Cells. *Nat. Energy* **2016**, *1*, 16149.

24. Stranks, S. D. Nonradiative Losses in Metal Halide Perovskites. *ACS Energy Lett.* **2017**, *2*, 1515–1525.

25. Buin, A.; Comin, R.; Xu, J.; Ip, A. H.; Sargent, E. H. Halide-Dependent Electronic Structure of Organolead Perovskite Materials. *Chem. Mater.* **2015**, *27*, 4405–4412.

26. Galisteo-López, J. F.; Calvo, M. E.; Rojas, T. C.; Míguez, H. Mechanism of Photoluminescence Intermittency in Organic–Inorganic Perovskite Nanocrystals. *ACS Appl. Mater. Interfaces* **2019**, *11*, 6344–6349.

27. Galland, C.; Ghosh, Y.; Steinbrück, A.; Sykora, M.; Hollingsworth, J. A.; Klimov, V. I.; Htoon, H. Two Types of Luminescence Blinking Revealed by Spectroelectrochemistry of Single Quantum Dots. *Nature* **2011**, *479*, 203–207.

28. Efros, A. L.; Nesbitt, D. J. Origin and Control of Blinking in Quantum Dots. *Nat. Nanotechnol.* **2016**, *11*, 661–671.

29. Peterson, J. J.; Nesbitt, D. J. Modified Power Law Behavior in Quantum Dot Blinking: A Novel Role for Biexcitons and Auger Ionization. *Nano Lett.* **2009**, *9*, 338–345.

30. Tian, Y.; Merdasa, A.; Peter, M.; Abdellah, M.; Zheng, K.; Ponseca, C. S.; Pullerits, T.; Yartsev, A.; Sundström, V.; Scheblykin, I. G. Giant Photoluminescence Blinking of Perovskite Nanocrystals Reveals Single-Trap Control of Luminescence. *Nano Lett.* **2015**, *15*, 1603–1608.

31. Wen, X.; Ho-Baillie, A.; Huang, S.; Sheng, R.; Chen, S.; Ko, H. C.; Green, M. A. Mobile Charge-Induced Fluorescence Intermittency in Methylammonium Lead Bromide Perovskite. *Nano Lett.* **2015**, *15*, 4644–4649.

32. Halder, A.; Pathoor, N.; Chowdhury, A.; Sarkar, S. K. Photoluminescence Flickering of Micron-Sized Crystals of Methylammonium Lead Bromide: Effect of Ambience and Light Exposure. *J. Phys. Chem. C* **2018**, *122*, 15133–15139.

33. Pathoor, N.; Halder, A.; Mukherjee, A.; Mahato, J.; Sarkar, S. K.; Chowdhury, A. Fluorescence Blinking Beyond Nanoconfinement: Spatially Synchronous Intermittency of Entire Perovskite Microcrystals. *Angew. Chemie - Int. Ed.* **2018**, *57*, 11603–11607.

34. Trinh, C. T.; Minh, D. N.; Ahn, K. J.; Kang, Y.; Lee, K. G. Organic-Inorganic $FAPbBr_3$ Perovskite Quantum Dots as a Quantum Light Source: Single-Photon Emission and Blinking Behaviors. *ACS Photonics* **2018**, *5*, 4937–4943.

35. Park, Y. S.; Guo, S.; Makarov, N. S.; Klimov, V. I. Room Temperature Single-Photon Emission from Individual Perovskite Quantum Dots. *ACS Nano* **2015**, *9*, 10386–10393.

36. Seth, S.; Mondal, N.; Patra, S.; Samanta, A. Fluorescence Blinking and Photoactivation of All-Inorganic Perovskite Nanocrystals $CsPbBr_3$ and $CsPbBr_2I$. *J. Phys. Chem. Lett.* **2016**, *7*, 266–271.

37. Merdasa, A.; Tian, Y.; Camacho, R.; Dobrovolsky, A.; Debroye, E.; Unger, E. L.; Hofkens, J.; Sundström, V.; Scheblykin, I. G. "supertrap" at Work: Extremely Efficient Nonradiative Recombination Channels in $MAPbI_3$ Perovskites Revealed by Luminescence Super-Resolution Imaging and Spectroscopy. *ACS Nano* **2017**, *11*, 5391–5404.

38. Eremchev, I. Y.; Tarasevich, A. O.; Li, J.; Naumov, A. V.; Scheblykin, I. G. Lack of Photon Antibunching Supports Supertrap Model of Photoluminescence Blinking in Perovskite Sub-Micrometer Crystals. *Adv. Opt. Mater.* **2021**, *9*, 2001596.

39. Trinh, C. T.; Minh, D. N.; Ahn, K. J.; Kang, Y.; Lee, K. G. Verification of Type-A and Type-B-HC Blinking Mechanisms of Organic–Inorganic Formamidinium Lead Halide Perovskite Quantum Dots by FLID Measurements. *Sci. Rep.* **2020**, *10*, 1–8.

40. Yu, J. C.; Kim, D. W.; Kim, D. Bin; Jung, E. D.; Park, J. H.; Lee, A.-Y.; Lee, B. R.; Di Nuzzo, D.; Friend, R. H.; Song, M. H. Improving the Stability and Performance of Perovskite Light-Emitting Diodes by Thermal Annealing Treatment. *Adv. Mater.* **2016**, *28*, 6906–6913.

41. Van-Cao, N.; Hiroyuki, K.; Fumio, S.; Hisao, Y. Single-Crystal Perovskite $CH_3NH_3PbBr_3$ Prepared by Cast Capping Method for Light-Emitting Diodes. *Jpn. J. Appl. Phys.* **2018**, *57* (4S), 04FL10.

42. Sharma, D. K.; Hirata, S.; Vacha, M. Single-Particle Electroluminescence of $CsPbBr_3$ Perovskite Nanocrystals Reveals Particle-Selective Recombination and Blinking as Key Efficiency Factors. *Nat. Commun.* **2019**, *10*, 4499.

43. Fassl, P.; Lami, V.; Bausch, A.; Wang, Z.; Klug, M. T.; Snaith, H. J.; Vaynzof, Y. Fractional Deviations in Precursor Stoichiometry Dictate the Properties, Performance and Stability of Perovskite Photovoltaic Devices. *Energy Environ. Sci.* **2018**, *11*, 3380–3391.

44. Falk, L. M.; Goetz, K. P.; Lami, V.; An, Q.; Fassl, P.; Herkel, J.; Thome, F.; Taylor, A. D.; Paulus, F.; Vaynzof, Y. Effect of Precursor Stoichiometry on the Performance and Stability of $MAPbBr_3$ Photovoltaic Devices. *Energy Technol.* **2020**, *8*, 1900737.

45. Schmidt, L. C.; Pertegás, A.; González-Carrero, S.; Malinkiewicz, O.; Agouram, S.; Mínguez Espallargas, G.; Bolink, H. J.; Galian, R. E.; Pérez-Prieto, J. Nontemplate Synthesis of $CH_3NH_3PbBr_3$ Perovskite Nanoparticles. *J. Am. Chem. Soc.* **2014**, *136*, 850–853.

46. Diab, H.; Arnold, C.; Lédée, F.; Trippé-Allard, G.; Delport, G.; Vilar, C.; Bretenaker, F.; Barjon, J.; Lauret, J. S.; Deleporte, E.; Garrot, D. Impact of Reabsorption on the Emission Spectra and Recombination Dynamics of Hybrid Perovskite Single Crystals. *J. Phys. Chem. Lett.* **2017**, *8*, 2977–2983.

47. Kim, H.; Zhao, L.; Price, J. S.; Grede, A. J.; Roh, K.; Brigeman, A. N.; Lopez, M.; Rand, B. P.; Giebink, N. C. Hybrid Perovskite Light Emitting Diodes under Intense Electrical Excitation. *Nat. Commun.* **2018**, *9*, 4893.

48. Ball, J. M.; Petrozza, A. Defects in Perovskite-Halides and Their Effects in Solar Cells. *Nat. Energy* **2016**, *1*, 16149.

49. Wang, F.; Bai, S.; Tress, W.; Hagfeldt, A.; Gao, F. Defects Engineering for High-Performance Perovskite Solar Cells. *npj Flex. Electron.* **2018**, *2*, 22.

50. Jin, H.; Debroye, E.; Keshavarz, M.; Scheblykin, I. G.; Roeffaers, M. B. J.; Hofkens, J.; Steele, J. A. It's a Trap! On the Nature of Localised States and Charge Trapping in Lead Halide Perovskites. *Mater. Horizons* **2020**, *7*, 397–410.

# Summary and perspectives

In this thesis, I studied the photoluminescence and electroluminescence properties of lead halide perovskite pellets and microcrystals. I utilized pressure-induced solid-state methods to synthesize perovskite pellets without using any harmful solvents or organic ligands. Although this method was used to study EL properties of perovskites, the sample was essentially thick and hence did not give good results. Hence, I switched to study the photon recycling phenomenon seen in such thick samples. I found that there exist closely spaced energy states within the pure lead halide perovskite pellets. These closely spaced state energy states allow for energy transfer within them. This was confirmed by using a mixed halide perovskite, where the closely spaced energy states allow for efficient energy transfer. Such an energy transfer is a means of efficient photon recycling in perovskites.

For studying the EL properties of lead halide perovskites, I synthesized lead halide perovskite microcrystals. I found that microcrystals showed an intriguing phenomenon called EL blinking. The studies showed that EL and PL blinking had different characteristics. Also, I observed two types of EL blinking in the perovskites. I modeled them as type-A and type-B EL blinking based on studies from microcrystals with multiple-emitting centers and an ensemble of microcrystals. In both the crystals, it was found that halide vacancy traps act as EL quenchers. These traps are migrating based on the observation of random switching of emitting centers.

For understanding the role of halide vacancies in the EL blinking mechanism clearly, I synthesized perovskite microcrystals of varying bromide composition by simply varying the precursor ratio namely, under-stoichiometric, stoichiometric, and over-stoichiometric precursor solution. It was found that an under-stoichiometric precursor solution showed a type-B blinking related to a trapping-de-trapping mechanism. Such a blinking results from the deficiency of halide ions which creates vacancy traps. When the charge carriers are generated by electrical excitation, some of them are trapped to the OFF-state in EL blinking. However, in a stoichiometric and over the stoichiometric sample, the density of halogen vacancy is less. Hence, other mechanisms such as Auger recombination of electrically generated trions contribute to EL blinking. This is seen by the truncated nature of power-law distribution due to the charging-discharging mechanism. Post-treatment of $MAPBbr_3$ crystals with MABr has shown that added Br ions can fill the vacancies leading to improved EL and PL properties.

# List of publications

1. **Nonradiative Energy Transfer through Distributed Bands in Piezochemically Synthesized Cesium and Formamidinium Lead Halide Perovskites**

   Bhagyalakshmi, S. B.; Ghimire, S.; Takahashi, K.; Takano, Y.; Nakamura, T.; Yuyama, K. -I.; Biju, V.

   *Chem. Eur. J.* **2020**, *26*, 2133–2137.

# List of papers presented in conferences

1. **Defect-filling in Lead Halide Perovskite Crystals Revealed by Single-Particle Electroluminescence Microspectroscopy**
   Bhagyalakshmi, S. B.; Takano, Y.; Biju, V.
   *The 101st CSJ Annual Meeting (2021),* Tokyo, Japan, 19-22 Mar **2021. [e-Oral]**

2. **Single Particle Electroluminescence Blinking Revealing Real-Time Switching Between Emitting and Quenching Sites in $MAPbBr_3$ Perovskites.**
   Bhagyalakshmi, S. B.; Biju, V.
   *Chemistry Association Hokkaido Branch 2021 Winter Research Presentation*, Sapporo, Japan, 26-27 Jan **2021. [e-poster]**

3. **Single Particle Electroluminescence Blinking Revealing Switching Between the Emitting and Quenching Sites in $MAPbBr_3$ Perovskites**
   Bhagyalakshmi, S. B.; Biju, V.
   *The 21st RIES-Hokudai International Symposium*, Sapporo, Japan, 10-11 Dec **2020. [e-poster]**

4. **Photon Recycling in Lead Halide Perovskites: Challenges and Prospects**
   Bhagyalakshmi, S. B.; Ghimire, S.; Takano, Y.; Yuyama, K. -I.; Biju, V.
   *International Webinar on "New Trends in Applied Chemistry (NTAC),* Cochin, India, 17-20 Dec **2020 [Student presentation]**

5. **Electroluminescence Intermittency and Spectral Fluctuations of $MAPbBr_3$ Perovskite Single Particles**
   Bhagyalakshmi, S. B.; Takano, Y.; Biju, V.
   *Annual Meeting of the Japanese Photochemistry Association 2020*, Japan, 9-11 Sep **2020. [e-poster]**

6. **Delayed Emission by Energy Transfer- Induced Photon Recycling in Close-Packed Perovskite Crystallites**
   Bhagyalakshmi, S. B.; Ghimire, S.; Takahashi, K.; Yuyama, K. -I.; Takano, Y.; Nakamura, T.; Biju, V.
   *2019 International Symposium of Research Institute for Electronic Science (RIES) and Center for Emerging Functional Matter Science (CEFMA)*, Sapporo, Japan, 3-4 Dec **2019. [Poster]**

7. **Photon Recycling via Energy Transfer- Induced Delayed Emission in Pressed Lead Halide Perovskites**

   Bhagyalakshmi, S. B.; Biju, V.

   *The 20th RIES-Hokudai International Symposium*, Sapporo, Japan, 2-3 Dec **2019. [Poster]**

8. **Delayed Red-Shifted Emission by Energy Transfer- Induced Photon Recycling in Pressed Lead Halide Perovskites**

   Bhagyalakshmi, S. B.; Ghimire, S.; Takano, Y.; Yuyama, K. -I.; Biju, V.

   *Annual Meeting of the Japanese Photochemistry Association 2019*, Nagoya, Japan, 10-12 Sep **2019. [Oral]**

9. **Delayed Emission from Close-Packed Crystals of Lead Halide Perovskites**

   Bhagyalakshmi, S. B.; Ghimire, S.; Takahashi, K.; Takano, Y.; Nakamura, T.; Yuyama, K. -I.; Biju, V.

   *Chemistry Association Hokkaido Branch 2019 Summer Research Presentation*, Sapporo, Japan, 20 Jul **2019. [Poster]**

10. **Lifetime of Photogenerated Charge Carriers in 0-, 1-, 2- and 3D Perovskite Structures**

    Bhagyalakshmi, S. B.; Ghimire, S,; Biju, V.

    *Chemistry Association Hokkaido Branch 2019 Winter Research Presentation*, Sapporo, Japan, 22 Jan **2019. [Oral]**

11. **Charge Carrier Dynamics in Low Dimensional Perovskite Structures**

    Bhagyalakshmi, S. B.; Ghimire, S.; Yuyama, K. -I.; Biju, V.

    *International Conference on "Materials for the Millennium - MATCON 2019,* Kochi, India, 14-16 March **2019. [Oral and Poster]**

12. **Delayed Emission by Energy Transfer-induced Photon Recycling in Close-Packed Perovskite Crystallites**

    Bhagyalakshmi, S. B.; Ghimire, S.; Takahashi, K.; Takano, Y.; Nakamura, T.; Yuyama, K.-I.; Biju, V.

    *The 19th RIES-Hokudai International Symposium*, Sapporo, Japan, 11-12 Dec **2019. [Poster]**